Scilight

Progress in Composite Materials
https://www.sciltp.com/journals/pcm

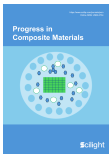

Review

Graphene Nanoplatelet-Reinforced Hybrid Aluminum Matrix Composites: Recent Advances and Future Perspectives

Sanoj Divakar [1], Santanu Sardar [2] and Debdulal Das [1,*]

[1] Department of Metallurgy and Materials Engineering, Indian Institute of Engineering Science and Technology, Shibpur, Howrah 711103, West Bengal, India
[2] Department of Mechanical Engineering, Indian Institute of Engineering Science and Technology, Shibpur, Howrah 711103, West Bengal, India
* Correspondence: debdulal_das@metal.iiests.ac.in or debdulal_das@yahoo.com

How To Cite: Divakar, S.; Sardar, S.; Das, D. Graphene Nanoplatelet-Reinforced Hybrid Aluminum Matrix Composites: Recent Advances and Future Perspectives. *Progress in Composite Materials* **2026**, *2*(1), 2. https://doi.org/10.53941/pcm.2026.100002

Received: 18 March 2026
Revised: 20 June 2026
Accepted: 13 July 2026
Published: 31 July 2026

Abstract: Hybrid aluminum matrix composites (HAMCs) reinforced with graphene nanoplatelets (GNPs) and secondary reinforcements have emerged as promising lightweight structural materials due to their superior strength, wear resistance, and multifunctional performance. This review critically evaluates recent developments in GNPs-reinforced HAMCs, categorizing them into carbide-assisted, oxide-assisted, carbonaceous, and emerging sustainable hybrid systems. The influence of processing routes including semi-solid stir casting (compocasting), ultrasonic-assisted stir casting (UASC), powder metallurgy (PM), friction stir processing (FSP), accumulative roll bonding (ARB), and laser powder bed fusion (L-PBF) on reinforcement dispersion, interfacial bonding, and resultant properties (grain refinement, load-transfer mechanisms, etc.) is systematically discussed. Further, particular emphasis is placed on the role of the hybrid reinforcements in improving the mechanical and tribological performances of the HAMCs in reference to their processing techniques. Comparative analysis reveals that carbide-assisted systems provide the highest strengthening response, where Al/(GNPs+SiC) composites achieve tensile strengths up to 589 MPa through severe grain refinement, while GNPs+WC systems exhibit nearly 350% relative strength enhancement. Among oxide-assisted systems, L-PBF fabricated AA2024/(0.2GNPs+1ZrO_2) (wt.%) composites attain a peak tensile strength of 624 MPa after T6 treatment due to the formation of a crack-free bimodal microstructure. Carbonaceous hybrids such as reduced graphene oxide (rGO)+CNTs systems demonstrate an excellent balance between strength (460 MPa) and ductility (31.6%) through interconnected carbon networks that suppress crack propagation. Tribologically, graphene-based tribo-films significantly reduce friction and wear, with GO+CNTs hybrids achieving a minimum coefficient of friction of 0.295, whereas GNPs+B_4C and GNPs+waste-derived Al hybrid systems exhibit excellent wear resistance with wear rates as low as 1.9×10^{-3} mm^3 m^{-1}. The review further highlights key challenges including reinforcement agglomeration, porosity, and interfacial instability at higher GNPs loadings (>1–2 wt.%). Overall, the study provides a comparative and data-driven framework for designing next-generation HAMCs for aerospace, automotive, defense, and thermal-management applications.

Keywords: Hybrid; composite; graphene; carbonaceous; processing; application; mechanical properties: tribological properties

Copyright: © 2026 by the authors. This is an open access article under the terms and conditions of the Creative Commons Attribution (CC BY) license (https://creativecommons.org/licenses/by/4.0/).
Publisher's Note: Scilight stays neutral with regard to jurisdictional claims in published maps and institutional affiliations.

1. Introduction

The growing demand for materials exhibiting superior combinations of strength, stiffness, toughness, and multifunctional performance has driven extensive research into advanced composite materials. Conventional engineering materials such as polymers, metals, and ceramics each possess inherent limitations when used independently. Polymers generally exhibit low stiffness and strength but offer good corrosion resistance and ease of processing, whereas ceramics are characterized by very high stiffness and strength though suffer from poor fracture toughness [1,2]. Metals provide a more balanced combination of strength, stiffness, and toughness; however, they often fall short of meeting the increasingly stringent performance requirements of modern engineering applications. To overcome such limitations, composite materials have been developed by combining two or more distinct constituents to achieve tailored and enhanced properties [3].

Based on the nature of the matrix material, composites are broadly classified into polymer matrix composites (PMCs), metal matrix composites (MMCs), and ceramic matrix composites (CMCs). Among those composites, MMCs have attracted significant attention due to their ability to retain the ductility and toughness of metals while incorporating reinforcements that improve stiffness, strength, wear resistance, and thermal stability [4]. Consequently, the search for effective reinforcing materials capable of enhancing the performance of the MMCs has become a major research concern [3]. MMCs consist of a metallic matrix reinforced with continuous or discontinuous fibers, whiskers, or particulate phases, which may range from micrometer to nanometer scale. Depending on the morphology and aspect ratio of reinforcement, MMCs are commonly classified into particulate-reinforced, short fiber or whisker-reinforced, and long fiber-reinforced systems. Notably, Aluminum matrix composites (AMCs) represent one of the most extensively studied classes due to their favorable balance of mechanical performance, density, cost, and process capability [5].

Aluminum and its alloys are widely regarded as MMC matrices because of their low density, relatively low melting temperature, good thermal and electrical conductivity, excellent corrosion resistance, and ease of fabrication [2,6]. These attributes make Aluminum-based composites particularly attractive for weight-sensitive applications, where reduced mass directly contributes to improved energy efficiency and performance, especially in the automotive and aerospace sectors [7,8]. Nevertheless, monolithic Aluminum alloys exhibit certain limitations, including inadequate wear resistance, moderate fatigue strength, and limited high-temperature capability. To overcome these shortcomings, various reinforcements such as silicon carbide (SiC), alumina (Al_2O_3), boron carbide (B_4C), carbon nano-tubes (CNTs), graphite, and graphene have been incorporated into Aluminum matrices to tailor their mechanical and functional properties [9,10]. Among the available reinforcements, graphene has emerged as one of the most promising candidates for Al-based MMCs owing to its exceptional intrinsic properties and unique two-dimensional structure. Graphene is a single-atom-thick carbon allotrope that serves as the fundamental building block for other carbon nanostructures, including zero-dimensional fullerenes, one-dimensional carbon nanotubes, and three-dimensional graphite. Its outstanding properties either in single-layer or few-layer forms, include an ultra high Young's modulus of approximately 1 TPa, ultimate tensile strength exceeding 125 GPa, exceptional stiffness, substantially high thermal conductivity (1000–5300 $W\ m^{-1}\ K^{-1}$), and a large specific surface area of about 2600–2630 $m^2\ g^{-1}$ [11]. These features enable strong interfacial interaction and efficient load transfer between graphene and Al matrices, making graphene a capable reinforcement for enhancing both mechanical and multifunctional properties of AMCs [3,10,12]. Notably, graphene-reinforced Al matrix composites have demonstrated significant improvements in strength, stiffness, thermal and electrical conductivities, offering potential applications in electronics, energy storage, sensing, and other advanced structural components. Nonetheless, several challenges remain, including graphene agglomeration, damage to its two-dimensional network during processing, and poor wettability and interfacial bonding with the Al [7,9]. Dispersing the second phase particles in the matrix and achieving a strong interfacial bond are the two main processing challenges. Most fabrication processes fall short of fulfilling these tasks. Clusters of particles and weak matrix-reinforcement interfaces compromise the ability of the composite material to function under extreme conditions, such as high temperature and pressure typical of automotive applications (especially diesel and jet engines) [8,13]. Uniform dispersion of graphene and other nano-carbon reinforcements remains a critical prerequisite for fully exploring their reinforcing potential in Al-matrix composites [14]. Researchers have reported optimized processing parameters and dispersion strategies to achieve simultaneous improvements in mechanical, thermal, and electrical properties of HAMCs [9,11,12,14]. To overcome the limitations of mono reinforced composites and to achieve more balanced property combinations, hybrid Aluminum matrix composites (HAMCs) have been developed, in which graphene is combined with secondary reinforcements like graphite, CNTs, ceramic oxides, carbides, borides, nitrides, or metallic phases (e.g., Cu, Ni, Cr, etc.) [12]. Such hybrid reinforcement strategies enable synergistic strengthening mechanisms and are reported to improve microstructural stability and performance,

addressing the core focus on graphene-reinforced hybrid AMCs, as addressed in this review article. To systematically understand the expanding landscape of advanced composite materials, a conceptual framework for HAMCs having graphene nanoplatelets (GNPs) as one of the hybrid reinforcements is presented in Figure 1. This framework categorizes HAMCs based on the nature of their secondary reinforcement, illustrating how the fundamental integration of 2D carbonaceous nanomaterials with various secondary phases, ranging from hard ceramics and metallic nanoparticles to industrial waste derivatives. The necessity for this categorization is underscored by the recent research trends. Based on a comprehensive review of the existing literature, a total of 115 journal articles published between 2015 and 2025 have been sorted for the current review.

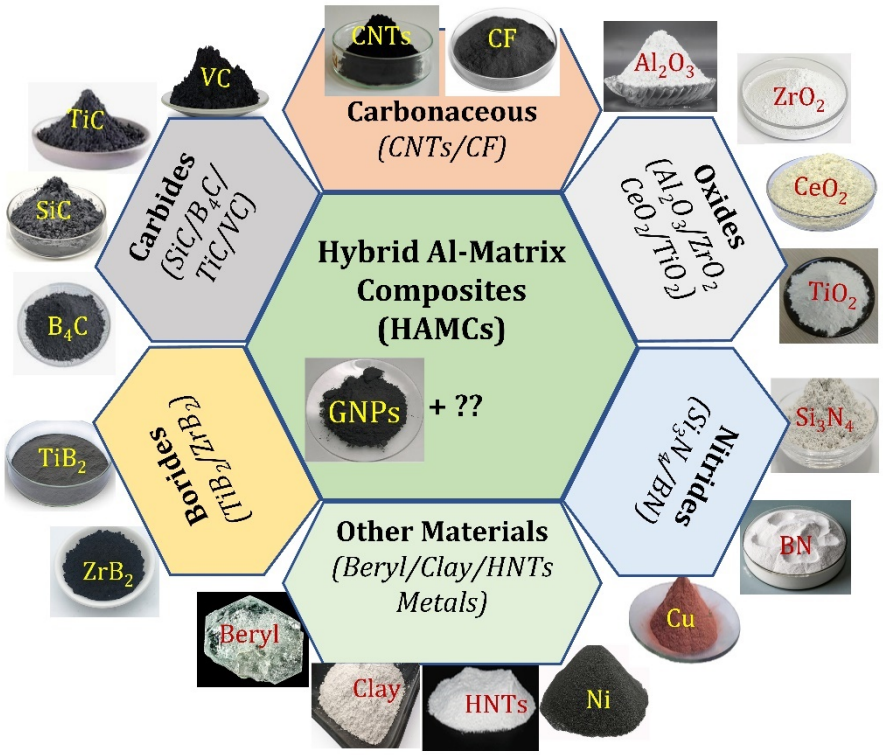

Figure 1. Conceptual framework of graphene nanoplatelets (GNPs) reinforced hybrid Al matrix composites (HAMCs) with secondary reinforcements.

A systematic bibliometric approach was adopted to ensure a transparent and reproducible literature survey. The Scopus database was searched using the Boolean query ("hybrid" AND "Graphene" AND ("metal matrix composite" OR "MMC" OR "AMC")) for publications from 2015 to 2025, yielding 455 initial records. After applying strict inclusion criteria (peer-reviewed English articles on aluminum-based hybrid composites reinforced with GNPs/graphene derivatives and secondary reinforcements) and excluding non-hybrid and non-aluminum systems, relevant studies were screened and analyzed. The selected articles were categorized based on matrix alloy, reinforcement combination, processing route, and mechanical/tribological performance. Additional validation through Google Scholar, citation tracking, and analysis of key review papers ensured comprehensive coverage and minimized bias. Finally, a focused dataset of 115 research articles was established for detailed evaluation of processing strategies, reinforcement effects, strengthening mechanisms, and future research directions in GNP-reinforced hybrid aluminum matrix composites. To comprehensively support the discussion of strengthening mechanisms, processing routes, and industrial applications, this repository was augmented by a secondary manual search using the Google Scholar database. Through forward-backward snowballing and the targeted inclusion of foundational research papers and high-impact review articles, the final reference count was expanded from 115 to 137, establishing a highly robust empirical baseline for this comprehensive review.

Figure 2 presents the statistical distribution of the secondary reinforcements utilized in current HAMCs having GNPs as the primary reinforcement. As depicted, the literature shows a clear preference for distinct architectural pairings such as combining the solid lubrication and strain-relief capabilities of GNPs with the load-bearing capacity of specific carbides, oxides, or waste derivatives to establish a universal strengthening synergy. These pairings are engineered to balance the traditional trade-offs between strength, microhardness, and ductility, while emerging categories like metal-anchored GNPs are at the forefront of preventing detrimental interfacial reactions.

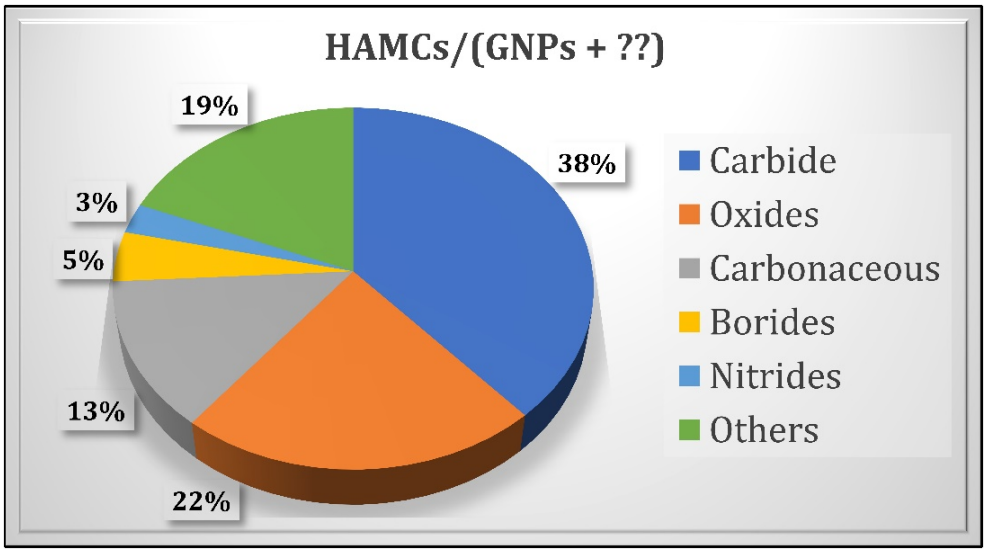

Figure 2. Distribution of the secondary reinforcements in HAMCs considering GNPs as the primary reinforcement.

The processing route plays a critical role in governing the microstructure, reinforcement distribution, and final properties of AMCs and HAMCs. Broadly, MMC fabrication techniques can be classified into liquid-state processing, solid-state processing, and gas- and vapour-phase techniques [15]. Liquid-state processing methods, particularly stir casting and compocasting, are widely adopted due to their simplicity, scalability, and cost-effectiveness. In stir casting, reinforcements are mechanically introduced into molten Aluminum under controlled stirring conditions, followed by solidification to produce the composite, making this technique attractive for industry-scale production [5,16]. Researchers such as Kumar and Singh [17], Kumar et al. [18], and Guan et al. [19] have adopted the compocasting technique to prepare graphene reinforced HAMCs. They have incorporated carbides (e.g., SiC and B_4C)/borides (e.g., ZrB_2) together with graphene into the semi-solid melt of the Al to synthesize HAMCs. Further, liquid-state processing variants such as squeeze casting and ultrasonic-assisted stir casting (UASC) are increasingly deployed to fabricate nano HAMCs [15]. The technique of UASC leverages acoustic cavitation along with localized fluid streams to systematically dismantle high-energy nanoparticle clusters, achieving uniform reinforcement distribution within the liquid melt before solidification [20].

Solid-state processing routes such as powder metallurgy (PM), friction stir processing (FSP), accumulative roll bonding (ARB), etc., have gained increasing attention for processing graphene- and nano-sized carbon-reinforced AMCs. The technique of PM offers better control over reinforcement distribution and minimizes interfacial reactions by avoiding complete melting of the Aluminum matrix, thereby preserving the structural integrity of graphene and other nano-sized reinforcements. The PM route has been widely explored for producing fine-grained and near-net-shape AMCs with improved mechanical and functional properties [15,21]. FSP and ARB, on the other hand, enable to cause severe plastic deformation and considerable grain refinement without melting, resulting in reduced defects, improved dispersion of reinforcements, and enhanced interfacial bonding [22]. Notably, FSP uses localized frictional heat and high-shear mechanical mixing to drive microstructural recrystallization [22], while ARB employs repetitive stacking and roll-bonding deformation cycles to produce highly oriented nanostructural layers [23]. Other processing techniques such as additive manufacturing, e.g., laser powder bed fusion (L-PBF), in-situ synthesis, etc., are emerging processing techniques for synthesizing HAMCs. The L-PBF route utilizes layer-by-layer laser melting paired with rapid cooling rates to engineer unique, crack-free bimodal grain configurations that bypass the solidification cracking limits of conventional alloys [15], while in-situ synthesis adopts a chemical approach, reacting master alloys directly inside the melt to generate pristine, contamination-free secondary ceramic phases like ZrB_2 or TiC [20].

A comparative overview of the commonly reported fabrication methods for the HAMCs is presented in Figure 3, highlighting the relative usage of the processing routes reported in the literature. The figure indicates that stir casting and powder metallurgy remain the most widely adopted fabrication approaches, while advanced techniques such as ultrasonic-assisted casting and FSP are increasingly being explored to improve reinforcement dispersion and interfacial characteristics.

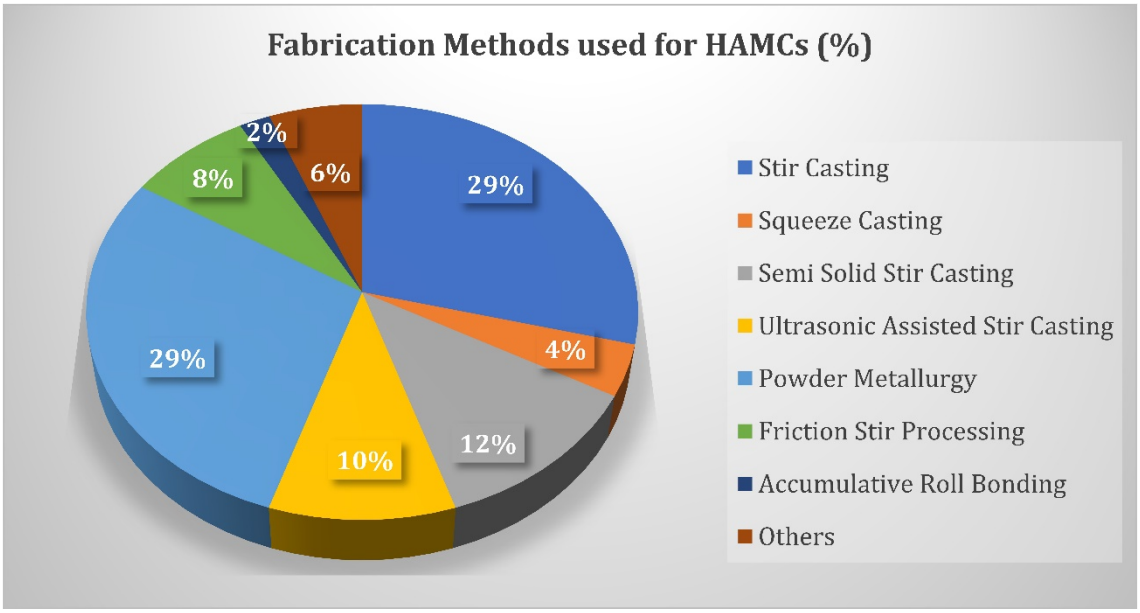

Figure 3. Percent distributions of the fabrication methods employed for manufacturing HAMCs.

This review provides a clear framework to compare various fabrication methods adopted for graphene-based hybrid Aluminum matrix composites (HAMCs). Given the rapid growth of such advanced materials, this work systematically reviews hybrid designs by grouping them into clear reinforcement families of carbide-assisted, oxide-assisted, all-carbonaceous, and sustainable or waste-derived systems together with graphene. By exploring those material combinations, the review article addresses microstructural activities, critical thresholds for nanoparticle dispersion, and mechanical and tribological performances of the HMACs. This review comprehensively addresses the variations in the mechanical and tribological properties of the graphene reinforced hybrid Al matrix composites with respect to their processing routes. Finally, this work outlines current and next-generation engineering applications of the HAMCs while identifying key research gaps in long-term performance evaluation and environmental degradation, and may be considered as a reference for researchers and engineers in designing advanced lightweight structures.

2. GNPs+Carbide Reinforced HAMCs

The increasing demand for advanced lightweight structural materials with enhanced mechanical and tribological performances has accelerated the development of nano HAMCs. In particular, graphene nanoplatelets (GNPs) and their derivatives, including graphene oxide (GO) and reduced graphene oxide (rGO), have been widely combined with carbide-based ceramic reinforcements to exploit complementary strengthening mechanisms. Carbide particles are known for their exceptional hardness, thermal stability, and load-bearing capability, while graphene-based nanomaterials contribute high tensile strength, improved load transfer, and solid lubrication characteristics. This dual-phase configuration creates a highly efficient reinforcement framework that structurally optimizes the strength, wear characteristics, and long-term durability of the composite [24,25]. In this section, 25 recent studies are reviewed and categorized considering carbide as one of the hybrid reinforcements along with graphene in the HAMCs.

2.1. GNPs+SiC Reinforced HAMCs

The integration of GNPs with silicon carbide (SiC) as reinforcements in AMCs is being extensively researched to develop next-generation materials for high-performance engineering sectors such as aerospace, automotive, and defense [26–28]. The studies demonstrated that the synergy between the enhanced hardness and the thermal stability of SiC and the exceptional mechanical strength and the self-lubricating characteristics of GNPs significantly enhanced the physical, mechanical, and tribological properties of monolithic Al alloys [29–31]. Researchers utilized a wide variety of fabrication techniques to ensure uniform dispersion of nano-sized reinforcements, which was identified as the primary challenge in composite manufacturing. Among a variety of processing techniques for composites, stir casting remains a preferred liquid-state method due to its scalability and cost-effectiveness [29,32–39]. To overcome clustering, especially for nano-sized particles, ultrasonic-assisted stir casting was employed, utilizing high-frequency vibrations to break down particle agglomerates in the melt [37,39,40]. In some instances,

electromagnetic stir casting was implemented to provide more vigorous and consistent stirring compared to mechanical methods, resulting in a more homogenous distribution of SiC and GNPs [37]. Parameters for these processes typically involved melting the Al alloy at temperatures mostly between 750 °C and 800 °C, with stirring intensities ranging from 300 to 600 RPM [29,37,41].

Powder metallurgy (PM) routes were frequently chosen for their ability to produce high-density components with refined microstructures. This typically involved ultrasonic liquid processing to disperse GNPs in solvents like acetone, followed by ball milling with SiC and Al powders to achieve encapsulation of the ceramic particles by graphene flakes [42–44]. Specifically, shift-speed ball milling (SSBM), which alternated between low-speed mixing and high-speed refinement, was found to be effective in embedding GNPs into the Al powder surfaces without damaging the reinforcements [28,45]. Consolidation of these powders was achieved through techniques such as uniaxial vacuum hot pressing or spark plasma sintering (SPS) [43,45,46]. Additionally, microwave hybrid sintering was explored as an innovative densification method, utilizing the high microwave absorption capacity of SiC to facilitate rapid, bidirectional heating, which reduced porosity and improved interfacial bonding [42,43]. Friction stir processing (FSP) was also highlighted as a solid-state surface modification technique. By inducing severe plastic deformation through a rotating tool, FSP not only refined the Al grain structure but also facilitated in-situ exfoliation of graphite into few-layer graphene [28,47,48]. Hybrid manufacturing approaches were also documented, such as combining the powder semi-solid processing (PSSP) with the FSP to enhance the distribution of SiC nano-rods grown on GNPs [26]. To further improve the compatibility between graphene and Al, surface-engineered hybrid reinforcements have also been investigated. One such strategy involves coating GNPs with SiC particles to enhance interfacial bonding, as illustrated in Figure 4.

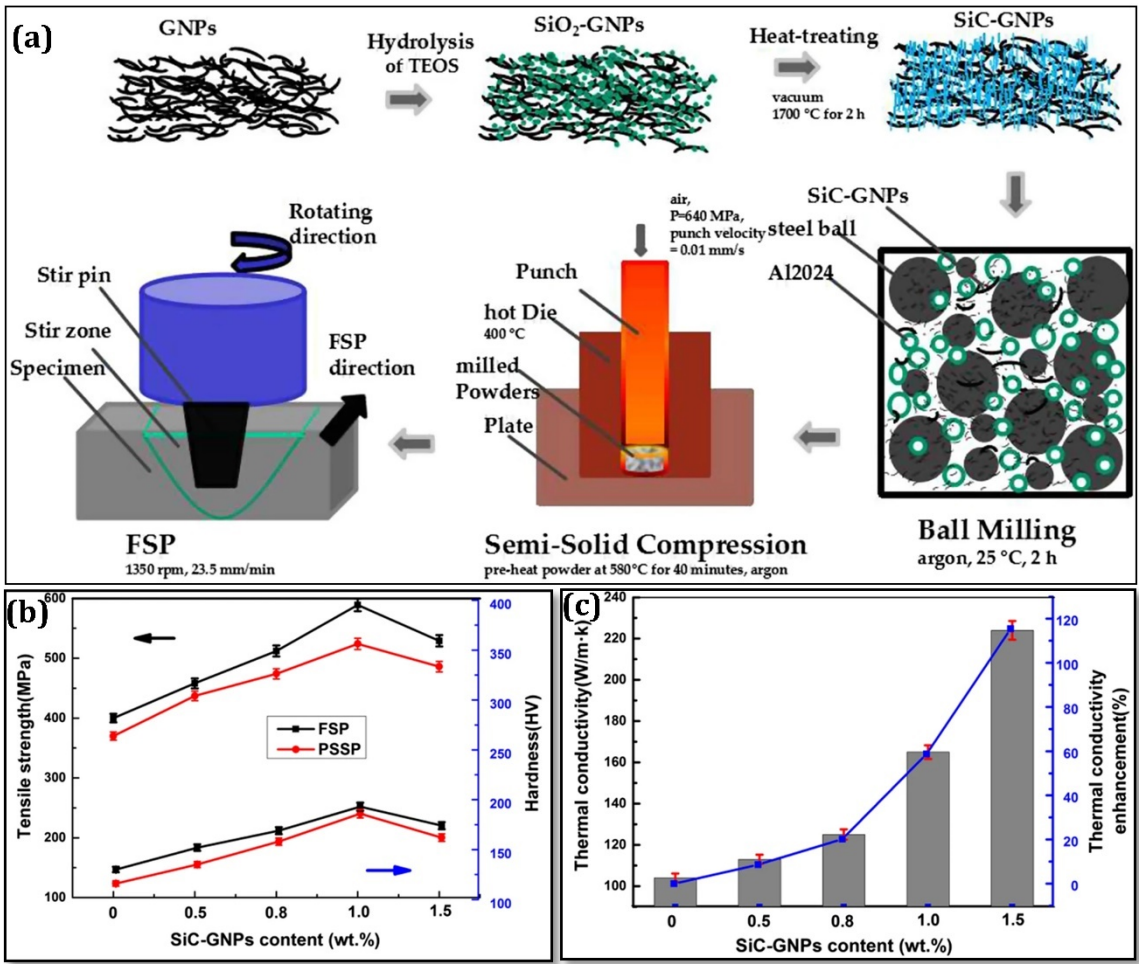

Figure 4. Processing scheme and thermo-mechanical behavior of Al2024 alloy matrix reinforced with SiC-coated GNPs: (**a**) hybrid synthesis and consolidation through PSSP and FSP; (**b**) tensile strength and hardness versus reinforcement content; (**c**) thermal conductivity enhancement. Adapted with permission from ref. [26]. Copyright 2021, Springer Nature.

Microstructural characterization was standard across the journal articles published to validate the successful fabrication of the composites. Scanning electron microscopy (SEM) and energy-dispersive X-ray spectroscopy

(EDS) were the primary tools employed to observe the morphology and spatial distribution of SiC particles and GNPs flakes inside the matrix [27,31,42]. High-resolution transmission electron microscopy (TEM) allowed for the detailed inspection of interfaces between the reinforcements and the matrix, revealing the presence of nanostructured bonding layers [27,45]. X-ray diffraction (XRD) was utilized to identify the phases present and to detect unwanted reactions, such as oxidation. While some studies reported no detectable Aluminum carbide (Al_4C_3) formation due to lower processing temperatures or microwave effects [42,43], others identified Al_4C_3 peaks, noting its role in improving interfacial load transfer when it existed in controlled amounts [28,48]. A typical processing-property correlation of GNPs+SiC reinforced HAMCs fabricated through ball milling followed by FSP is illustrated in Figure 5, where improved tensile properties and reduced friction coefficient are achieved due to the combined strengthening and lubrication effects of the reinforcements.

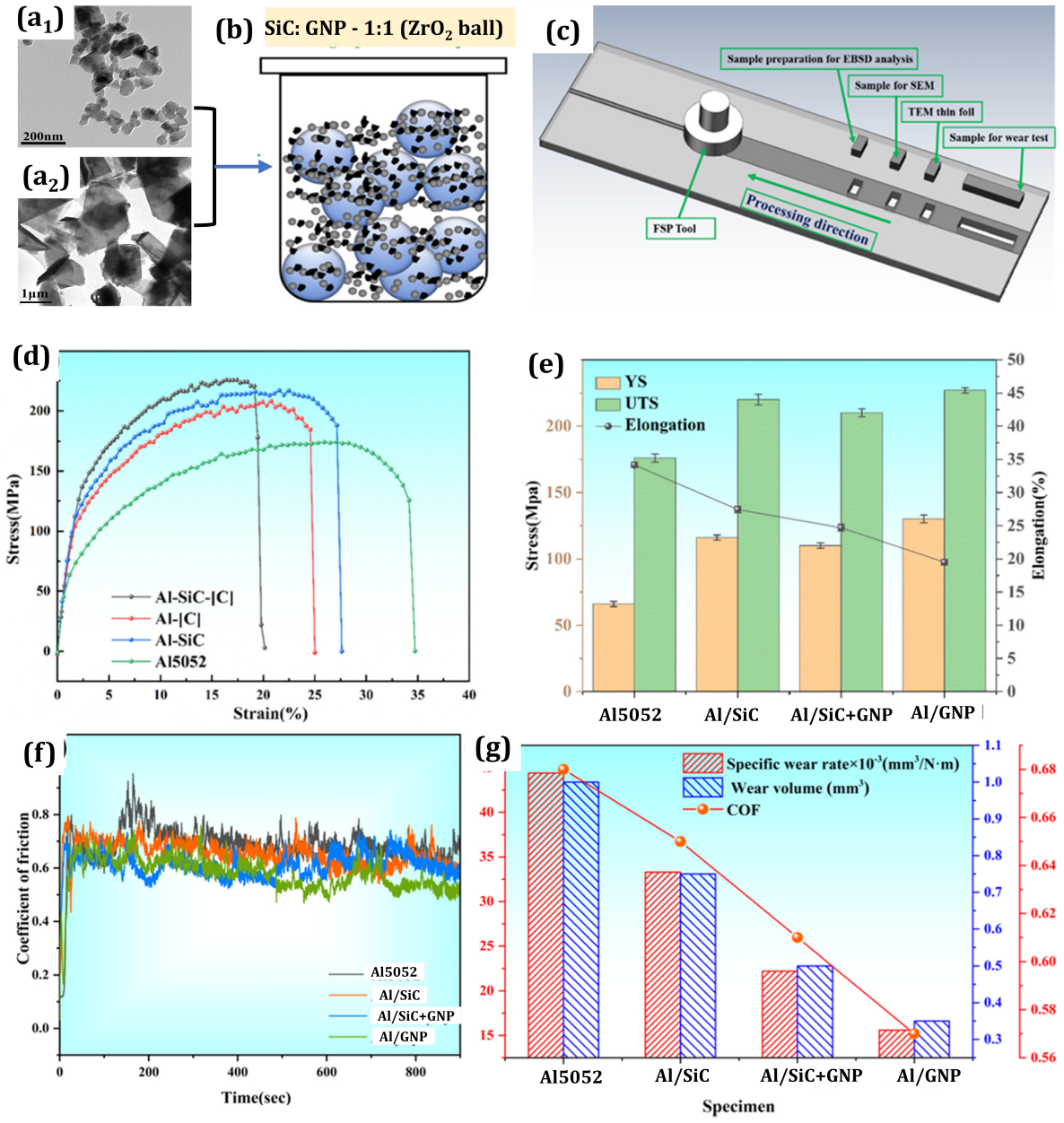

Figure 5. Processing route and mechanical-tribological performances of Al5052/(GNPs+SiC) hybrid composites: (**a**$_1$,**a**$_2$) micrographs of SiC particles and GNPs; (**b**) schematic of ball milling (SiC:GNPs = 1:1, ZrO_2 balls); (**c**) friction stir processing setup and specimen extraction; (**d**,**e**) stress–strain curves and comparison of YS, UTS, and elongation; (**f**,**g**) coefficient of friction and wear behavior. Adapted with permission from ref. [48]. Copyright 2026, Elsevier.

Raman spectroscopy served as a vital technique for assessing the structural integrity of graphene [43,44,48]. Furthermore, atomic force microscopy (AFM) was used to evaluate surface topographies, providing a quantitative measure for surface quality of specimens [43]. It was obvious that the hybrid reinforcement approach consistently

yielded superior mechanical performance compared to monolithic Al metal/alloys. Hardness values of HAMCs measured via Vickers or Rockwell scales, showed significant increases compared to Al alloys. For example, an AA5457 alloy reinforced together with 6% SiC and 6% GNPs showed a 57% increase in Brinell hardness [30], while other studies reported hardness of HAMCs reaching up to 128 HV through stir casting optimization [17,31]. This enhancement was attributed to the high hardness of SiC and the grain refinement induced by the reinforcements, which acted as barriers to dislocation motion [32]. Tensile strength also improved substantially.

Vishnoi et al. [31] employed a stir-casting set-up to mix the reinforcing elements of SiC, graphene, and fly ash into the AA6063 alloy. The alloy was first heated in a graphite crucible, and then the preheated reinforcing elements were added in two phases (50:50) in the alloy through a mechanical stirrer at 650 rpm. Results indicated a 119% increase in ultimate tensile strength (UTS) with a 4 wt.% graphene addition together with SiC (10 wt.%) and fly ash (2 wt.%) in AA6063 matrix [31]. Chen et al. [26] adopted the hydrolysis steps involved in the fabrication of SiO_2-decorated GNPs. The SiC-GNPs powders were obtained through heat-treating of SiO_2-GNPs in a vacuum furnace at 1700 °C for 2 h. The acquired SiC-GNPs powders were then mixed with Al2024 powder by different weight ratios and ball milled for 2 h with stainless steel balls. The powder mixture was heated to 580 °C for 40 min in the semisolid range of Al2024 in a furnace (argon atmosphere), with a liquid fraction of 17.8%, then compressed in a hot mold (mold temperature of 400 °C, pressure of 640 MPa, punch velocity of 0.01 mm s^{-1}). This study reported a UTS of 589 MPa for a hybrid combination of GNPs+SiC of 1 wt.% in Al2024 matrix [26].

Researchers identified several strengthening mechanisms, including Orowan looping, Hall-Petch grain refinement, and thermal mismatch strengthening due to the different coefficients of thermal expansion between the Al and the reinforcing elements [20,45,48,49]. The mechanical enhancement in graphene-based hybrid Aluminum matrix composites relies on the simultaneous activation of multiple microstructural strengthening mechanisms, namely load transfer ($\Delta\sigma_{LT}$), Orowan looping ($\Delta\sigma_{OR}$), Hall-Petch grain refinement ($\Delta\sigma_{HP}$), and thermal mismatch dislocation foresting ($\Delta\sigma_{CTE}$) [12]. A critical cross-examination of the literature revealed that the dominance of these mechanisms was strictly partitioned by the hybrid filler system configuration and processing route. In oxide- and carbide-assisted systems (e.g., GNPs+Al_2O_3 or GNPs+B_4C), load transfer and thermal mismatch typically prevailed due to the large elastic modulus mismatch and high thermal expansion variance between the rigid ceramic particles and the Al matrix, frequently accounting for over 45% of the total quantified strength increment [18,50]. Conversely, in all-carbonaceous networks (GNPs+CNTs), Orowan looping and Hall-Petch grain boundary pinning became the dominant contributors due to the ultra-fine grain refinement induced by the interlocking multi-dimensional carbon network in the HAMCs [51].

Nonetheless, deep conflicts existed between the mathematical modeling studies regarding the synergistic or competitive nature of those mechanisms. While classical analytical frameworks utilized a simple linear summation $\Delta\sigma_{total} = \Delta\sigma_{LT} + \Delta\sigma_{OR} + \Delta\sigma_{HP} + \Delta\sigma_{CTE}$, recent micro-mechanical evaluations reveal that this approach frequently overestimates empirical yields. Conflicts arise because high thermal dislocation densities ($\Delta\sigma_{CTE}$) often restrict the mobility of dislocations required to trigger effective Orowan looping ($\Delta\sigma_{OR}$), making the mechanisms mutually competitive rather than additive [12]. For a comprehensive breakdown of the complex mathematical models, explicit root-sum-square modifications, and structured state-of-the-art modelling equations, the foundational reviews by Sharma et al. [20] and Liu et al. [3] may be referred to.

Excessive reinforcement content, typically beyond 1.0–2.0 wt.% for GNPs or 15–20% for SiC, often led to agglomeration and increased porosity, thus facilitating crack initiation and reduced elongation [17,28,31,45]. Notably, heat treatments at elevated temperatures (e.g., at 600 °C) were shown to optimize the intra-granular nano-phase distribution, helping to balance strength and plasticity by promoting controlled Al_4C_3 formation at the interfaces [45]. Impact toughness and flexural strength were also evaluated for HAMCs, demonstrating higher energy absorption and bending capacity [29,31,43]. For instance, adding 4% graphene to an Al6063/(SiC+fly) ash system enhanced impact strength by 75.7% and flexural strength by 98.8% [31]. The presence of SiC and fly ash improved stiffness, while GNPs inhibited crack propagation through mechanisms like crack bridging and deflection [31,43]. Tribological investigations using pin-on-disk testers revealed that the hybrid composites possessed remarkable wear resistance properties and lower coefficients of friction (COF) [17,27,43,48]. Notably, SiC particles served as hard load-bearing elements that resisted abrasive wear, while GNPs acted as a solid lubricant. During sliding, GNPs were smeared onto the worn surface, forming a carbon-rich tribo-layer, thus preventing direct metal-to-metal contact and reducing frictional forces [37,43,48]. Experimental results indicated that rising sliding speed often diminished COF due to the faster formation of that protective film, whereas enhancing normal load initially increased wear loss until an optimal lubrication state was reached [17]. The machinability of MMCs was also a matter of concern as their increased hardness imposed challenges for traditional

cutting tools. Studies related to machining of HAMCs adopted design of experiments (DOE) techniques such as Taguchi's L_{27} orthogonal array and response surface methodology (RSM), followed by multi-objective optimization techniques like grey relational analysis (GRA), particle swarm optimization (PSO), genetic algorithm (GA), etc., to identify optimal cutting parameters [17,30,37]. Advanced machine learning (ML) models, including artificial neural networks (ANN), random forests and decision trees, deep learning (e.g., VGG 16/VGG 19), etc., were successfully trained to predict tool wear, surface roughness, dimensional accuracies, kerf width, and material removal rates of machined HAMCs [30,35,41]. Those models demonstrated that optimizing machining parameters and reinforcement content could significantly improve surface integrity and tool life during machining of HAMCs [30,41,52–54]. The influence of the reinforcement content on mechanical and tribological performances is demonstrated in Figure 6, indicating microstructural and property evolution of AA5457/(GNPs+SiC) hybrid composites.

Composite System	Hardness (BHN)	Yield Strength (MPa)	Tensile Strength (MPa)	Impact Strength (Jcm^{-2})	Specific Wear Rate ($mm^3N^{-1}m^{-1}$)	Coefficient of Friction
AA5457	65	160	230	12	0.023	0.53
AA5457/(2SiC+2GNPs)	78	185	270	15	0.018	0.51
AA5457/(4SiC+4GNPs)	89	200	290	18	0.016	0.49
AA5457/(6SiC+6GNPs)	102	215	310	21	0.014	0.47

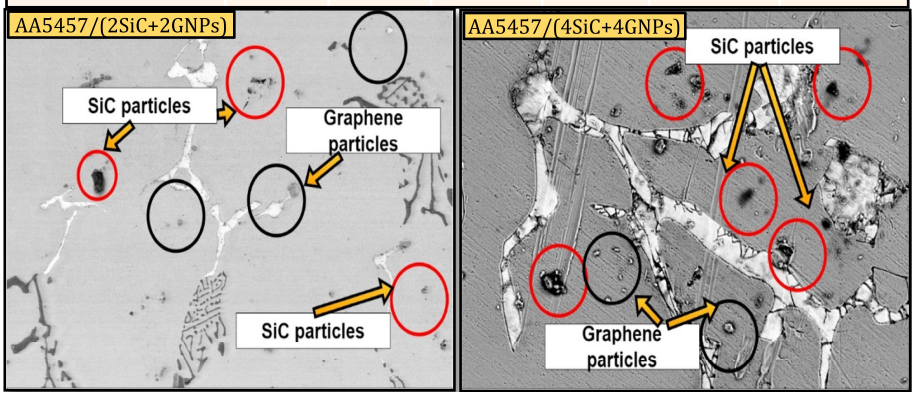

Figure 6. Mechanical, tribological, and microstructural characteristics of AA5457/(GNPs+SiC) hybrid composites showing (**top**) hardness, tensile, impact, and wear properties versus reinforcement content and (**bottom**) SEM micrographs illustrating dispersion of SiC particles and GNPs. Adapted with permission from ref. [30]. Copyright 2025, Elsevier.

In summary, the collective research demonstrated that the hybrid combination of SiC and GNPs effectively overcame the limitations of individual reinforcing elements. The processing route, whether liquid-state/solid-state, happened to be the most critical factor in determining the final composite properties through dispersion of reinforcements and their bonding with the matrix [26,28,42]. While the addition of SiC and GNPs provided substantial gains in hardness, strength, and wear resistance, maintaining a balance of the two to prevent agglomeration was essential to retain ductility [17,31]. Adoption of advanced optimization techniques and machine learning algorithms further validated HAMCs' readiness for complex industrial applications by providing strategies for efficient machining and performance prediction [17,30,37,41]. To compare the effects of the geometries of the reinforcements, Ajithkumar and Xavior [55] have fabricated AA7075/SiC hybrids with 0.1 wt.% additions of graphene, CNTs, and B_4C via squeeze casting. The study has revealed that graphene provided superior strengthening (324 MPa) compared to CNTs (308 MPa) and B_4C (239 MPa). This may be attributed to the planar 2D geometry of graphene, which offered more effective grain refinement and load transfer than the 1D tubular structure of CNTs at equivalent low loadings.

2.2. GNPs+B_4C Reinforced HAMCs

The research and development of HAMCs with graphene nanoplatelets (GNPs) and boron carbide (B_4C) as reinforcements were conducted to produce advanced materials for aerospace, automotive, and defense sectors [18,56,57]. Those hybrid systems were sought to explore high hardness and low density of B_4C particles alongside the superior mechanical strength and self-lubricating nature of GNPs to overcome the performance limitations of monolithic Al alloys such as AA6061, AA7075, and AA2024 [18,58–60]. Researchers dispersed various weight percentages of GNPs in solvents like acetone or ethanol using probe sonication to prevent clustering

before adding Al and B_4C powders [56]. It was typically followed by planetary ball milling with process control agents like stearic acid to embed reinforcements into the Al powder surfaces [56]. Consolidation of those powders was achieved through techniques such as uniaxial vacuum hot pressing, SPS, hot isostatic pressing (HIP), and microwave sintering, which significantly improved densification and reduced porosity [56,61].

One study successfully utilized a semi-powder route in which GNPs were uniformly coated onto B_4C particle surfaces before the gas-pressure infiltration of a molten Al-Si alloy into the reinforcement preform [58]. The overall fabrication strategies adopted for those Al/(GNPs+B_4C) HAMCs are illustrated in Figure 7, highlighting both liquid-state infiltration and solid-state powder metallurgy consolidation routes.

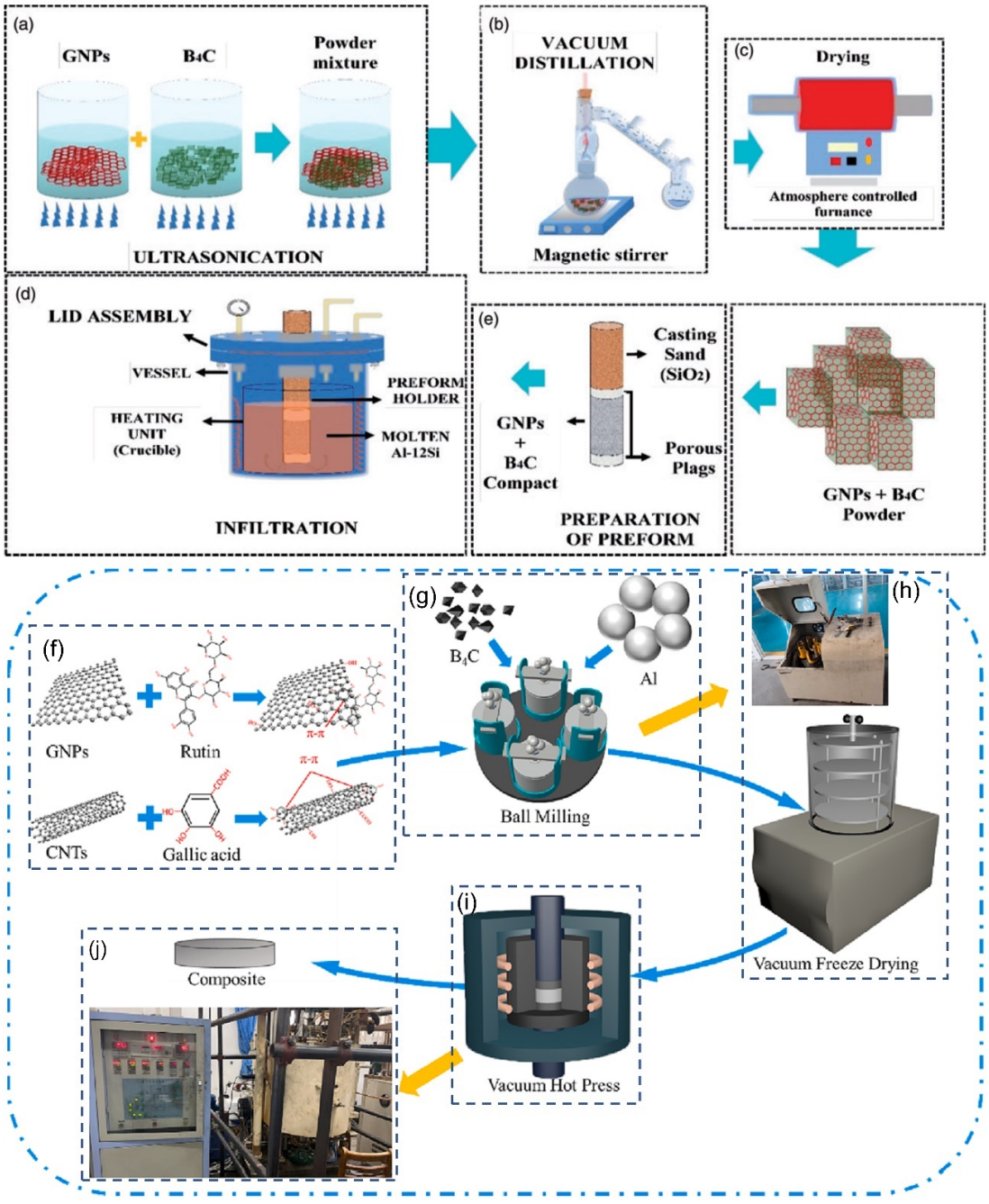

Figure 7. Processing routes for Al/(GNPs+B_4C) hybrid composites: (**a**–**e**) ultrasonic assisted powder mixing, preform preparation, and melt infiltration. Adapted with permission from ref. [58]. Copyright 2019, SAGE; (**f**–**j**) functionalization, ball milling, freeze drying, and vacuum hot-pressing consolidation steps. Adapted with permission from ref. [62]. Copyright 2023, Elsevier.

Figure 7 represents two processing strategies for producing hybrid Al/(GNPs+B_4C) composites. The first approach in Figure 7a–e involved ultrasonic-assisted dispersion of GNPs and B_4C particles followed by preform fabrication and melt infiltration using molten Al-Si alloy. The second route (Figure 7f–j) employed chemical

functionalization of GNPs and CNTs to improve interfacial compatibility, followed by ball milling with Al and B_4C powders, freeze-drying to prevent agglomeration, and final densification through vacuum hot pressing. These complementary routes demonstrated the importance of dispersion control, surface modification, and pressure-assisted consolidation in achieving homogeneous reinforcement distribution and improved interfacial bonding in the HAMCs [58].

The addition of GNPs (with CNTs as co-reinforcement) significantly enhanced the mechanical performances of Al/30%B_4C composites fabricated via ball milling and hot pressing [62]. The B_4C particles were uniformly distributed with strong interfacial bonding facilitated by in-situ formation of AlB_2 and Al_3BC phases. The optimized hybrid composition (0.25% GNPs+0.75% CNTs) achieved a ~46% increase in compressive strength compared to Al/30%B_4C, attributed to improved load transfer along with Orowan, dislocation, and grain refinement strengthening mechanisms [62]**.** As discussed previously, stir casting has remained a widely utilized liquid-state processing method due to its cost-effectiveness and scalability for industrial applications [18,57,59,61,63,64]. In those processing routes, Al alloy was melted at temperatures ranging from 750 °C to 800 °C, and reinforcements often preheated to remove moisture were introduced into the melt via a vortex created by a rotating impeller [18,59,60]. Some studies implemented ultrasonic-assisted stir casting technique to break down agglomerates of nanoparticles and two-stage stir casting to enhance wettability [57,59].

Post fabrication treatments, particularly T6 and T651 tempering, were frequently applied to optimize the secondary phase precipitates and to refine the grain structure [60,61]. Microstructural characterizations were essential to confirm the successful integration of the dual reinforcements. SEM and EDS were the standard tools employed to observe the distribution of GNPs and B_4C and to identify potential defects like porosity or discontinuities at the interfaces [18,56,58,59]. Microstructural characterizations showed GNPs adhered to the Al particles after milling and were dispersed uniformly within the matrix after casting, though agglomeration was noted when reinforcement content exceeded optimal limits (typically >0.6–1.0 wt.% for GNPs and >10–15 wt.% for B_4C) [18,56–58]. TEM provided high-resolution insights into grain boundary precipitation and interfacial bonding, revealing the presence of nanostructured layers between the reinforcements and the matrix [59]. XRD was used to identify phases and confirm the rhombohedral structure of B_4C and the crystalline integrity of graphene [18,56,58]. Furthermore, Raman spectroscopy was critical in evaluating the structural quality of the graphene, with the intensity ratios of D, G, and 2D bands used to assess defect density and exfoliation levels [58]. Thermal analyses using differential scanning calorimetry (DSC) and thermal gravimetric analysis (TGA/DTA) helped in determining the oxidation behavior and the thermal stability of the HAMCs, which were found to significantly improve compared to the base alloys [58,59]. The combined incorporation of B_4C and GNPs consistently drove substantial mechanical improvements. For example, adding 1.2 wt.% GNPs to an Al6061/B_4C system raised the hardness by 225% (i.e., from 28 HRB to 91 HRB) [56]. The fabrication procedure of the composite system was based on the PM technique discussed at the start of this section. Compressive strength was reported to increase by up to 145% after HIP treatment in reference to the base alloy (110 MPa), eliminating internal voids and improving interfacial load transfer [56]. Another study on Al6061 reported a significant increase in hardness of 52% with the addition of 6 wt.% B_4C and 0.5 wt.% GNPs compared to their base alloy [60]. Those enhancements were primarily attributed to the presence of the hard-ceramic phase and the Hall-Petch grain refinement induced by the dual reinforcements [56,57]. Tensile and compressive strengths of the HAMCs also showed marked improvements. One study achieved a maximum UTS of 214.95 MPa in an Al2024 hybrid composite with 0.75 wt.% GNPs and 10 wt.% B_4C [18].

However, a strength-ductility trade-off has often been observed. While initial additions of GNPs and B_4C increased strength, excessive amounts (beyond 0.2–0.75 wt.% for GNPs) led to agglomeration and wettability issues, which diminished UTS and elongation [18,56,57,60]. Heat treatment and tempering played a vital role in mitigating those effects; the combination of solution treatment, cold rolling, and artificial ageing (T651) was found to be the most effective temper condition, resulting in fully recrystallized grain structures and the formation of intermetallic secondary phases like Mg_2Si and AlB_2, which further bolstered the composite's mechanical integrity [60,61]. Additionally, impact toughness and flexural strength were shown to increase by up to 75% and 98%, respectively, with optimal graphene levels, as the GNPs acted as crack bridges and deflector agents [57,59]. The HAMCs demonstrated superior wear resistance and lower COF in dry sliding conditions to the unreinforced base alloys [56,57,59]. B_4C acted as a hard load-bearing phase that resisted abrasive action, while GNPs served as a solid lubricant. During sliding, the GNPs were smeared onto the worn surface, forming a carbon-rich tribo-layer that prevented direct metal-to-metal contact and reduced wear loss by up to 45% [56,61]. The specific wear rates of the HAMCs were found to diminish with increased sliding distance and the addition of graphene up to a certain limit [57,59]. The fracture behavior and strengthening mechanisms associated with those HAMCs are illustrated in Figure 8, providing fractographic evidence of the reinforcement interactions during deformation.

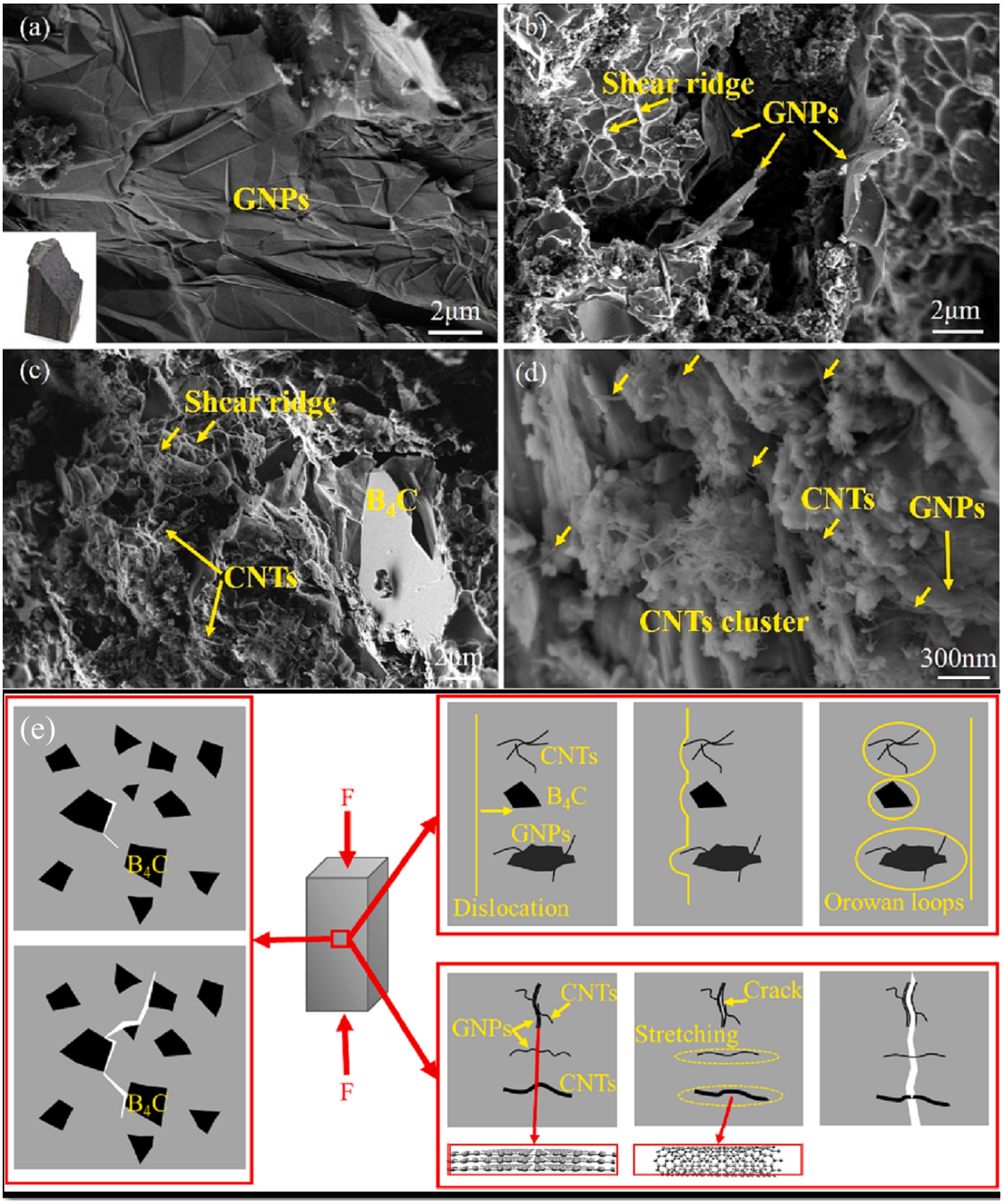

Figure 8. Fractography and strengthening mechanisms of Al-30%B_4C/(0.25GNPs+0.75CNTs) hybrid composites: (**a**–**d**) SEM images showing reinforcement dispersion, shear ridges, and CNT clustering; (**e**) schematic illustration of dislocation pinning, Orowan looping, and crack-bridging mechanisms. All are in wt.%. Adapted with permission from ref. [62]. Copyright 2023, Elsevier.

Figure 8 reveals characteristic fractographic features observed in the HAMCs reinforced with B_4C, GNPs, and CNTs. The SEM micrographs exhibit shear ridges, embedded graphene sheets, CNT networks, and localized reinforcement clusters, indicating active load transfer and plastic deformation during fracture. Notably, B_4C particles primarily contributed to load-bearing and crack deflection, while nano-carbon reinforcements promoted crack bridging and pull-out mechanisms that enhanced fracture resistance. The schematic representation further illustrates the combined strengthening mechanisms, including dislocation pinning, Orowan looping around rigid particles, and crack arrest through nano-reinforcement networks, which collectively improved the strength and toughness of the HAMCs.

Electrochemical behavior was also evaluated, with findings indicating that while B_4C alone could increase the corrosion rate, the addition of graphene often shifted the free corrosion potential to more positive values, thereby lowering the corrosion rate in certain environments, such as boric acid [56,58,61]. However, the effect was sensitive to the medium; for instance, corrosion rates increased with graphene addition in NaCl solutions but

reduced in boric acid [56]. In summary, the integration of GNPs and B_4C reinforcements through PM or stir casting proved highly effective in creating high-performance HAMCs. The combination of high-density ceramic particles and nano-carbonaceous flakes significantly improved the hardness, tensile and compressive strength, and wear resistance of the HAMCs [18,56,59,60]. While processing parameters such as stirring speed, milling time, and consolidation pressure were critical to ensuring uniform dispersion, the post-fabrication heat treatments are equally vital for optimizing the microstructure and balancing the strength-plasticity relationship of the HAMCs [60,61]. Despite the challenges of reinforcement agglomeration at larger concentrations, those HAMCs showed exceptional promise for advanced structural applications, satisfying the need of light weight and high durability [18,56,57].

2.3. GNPs+Other Carbide Reinforced HAMCs

The synthesis of Al matrix alloys reinforced with GNPs and alternative carbides, specifically tungsten carbide (WC), vanadium carbide (VC), titanium carbide (TiC), etc., was explored to develop materials with enhanced load-bearing capacity and shock resistance for aeronautical and automotive applications [65–69]. Fabrication routes for those HAMCs include both liquid-state and solid-state techniques tailored to the specific carbide reinforcements. The stir casting route was employed for bulk AA2024-based hybrids containing WC and graphene, using a stirring speed of 750 rpm to ensure adequate turbulence for reinforcement dispersion [65]. Ultrasonic-assisted stir casting was used for AA7010/(GNPs+TiC) HAMCs, where high-frequency vibrations helped in mitigating nanoparticle clustering and improving reinforcement distribution [67,68]. For surface modification approaches, FSP was applied to integrate VC and boron nitride (BN) into AA7075, resulting in significant grain refinement due to severe plastic deformation during processing [66]. Notably, a study using a recycled Al431+1050 matrix implemented a combined sintering and forging route, which enabled the incorporation of high TiC contents (up to 20 wt.%) along with secondary reinforcements such as Mo, Cu, and γ-Al_2O_3 fibres [69]. That solid-state approach facilitated the development of a dense composite structure suitable for high-load applications. Microstructural characterizations in those studies primarily relied on scanning electron microscopy (SEM) and energy-dispersive spectroscopy (EDS) to evaluate the dispersion and the homogeneity of the hybrid reinforcements within the Al matrix [65–67,69]. SEM analysis of WC- and TiC-reinforced HAMCs with graphene revealed that the hard carbide nanoparticles contributed to grain refinement and acted as effective barriers to crack propagation during mechanical loading [65,67]. In the recycled Al431+1050 system, microstructural characterizations focused on comparing the structural roles of metallic powders (Mo and Cu) with those of GNPs and alumina fibres to achieve a high-strength composite architecture [69]. In addition, X-ray diffraction (XRD) analyses were commonly adopted to identify the crystalline carbide phases and confirm the structural integrity of GNPs within the Al matrix [67,69]. The influence of hybrid reinforcements on thermal and electrical transport properties of the composites was also investigated.

Figure 9 illustrates the variation in thermal and electrical conductivities of the AA7075-based composites reinforced with GNPs along with BN and VC. The addition of GNPs significantly enhanced the thermal conductivity of the Al matrix due to the intrinsically high thermal conductivity of graphene and the formation of efficient heat-transfer pathways within the composite. Nonetheless, when BN and VC were incorporated alongside GNPs, a gradual decrease in thermal conductivity was observed, though the values remain comparable to or slightly higher than that of the base alloy. That behaviour was primarily attributed to enhanced phonon scattering at the interfaces and the comparatively lower thermal conductivity of the ceramic reinforcements relative to graphene. A similar trend was observed in electrical conductivity, where the AA7075/GNPs composite exhibited relatively greater conductivity owing to the excellent electron transport capability of GNPs [66]. With the addition of BN and VC, the electrical conductivity decreased progressively due to the insulating nature of BN and the augmented number of interfaces that hindered electron mobility. Those results highlighted that although hybrid reinforcement strategies improved mechanical and thermal performances, the incorporation of ceramic phases might moderately reduce electrical conductivity because of enhanced electron scattering and interfacial resistance [66].

The incorporation of alternative carbides along with GNPs consistently resulted in improved mechanical performance compared with monolithic Al alloys. For example, AA2024/(GNPs+WC) hybrid composites demonstrated a significant increase in tensile strength, with the optimal reinforcement content reported at 2 wt.% WC and 0.15 wt.% graphene [65]. Beyond those levels of reinforcement, strength decreased due to graphene agglomeration within the matrix [65]. Similarly, compressive strengths in AA7010/(GNPs+TiC) systems reached approximately 428.33 MPa, where the hard TiC nanoparticles enhanced load transfer and restricted plastic deformation within the matrix [67]. The study on the recycled Al431+1050 composite further revealed that the TiC-reinforced structures exhibited high resistance to both static and dynamic compression loading, making them suitable for aeronautical service conditions requiring shock resistance [69]. Tribological evaluations also indicated significant improvements in wear resistance when carbides were combined with graphene reinforcements.

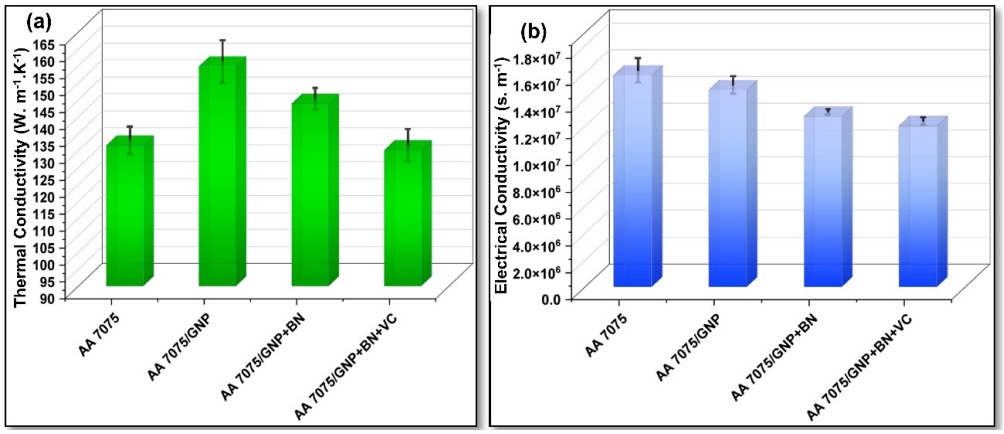

Figure 9. Thermal and electrical conductivity of AA7075-based hybrid composites with graphene nanoplatelets (GNPs), boron nitride (BN), and vanadium carbide (VC): (**a**) thermal conductivity and (**b**) electrical conductivity comparison for AA7075, AA7075/GNPs, AA7075/(GNPs+BN), and AA7075/(GNPs+BN+VC) composites. Adapted from Ref. [66] under the Creative Commons Attribution (CC BY) license.

Figure 10 presents wear rate, coefficient of friction (COF), and worn surface morphology of the Al7075/(GNPs+TiC) HAMCs under varying sliding conditions. The results showed that the wear rate of the base Al7075 alloy decreased substantially with the addition of the reinforcements, reaching a minimum at 1.0 wt.% of TiC. The COF also reduced progressively with increasing TiC content, reflecting the combined effects of the lubricating behaviour of graphene and the load-bearing capability of TiC particles [68]. SEM observations of the worn surfaces revealed distinct differences in wear mechanisms. The base alloy exhibited severe ploughing, deep grooves, and large debris particles, indicating dominant abrasive and adhesive modes of wear. In contrast, the HAMCs showed shallower wear tracks and smaller debris, suggesting improved wear resistance due to the combined action of graphene-induced solid lubrication and TiC-induced hardness enhancement [68]. Nonetheless, at higher TiC contents (≥2 wt.%), localized delamination and debris accumulation became more prominent, causing the slight increase in wear rate beyond the optimum reinforcement level [68].

Composite system	Al7075	Al7075/ (0.25GNPs +0.5TiC)	Al7075/ (0.25GNPs +1.0TiC)	Al7075/ (0.25GNPs +1.5TiC)	Al7075/ (0.25GNPs +2.0TiC)	Al7075/ (0.25GNPs +2.5TiC)
Wear rate (x10^{-4}, mm^3 N^{-1} m^{-1})	6	4	3.85	4.29	4.5	5.00
Coefficient of friction	0.42	0.30	0.32	0.36	0.35	0.29

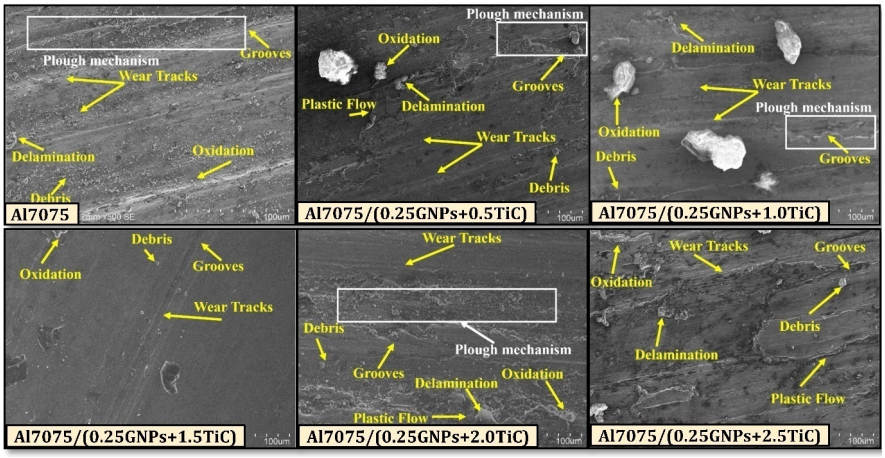

Figure 10. Wear rate, coefficient of friction, and worn surface morphology of Al7075/(GNPs+TiC) hybrid composites under varied sliding wear conditions. Adapted with permission from ref. [68]. Copyright 2024, Springer Nature.

3. GNPs+Oxide Reinforced HAMCs

The engineering demand for lightweight materials with high specific strength has led to the development of HAMCs having nano-sized reinforcing elements. GNPs and their derivatives, such as graphene oxide (GO) and

reduced graphene oxide (rGO), are increasingly paired with ceramic oxide reinforcements to establish a complementary framework, where ceramic oxides provide high stiffness and hardness while carbonaceous nanomaterials offer exceptional strength and solid lubrication properties [70,71]. The current review article has evaluated and categorised published studies into two primary hybrid systems: HAMCs possessing alumina (Al_2O_3) and those utilizing alternative oxides such as zirconia (ZrO_2) [72], Ceria (CeO_2) [73–75], and titania (TiO_2) [76].

3.1. GNPs+Al_2O_3 Reinforced HAMCs

The combination of alumina and graphene is the most established hybrid system, investigated across a variety of Al alloys including AA6061, AA7075, and recycled scrap aluminum [70,77,78]. Researchers utilized a wide spectrum of liquid-state and solid-state processing techniques to overcome the inherent challenges of nanoparticle agglomeration. Fluid metallurgy, specifically stir casting, remained a popular choice for its cost-effectiveness and scalability, though poor wettability often necessitates modifications [70,79–81]. For instance, preheating reinforcements to 400 °C was commonly used to remove moisture and improve integration of the reinforcement into the melt [70]. Notably, ultrasonic-assisted melt-stirring was frequently employed to achieve more uniform dispersion, often combined with ball-milling at pre-processing to break down initial agglomerates [82]. PM techniques allowed for even more precise control over the distribution of nanoparticles, with advanced consolidation via spark plasma sintering (SPS) regarded for its ability to produce denser composites at lower temperatures and faster rates, which limited undesirable interfacial reactions [83,84]. Furthermore, novel chemical approaches emerged, such as the first-ever in-situ synthesis of alumina microparticles and graphene films via the reaction of a salt melt containing yttria and B_4C with molten Al [85]. Another innovative method involved electroless Ag plating of the reinforcements to significantly enhance their wettability and dispersion during mechanical milling and hot compaction [86].

Investigating Al/(GNPs+Al_2O_3) composites fabricated via ARB, Jafarzadeh et al. [87] demonstrated that processing up to five cycles progressively improved reinforcement dispersion and reduced matrix porosity. Consequently, mechanical properties such as tensile strength and microhardness reached their maximum values at the fifth cycle. However, a critical processing trade-off was observed: while mechanical strength peaked at five cycles, optimal corrosion resistance was achieved at the third cycle before deteriorating during subsequent rolling. An example of a combined dispersion strategy involving mechanical mixing and ultrasonic treatment during stir casting is illustrated in Figure 11, outlining the processing route used for fabricating Al6061/(GNPs+Al_2O_3) HAMCs by Soni et al. [82].

The reinforcements were first ball milled for uniform mixing and preheated to improve wettability before incorporation into the molten Al6061 alloy. Mechanical stirring combined with ultrasonic treatment was employed to enhance dispersion, followed by casting into a preheated iron die under controlled conditions. The microstructural characteristics of these HAMCs were primarily defined by the dispersion of the dual reinforcements and the resulting grain modifications. Alumina and graphene were typically found distributed along the grain boundaries of the Al matrix, where they acted as physical barriers [70,83]. Their presence facilitated significant grain refinement by providing heterogeneous nucleation sites and pinning grain boundaries during solidification, a process known as Zener pinning [70,82]. Well-processed samples exhibited barrier-pin-holes where the graphene structure blocked the diffusion of corrosive ions [84]. Nonetheless, higher concentrations of the reinforcements, typically exceeding 10 wt.% for Al_2O_3 or 1 wt.% for GNPs, led to significant clustering of particles [77,83,88]. Such clustering triggered porosity, formed micro-cracks, and created porous interface regions that could trap air and degrade the material's integrity [70,84]. The microstructural refinement and the fracture behavior associated with increasing reinforcement content in Al6061/(1GNPs+$x$$Al_2O_3$) are illustrated in Figure 12.

Figure 12 illustrates the influence of hybrid reinforcement (1 wt.% GNPs combined with varying Al_2O_3 contents) on the mechanical performance and fracture behavior of Al6061 composites. The results demonstrated a consistent improvement in yield strength (YS), ultimate tensile strength (UTS) and hardness with increasing Al_2O_3 content, while ductility decreased. Optical micrographs revealed a transition from relatively coarse grains in the unreinforced alloy to refined and more homogeneous microstructures in the hybrid composites. The SEM fractography confirmed that trend, showing shallow dimples in the base alloy associated with ductile fracture, whereas reinforced composites displayed embedded Al_2O_3 particles, graphene sheets and evidence of graphene pull-out. At higher reinforcement levels, reduced dimple depth and interfacial debonding indicated a shift toward mixed ductile-brittle fracture behavior. The mechanical and functional findings for Al/(GNPs+Al_2O_3) hybrids consistently showed substantial improvements over monolithic alloys. Significant enhancements in Vickers hardness, YS, and UTS were reported across the literature. For example, adding 15 wt.% Al_2O_3 and 1 wt.% GNPs to Al6061 could increase hardness by 69% [70]. In-situ synthesized hybrids demonstrated a unique combination

of doubled hardness and strength alongside a threefold increase in relative elongation [85]. Tribologically, graphene served as an exceptional solid lubricant, forming a carbon-rich tribo-layer that reduced the COF and mass loss during sliding, effectively filling porosities and voids [86,88]. The improvement in wear resistance and frictional behavior with increasing graphene nanosheet content is shown in Figure 13, which compares wear rates and COF under varied applied loads.

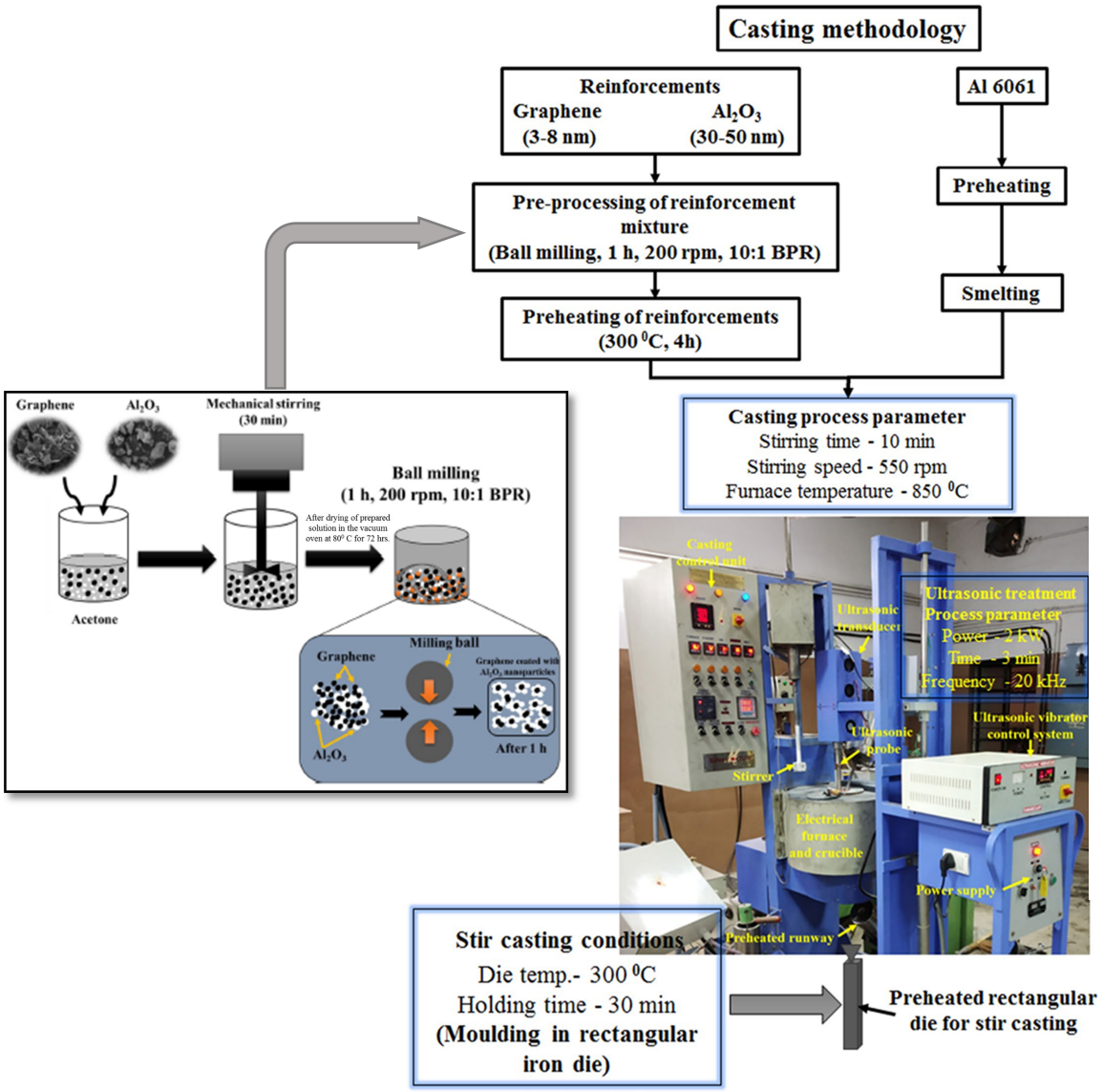

Figure 11. Stir casting methodology for fabrication of Al6061/(GNPs+Al_2O_3) hybrid composites showing reinforcement characteristics, ball milling pre-processing (200 rpm, 1 h, 10:1 BPR), reinforcement preheating (300 °C, 4 h), mechanical stirring (550 rpm, 10 min), ultrasonic treatment (2 kW, 20 kHz, 3 min), and casting into a preheated rectangular iron die. Adapted with permission from ref. [82]. Copyright 2022, Springer Nature.

Figure 13 demonstrates that the incorporation of graphene nanosheets significantly reduces wear rate and COF. The graphene-free composite exhibited severe abrasive wear characterized by deep grooves and particle pull-out, whereas graphene-reinforced HAMCs showed smoother surfaces and retained graphene layers that act as protective solid-lubricant films. Hybridization also impacted thermal and electrochemical properties; HAMCs often demonstrated lower coefficients of thermal expansion and higher thermal conductivities compared to pure Al [83]. Electrochemically, the honeycomb structure of GO-reinforced MMCs could block the diffusion of chloride and sulphate ions, significantly reducing corrosion rates [84]. However, that benefit was often lost in hybrid systems where poor Al_2O_3 wettability created porous interfaces that served as sites for aggressive pitting [84]. Corrosion behaviors of the Al composites reinforced with Al_2O_3 and GO in different environments are illustrated in Figure 14.

Composite system	Yield strength (MPa)	Tensile strength (MPa)	Elongation (%)	Hardness (BHN)
Al6061	83	117	11.2	51
Al6061/(1GNPs+5Al_2O_3)	91	128	5.2	58
Al6061/(1GNPs+10Al_2O_3)	108	158	4.6	70
Al6061/(1GNPs+15Al_2O_3)	142	190	4.1	87

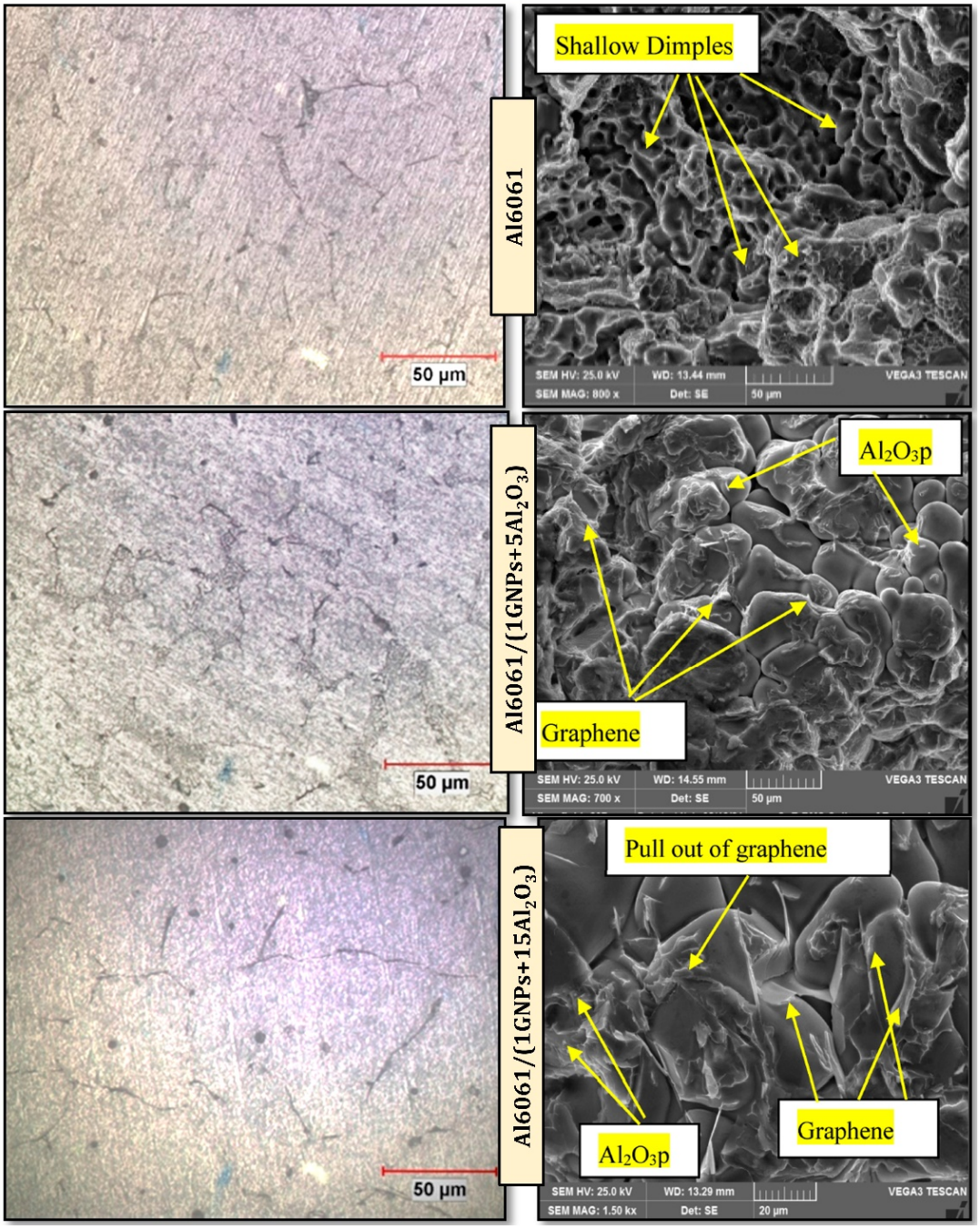

Figure 12. Mechanical properties, microstructure and fractography of Al6061 and Al6061/(1GNPs+xAl_2O_3, x = 5, 10 and 15) hybrid composites: tensile strength, yield strength, elongation and hardness variation with reinforcement content; optical micrographs showing grain refinement; SEM images illustrating shallow dimples in base alloy, graphene dispersion and Al_2O_3 particle reinforcement, and graphene pull-out features at higher ceramic content. All are in wt.%. Adapted from Ref. [70] under the Creative Commons Attribution (CC BY) license.

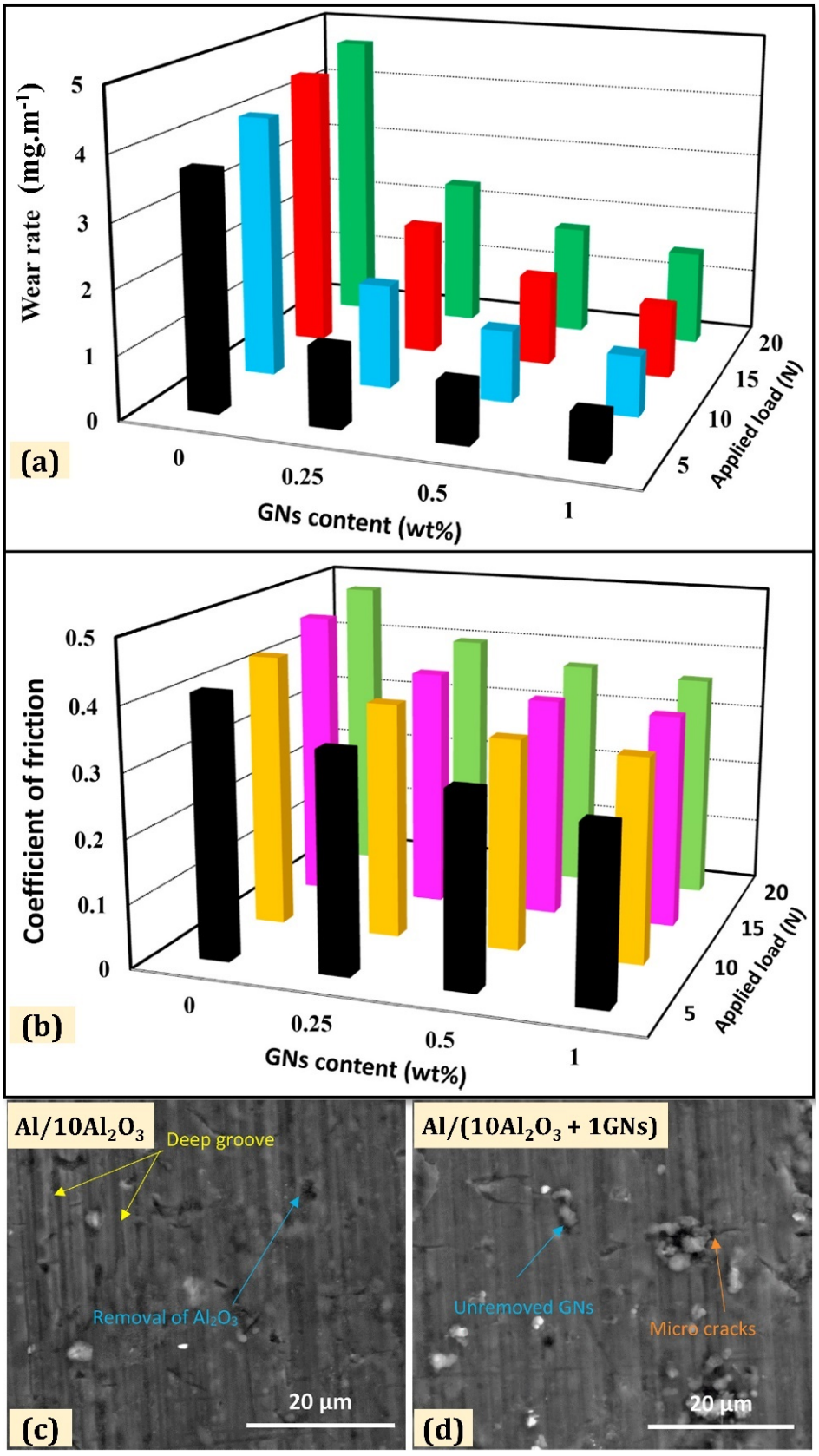

Figure 13. Effect of graphene nanosheets (GNs) content on the tribological performance of Al/10Al_2O_3 composites: (**a**) wear rate variation with applied load and GNs content at a sliding speed of 1 m s^{-1}, (**b**) coefficient of friction variation with applied load and GNs content at sliding speed of 1 m s^{-1}, and (**c**,**d**) SEM images of worn surfaces showing deep grooves and Al_2O_3 particle removal in Al/10Al_2O_3 composite, and presence of unremoved GNs along with micro-crack formation in Al/(10Al_2O_3+1GNs) hybrid composite. All are in wt.%. Adapted with permission from ref. [86]. Copyright 2021, Elsevier.

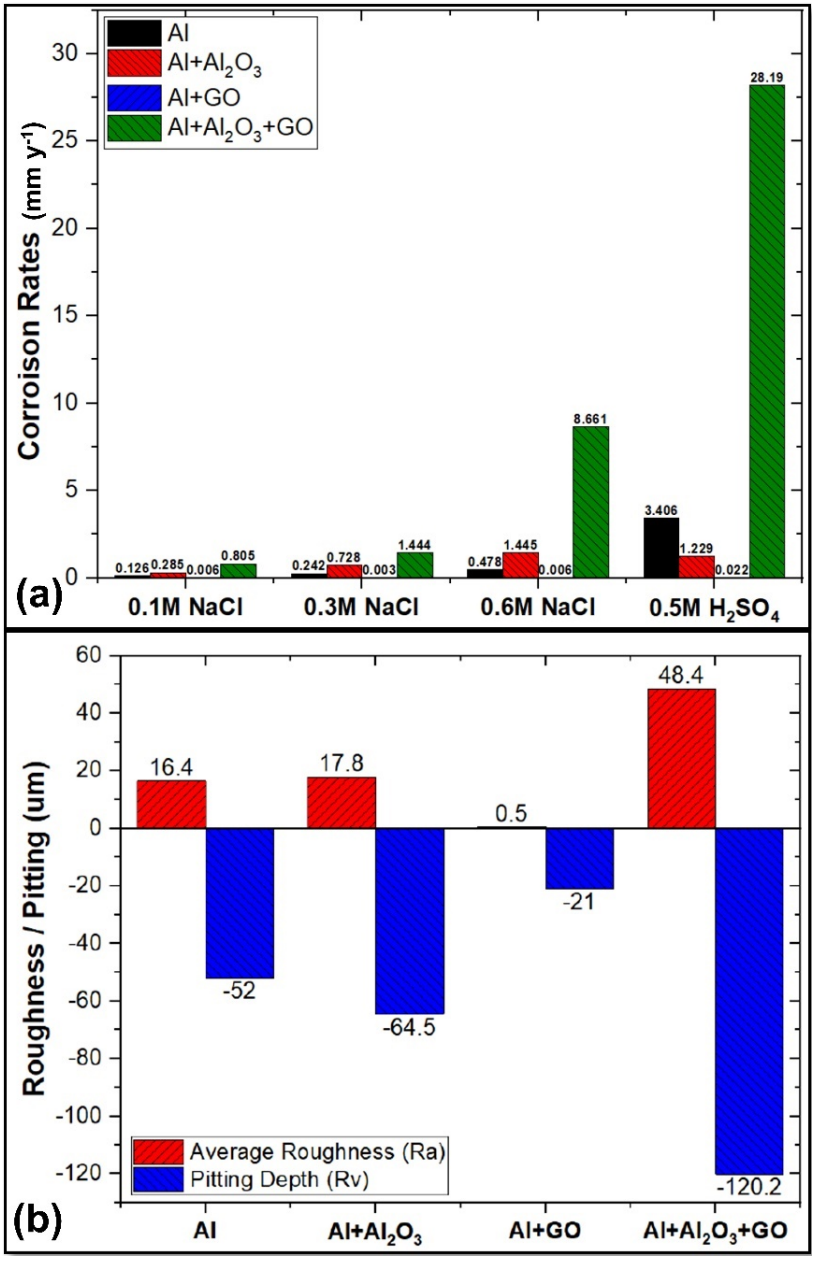

Figure 14. Corrosion and surface degradation behavior of Al-based hybrid composites: (**a**) corrosion rates of Al, Al+Al_2O_3, Al+GO, and Al+Al_2O_3+GO in different media (0.1 M, 0.3 M, 0.6 M NaCl and 0.5 M H_2SO_4), and (**b**) corresponding average surface roughness (Ra) and pitting depth (Rv) after corrosion testing. GO: graphene oxide. Adapted from Ref. [84] under the Creative Commons Attribution (CC BY) license.

Figure 14 shows that corrosion rates increase with rising NaCl concentration and are the highest in acidic environments. While GO reinforcement alone could reduce corrosion in chloride solutions, the hybrid Al/(Al_2O_3+GO) system exhibited higher corrosion rates and deeper pitting due to interfacial heterogeneity and possible galvanic interactions between reinforcing phases. Expanding beyond conventional systems, recent research highlights the development of sustainable HAMCs utilizing recycled matrices and waste-derived reinforcements. For instance, Oraimi et al. [78] utilized stir casting to fabricate HAMCs from scrap Al with Al_2O_3, GO, and waste particles like spent catalysts and seashells as the reinforcements. The study has demonstrated that an optimal 2.5 wt.% reinforcement fraction achieved uniform dispersion and peak mechanical hardness (65 HRB), where the hard particles enhanced load transfer and the GO networks effectively inhibited crack propagation before agglomeration could occur at larger concentrations [78].

3.2. GNPs with Other Oxide Reinforcements

HAMCs using alternative oxides like Zirconia (ZrO_2), Ceria (CeO_2), and Titania (TiO_2) were shown to have unique benefits, particularly in maintaining ductility and improving specialized manufacturing characteristics.

Processing those composites often involved thermo-mechanical and additive manufacturing techniques. ARB was successfully used to create filler rods for TIG welding, achieving uniform distribution of ZrO_2/rGO through eight cycles of bonding [89]. FSP was another effective route, with research suggesting that solvent-based mixing of powders utilizing ethanol and sonication was superior to dry mixing for preventing oxide agglomeration before the FSP passes [73].

A major recent advancement has been the use of laser-powder bed fusion (L-PBF) to create crack-free AA2024 composites [72]. In that process, nanoparticles were adhered to the surface of the base alloy particles to form a composite powder, which was then melted by laser [72]. For TiO_2 and CeO_2-based systems, ultrasonic stir casting remained a standard fabrication method, where reinforcement powders were typically preheated before addition into the molten alloy to improve wettability and dispersion [75]. An example of the stir casting route used for fabricating Al6061/(GNPs+CeO_2) HAMCs is illustrated in Figure 15, outlining the reinforcement preheating, the vortex generation during mechanical stirring, and the casting into molds for solidification.

Figure 15 presents the fabrication methodology, wear performance, and worn surface characteristics of Al6061 HAMCs reinforced with GNPs and CeO_2 particles. The schematic in Figure 15a illustrates the stir casting route, where reinforcement powders were first preheated (~300 °C) and then introduced into molten Al6061 followed by mechanical stirring to generate a vortex and achieve improved particle dispersion before casting into mold. The wear performance of the composites shown in Figure 15b indicated the variation of wear rates of the composite specimens (Z1-Z4) under the applied loads of 15, 30, 45, and 60 N. A general trend of increasing wear rate with enhanced load was observed, while the HAMCs exhibited relatively improved wear resistance compared with the base alloy due to the load-bearing effect and enhanced hardness imparted by the reinforcements. Microstructurally, those alternative oxide systems offered specialized grain structures and reinforcement interactions. In Al/(GNPs+ZrO_2) systems processed through L-PBF, the nanoparticles induced a columnar-to-equiaxed transformation (CET), resulting in a bimodal microstructure consisting of ultra-fine equiaxed grains and coarse columnar grains [72]. That structure was critical for printing Al alloys that were traditionally difficult to weld [72]. Furthermore, ceramic nanoparticles in those systems could act as “nails” on the graphene surface, helping to bridge matrix cracks and enhance load transfer through high-density dislocation accumulation [72]. In CeO_2 and TiO_2 systems, the nanoparticles sat uniformly on graphene layers, retarding grain growth during processing through pinning effects and resulting in highly refined matrix grain structures [73,75]. Similar to GNPs+alumina hybrids, maintaining dispersion remained the primary challenge, as excessive loading (e.g., >3 wt.% CeO_2) caused clustering that deteriorated mechanical performance [75]. The mechanical responses of Al/(GNPs+ZrO_2) HAMCs fabricated via L-PBF are illustrated in Figure 16, comparing the tensile strength and ductility of AA2024 alloy with different reinforcement combinations of the HMACs.

The figure (Figure 16) shows the effect of the hybrid reinforcement (ZrO_2 and GNPs) on the tensile properties of AA2024 alloy. The addition of 1 wt.% ZrO_2 improved tensile strength compared to the base alloy due to particle strengthening and dislocation hindrance. Further, the addition of GNPs enhanced both strength and ductility, with the composite containing 1 wt.% ZrO_2+0.2 wt.% GNPs exhibiting the highest tensile strength and elongation. However, increasing the GNPs content to 0.4 wt.% slightly reduced the mechanical performance, likely due to their agglomeration and inefficient load transfer. The findings for those alternative HAMCs often highlighted a rare synergy between strength and ductility. A breakthrough in Al/(GNPs+ZrO_2) hybrids fabricated by L-PBF was the simultaneous enhancement of both properties, achieving a UTS of 382 MPa with 16% elongation in AA2024, indicating a 77.8% increase in ductility compared with the base alloy [72]. In CeO_2/GNPs systems, a 50/50 volume percentage ratio was identified as the optimum for enhancing both microhardness and tensile strength [73]. For Al/(GNPs+TiO_2) hybrids, a combination of 1 wt.% GNPs and 3 wt.% TiO_2 showed an optimal UTS improvement of 72% [71]. Across all those alternative systems, T6 heat treatments could further improve tensile properties by precipitating secondary phases at cell boundaries [72]. Tribologically, HAMCs containing CeO_2 and TiO_2 exhibited significantly lower wear rates due to the concurrent action of the hard ceramic particles and the compliant graphene phase, which collectively formed a protective tribo-film between the sliding surfaces [75,76]. Additionally, those hybrid reinforcements were shown to improve wire-cut electric discharge machining (WEDM) performances of Al alloys by preventing dislocation movements, which influenced the material removal rate and surface roughness [90].

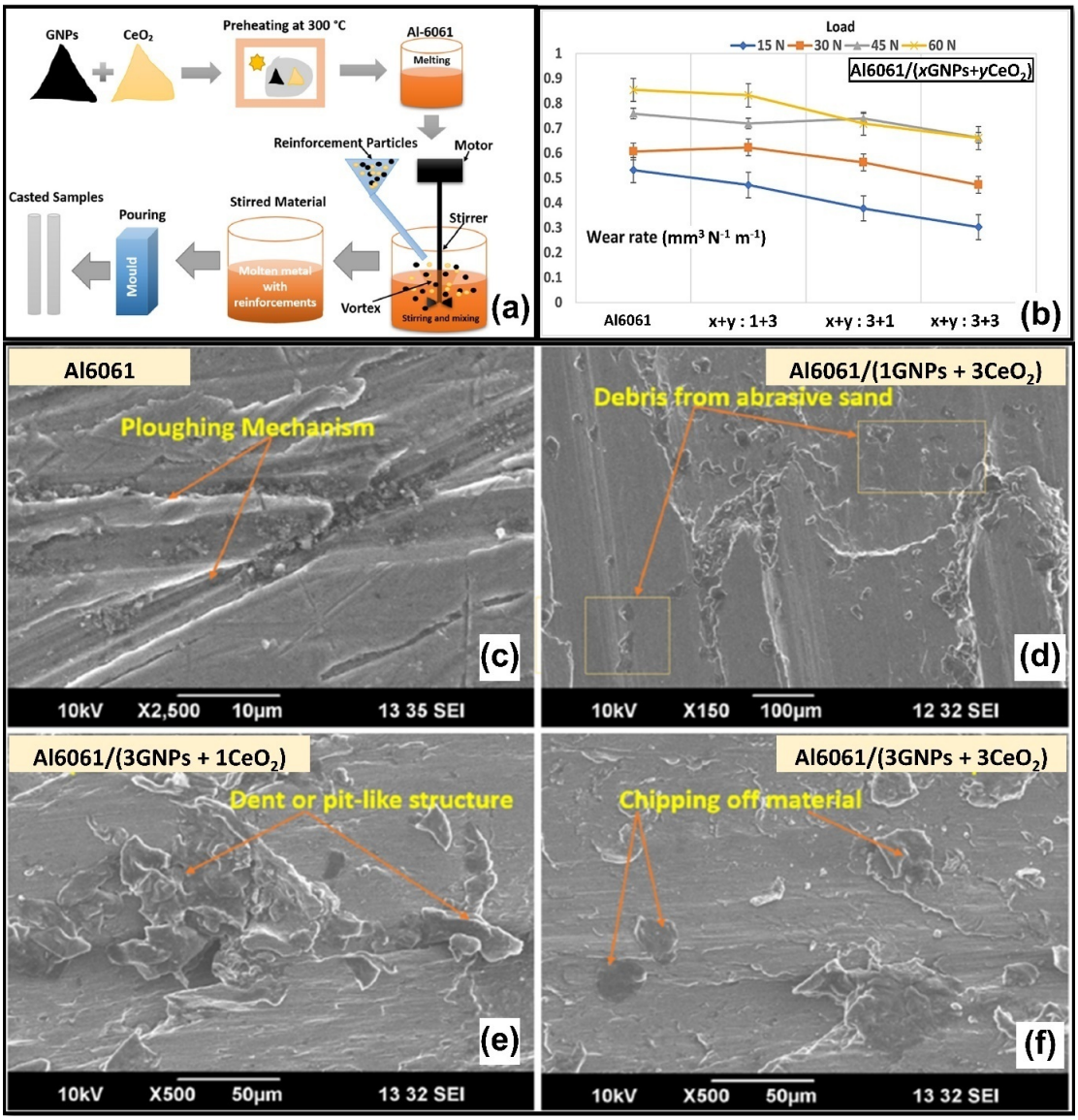

Figure 15. Fabrication process, wear behavior, and worn surface morphology of Al6061/(GNPs+CeO_2) hybrid composites of varying wt.% of GNPs and CeO_2: (**a**) stir casting fabrication route, (**b**) wear rate variation under different loads, and SEM micrographs of worn surfaces showing (**c**) ploughing mechanism in Z1 specimen, (**d**) abrasive debris formation in Z2 specimen, (**e**) pit-like surface damage in Z3 specimen, and (**f**) material chipping in Z4 specimen. Z1: Al6061, Z2: Al6061/(1GNPs+3CeO_2), Z3: Al6061/(3GNPs+1CeO_2), Z4: Al6061/(3GNPs+3CeO_2). All are in wt.%. Adapted with permission from ref. [75]. Copyright 2023, Elsevier.

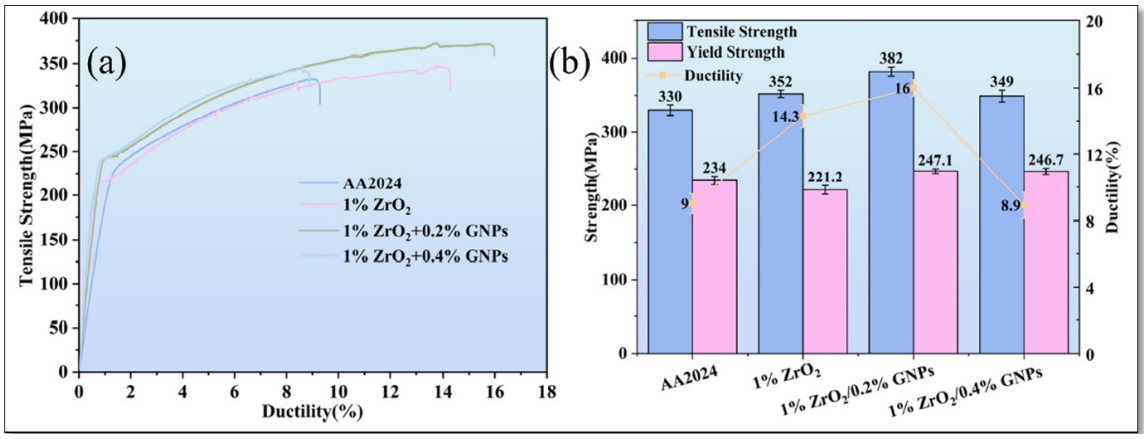

Figure 16. Tensile properties of AA2024 alloy and AA2024/(GNPs+ZrO_2) hybrid composite: (**a**) tensile strength-ductility curves and (**b**) comparison of tensile strength, yield strength, and ductility. All are in wt.%. Adapted with permission from ref. [72]. Copyright 2024, Elsevier.

4. GNPs+Carbonaceous Reinforced HAMCs

The incorporation of carbonaceous reinforcements into Al matrices revolutionized the development of lightweight, high-strength structural materials. While distinct carbon allotropes such as carbon nanotubes (CNTs), graphene nanoplatelets (GNPs), and carbon fibers (CFs) individually offered exceptional specific strength, good thermal conductivity, and self-lubricating properties, their application as single reinforcements was limited owing to the agglomeration and anisotropic behavior. Consequently, the trend shifted toward HAMCs that utilized multiple carbonaceous fillers. The hybridization of 2D planar graphene with 1D tubular CNTs offered a unique bridging effect that prevented the stacking of graphene sheets and inhibited the agglomeration of nanotubes, creating a continuous conductive and reinforcing network. This section reviews recent advances in HAMCs containing GNPs plus CNTs and other carbon derivatives [91,92].

4.1. GNPs+CNTs Reinforced HAMCs

The combination of GNPs and CNTs represents the most investigated carbon-hybrid reinforced composite system. The primary challenge remained the homogeneous dispersion of those nano-scale fillers and the mitigation of deleterious interfacial carbides (Al_4C_3). Research indicated a critical dependence on processing methods to achieve uniform dispersion of GNPs and CNTs. Naik et al. [91] utilized stir casting to fabricate pure Al composites with 1–5 wt.% graphene and 2 wt.% CNTs, finding that, while wettability was challenging, the hybrid successfully shifted the wear mechanism from adhesive to mild abrasive. Similarly, Elshalakany et al. [93] employed squeeze casting to reduce porosity in graphene nano sheets (GNSs)/MWCNTs hybrids, achieving superior densification compared to gravity casting. To further enhance dispersion, Perla et al. [94] and Somayajula et al. [95] applied stir casting with optimized parameters, ensuring minimal agglomeration.

Kumar et al. [96] and Reddy et al. [97] also utilized PM and ball milling strategies; Kumar et al. [96] reported that high-energy ball milling effectively exfoliated graphene layers while embedding CNTs, creating a robust interface. Li et al. [98] and Heydari et al. [99] (using graphene oxide+MWCNTs) further confirmed that the solid-state routes like ARB could align CNTs along the rolling direction, enhancing significantly directional strength. Yang et al. [92] developed an in-situ composite containing Cu-decorated GNSs and CNTs. The Cu coating acted as an intermediate layer, promoting load transfer and preventing Al_4C_3 formation, resulting in excellent tensile strength without sacrificing ductility. Chen et al. [100] introduced a novel unzipping technique, converting CNTs into in-situ graphene nano-ribbons (GNRs), which fostered a controlled nucleation-growth of nano-carbides that could lock the reinforcement in place more effectively than ex-situ addition. Xu et al. [101] also explored in-situ growth within a PM context to tailor the interface for high-temperature stability. Sadeghi et al. [102,103] investigated HAMCs containing reduced graphene oxide (rGO) and CNTs, finding that the removal of oxygen functional groups during processing restored the sp^2 carbon network, leading to greater electrical conductivity and wear resistance compared to only GO-based equivalents.

4.2. GNPs+Other Carbonaceous Reinforced HAMCs

Beyond CNTs, hybridization with micro-scale CFs attempted to bridge the nano-micro length scale. Patil et al. [104] fabricated an AA7076 composite system reinforced with graphene and CFs via motorized stir casting. With just 0.5 wt.% of each, the hybrid composite exhibited a 50% increase in hardness and 42% in tensile strength. That suggested the presence of a dual-reinforcement mechanism: graphene lubricated the grain boundaries while carbon fibers bore the macroscopic load, offering a balanced enhancement in both strength and tribology that single-scale reinforcements could not achieve. The review of Naik et al. [91] through Reddy et al. [97] confirmed that Al/(GNPs+CNTs) hybrids offered a versatile pathway to high-performance AMCs. Liquid processing (stir/squeeze casting) was viable for complex shapes but required ultrasonic or chemical assistance for dispersion of particles [91,93,94]. Solid-state routes (PM/ARB) provided superior microstructural control, critical for aligning CNTs with other reinforcing elements [96,98]. Finally, in-situ methods represented the frontier of interface engineering, turning the chemical reactivity of carbon from a liability into a strengthening asset [92,100].

5. GNPs+Emerging and Sustainable Reinforced HAMCs

5.1. GNPs+Metal Reinforced HAMCs

The hybridization of graphene with metallic nanoparticles was primarily aimed at enhancing thermal and electrical conductivities while maintaining ductility properties often compromised by ceramic reinforcements.

Kumar et al. [105] manufactured Al6061 matrix composites reinforced with GNPs and separate nanoparticles of nickel (Ni) and chromium (Cr) via stir casting. The study has established that while Ni and Cr additions

improved hardness and self-lubricating properties, their contribution to thermal conductivity was non-linear. In fact, excessive metallic additions led to phonon scattering at the multiple interfaces, reducing the overall thermal efficiency of the HAMCs.

Pu et al. [106,107] explored the sintering and in-situ formation of Al/(GNPs+Cu) composites. They found that the metallic Cu phase facilitated liquid phase sintering, significantly improving densification [106]. In another study, Pu et al. [107] demonstrated that in-situ reaction control could tailor the interface behavior to minimize electron scattering, maintaining high electrical conductivity. Saxena and Bongale [108] also investigated performances of the HAMCs for Cu additions, reinforcing the trend that ductile metal phases could mitigate the embrittlement often seen in ceramic-reinforced AMCs. Additionally, Puchy et al. [46] investigated the concurrent effect of Ag nanoparticles in Al/(GNPs+SiC) systems produced via SPS. Electrical testing showed that Ag nanoparticles formed conductive bridges between the graphene sheets and the matrix, significantly reducing electrical contact resistance. In liquid metallurgy processing of hybrid aluminum matrix composites, magnesium (Mg) is widely utilized by researchers as a proactive wetting agent. Its incorporation significantly lowers the surface tension of the molten aluminum pool during processing operations like stir casting, which fundamentally enhances matrix-to-reinforcement wettability and ensures a highly uniform spatial dispersion of secondary phases such as GNPs and Al_2O_3 [79].

Gatamorta et al. [69] utilized molybdenum (Mo) alongside TiC and Al_2O_3, finding that the refractory metal improved the high-temperature stability of the HAMCs. Lingaraju et al. [68] investigated TiC additions where the metallic Ti precursor played a crucial role in the in-situ formation of the carbide phase. By acting as an interfacial bridge, the metallic nanoparticles could prevent the severe interfacial degradation often seen in bare Al/GNPs systems. For instance, Yang et al. [21] developed a novel hybrid reinforcement utilizing nickel nanoparticles (Ni NPs@GNS) together with graphene nanosheets (GNS) via an in-situ synthesis. During sintering, this metal-anchored design successfully established a continuous, covalently bonded Al-Al_3Ni-Ni-GNS interlocking structure.

The macroscopic benefits of this engineered metallic interface are vividly illustrated in Figure 17. As depicted in the stress-strain curves and comparative charts (Figure 17a,b), the composite achieved a remarkable strength-ductility balance, effectively bypassing the severe embrittlement typical of standard AMCs. Furthermore, Figure 17c highlights the exceptional strengthening efficiency unique to this metal+GNPs hybrid system. The coherently bonded Al_3Ni/Ni metallic nodes acted as nanoscopic anchors that dramatically improved load transfer efficiency to the GNs and induced a tortuous crack propagation path, resulting in superior energy dissipation and matrix toughening [21].

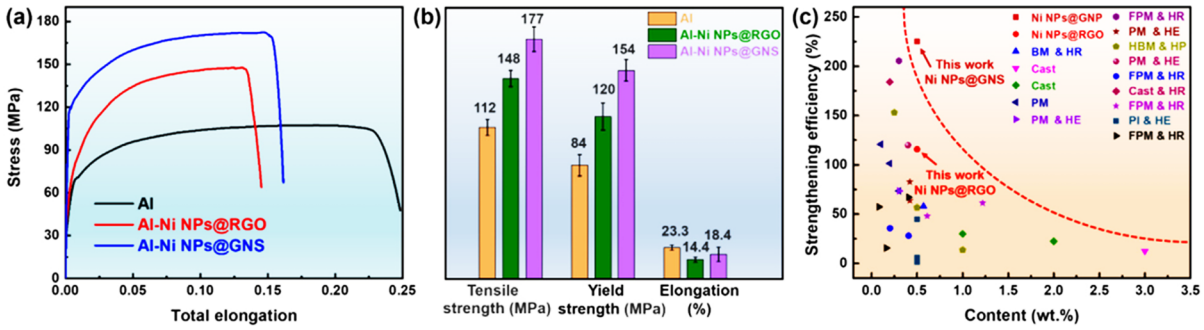

Figure 17. Mechanical properties of Al-based composites reinforced with Ni nanoparticles and graphene derivatives: (**a**) stress–strain curves, (**b**) tensile strength, yield strength, and elongation comparison, and (**c**) strengthening efficiency as a function of reinforcement content. NPs: nanoparticles, GNS: graphene nanosheets, RGO: reduced graphene oxide. Adapted with permission from ref. [21]. Copyright 2021, Elsevier.

5.2. GNPs+Boride/Nitride Reinforced HAMCs

This category of the HAMCs combines the extreme stiffness and hardness of borides/nitrides with the lubrication property of graphene, targeting high-wear applications. Kumar et al. [109] synthesized an Al7075/(GNPs+TiB_2) composite using high-energy ball milling and sintering. FESEM micrographs and EDX mappings revealed that TiB_2 particles pinned grain boundaries, inhibiting growth, while graphene provided lubrication. This dual-reinforcement network resulted in a 71% increase in wear resistance. Rao et al. [110] corroborated those benefits in a corrosion study, reporting that the TiB_2/Graphene network formed a barrier that increased polarization resistance to 2.01×10^{-5} A cm^{-2}. Vishnoi et al. [111] developed a sustainable variant of HAMC by stir casting AA6351 with TiB_2, GNPs, and rice husk ash (RHA). Characterizations confirmed that TiB_2

compensated for the lower strength of the ash, creating a balanced composite that utilized waste materials without sacrificing structural integrity. Guan et al. [19,112–114] developed high-performance AA6111 composites by co-incorporating Cu-coated GNPs and in-situ ZrB_2 nanoparticles via ultrasonic assisted stir casting and hot rolling. By optimizing thermomechanical deformation to induce dynamic recrystallization, that mutually beneficial system bypassed the strength-ductility trade-off, achieving up to 442 MPa UTS with >10% elongation [19,112,113] while the thermally stable in-situ ZrB_2 provided superior high-temperature creep resistance [114]. Complementing those regular strategies, parallel research findings highlighted acoustic processing for microstructural optimization. Guan et al. [115] demonstrated an AA6111/(GNP+ZrB2) HAMC fabricated via in-situ casting, revealing that the co-fillers directly control dislocation initiation, motion, and annihilation to yield a nanolaminated microstructure. This dual-reinforcement network strategy increased the ultimate tensile strength to 455 MPa (a 31.5% improvement over the 346 MPa matrix baseline) while maintaining an impressive 11.6% elongation, a balanced performance validated by strain-hardening rate analysis [115].

Agarwal et al. [116] produced Al/(GNPs+h-BN) hybrids via ball milling and stir casting. Hexagonal boron nitride (h-BN) worked synergistically with GNPs to lower COF, achieving a 31.25% improvement in UTS. Khoshaim et al. [66] employed FSP to incorporate BN and vanadium carbide (VC) into AA7075. The intense plastic deformation broke down agglomerates effectively, reducing grain size by over 10 times. Reddy et al. [117] focused on silicon nitride (Si_3N_4) hybridized with GNPs, where the nitride phase contributed to retaining mechanical strength at elevated temperatures. While nitride reinforcements provided exceptional thermal and mechanical stability, achieving a strong, defect-free interfacial bonding with graphene remained a persistent challenge.

5.3. GNPs+Waste-Derived/Clay-Based Reinforced HAMCs

Patil et al. [118–122] in their studies extensively characterized Al7075 alloy matrix composites reinforced with GNPs and beryl (a mining by-product). In one study**,** they reported that the hybrid combination (i.e., 2 wt.% GNPs+ 6 wt.% beryl) in Al7075 alloy achieved a remarkable 66% increase in UTS as the hard beryl particles bore the macroscopic load while graphene arrested micro-cracks [118]. In another study, they validated the tribological performances of the HAMCs, finding wear rates comparable to SiC-reinforced Al composites [120]. Wadi et al. [123] synthesized the HAMCs using halloysite nanotubes (HNTs)- natural clay nanotubes and GNPs, finding that the hybrid tribo-film in the composites reduced wear rates by 36%. Chaurasia et al. [124] utilized marble dust (MD) paired with GNPs in a stir-cast Al alloy; while marble dust reduced density, graphene was necessary to restore toughness, achieving a 57% improvement in microhardness. Bawaneh et al. [125] utilized bentonite nano clay with graphene in Al6061 alloy, finding it to be a cost-effective reinforcement for stiffness with anti-microbial properties. Kumar et al. [126] investigated the hybridization of GNPs with R-glass fibers in Al2024 alloy, finding that the fibers provided a bridging mechanism that significantly improved impact toughness. Ahmed et al. [127] investigated the combined reinforcing effect of GNPs and locally sourced clay particles in an AA6061 alloy processed via the PM route. The study demonstrated that the solid-state processing route effectively preserved the structural integrity of the reinforcements, where the addition of clay improved microhardness and wear resistance by hindering dislocation motion, while the graphene phase reduced porosity and the COF.

6. Comparative Assessments of the HAMCs

A comparative evaluation of the reviewed graphene-reinforced HAMCs reveals that while the type of secondary reinforcement significantly influences performance metrics, the overarching improvements are driven by a universal structural synergy. Across all configurations, the harder secondary phases (such as carbides, oxides, or waste derivatives) establish a high macro-hardness ceiling and bear primary structural loads, while the primary graphene phase simultaneously mitigates localized stress concentrations and provides in-situ solid lubrication via protective tribo-film formation. Within this synergistic framework, carbide-assisted systems maximize load transfer and dislocation pinning, oxide-assisted systems optimize interfacial stability and ductility retention, and dual-carbonaceous networks maximize toughness through interconnected elastic boundaries. Ultimately, the efficiency of these multi-phase interactions is dictated by the processing route whether liquid-state ultrasonic casting or solid-state powder metallurgy which governs reinforcement dispersion and prevents the local agglomeration defects that disrupt this collective strengthening behavior.

6.1. Assessment of the Mechanical Properties of the HAMCs

The mechanical integrity of HAMCs is a function of reinforcement synergy and the efficacy of the processing route. Processing strategies range from cost-effective liquid-state casting to advanced solid-state and additive

manufacturing techniques, each impacting the microstructure and resultant properties differently. Table 1 presents the mechanical properties of the graphene reinforced HAMCs together with their processing techniques.

Moreover, Figure 18 also presents the variations in the mechanical properties of the graphene reinforced HAMCs along with their synthesizing routes in the form of bar charts. Stir casting and its variants remain the most economical routes for HAMCs. Conventional stir casting often struggles with reinforcement agglomeration and poor wettability [59,118]. To address this, UASC uses high-frequency vibrations to break clusters and ensure uniform dispersion [67,82]. For instance, Al6061-based hybrids processed via UASC and ball milling achieved a 171.70% improvement in UTS, justified by the enhanced interfacial bonding and grain refinement [82]. Similarly, AA7010 reinforced with TiC and graphene via UASC reached a hardness of 170 HV, attributed to low porosity and strong mechanical interfacing between the matrix and the reinforcement [67].

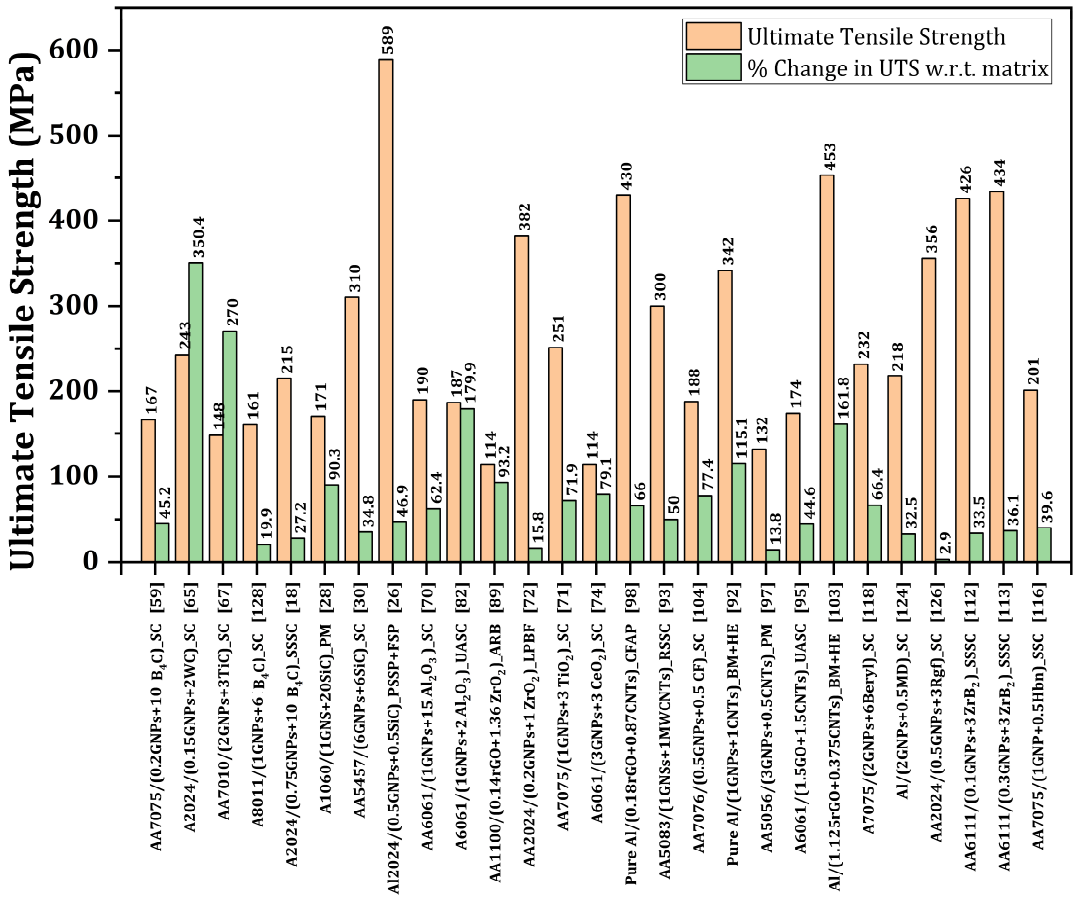

Figure 18. Comparison of ultimate tensile strength (UTS) and percentage change relative to the unreinforced matrix for various graphene-reinforced HAMC systems. (ARB: Accumulative roll bonding; BM: Ball milling; FSP: Friction stir processing; HE: Hot extrusion; LPBF: Laser powder bed fusion; MD: Marble dust; PM: Powder metallurgy; PSSP: Powder semi solid processing; Rgf: R-glass fiber; RSSC: Rheo squeeze stir casting; SC: Stir casting; SSC: Squeeze stir casting; SSSC: Semi solid stir casting or compocasting; UASC: Ultrasonic assisted stir casting.).

Table 1. Comparison of mechanical properties of graphene reinforced hybrid Al matrix composites.

Sl. No.	Composite System (wt.%)	Manufacturing Method	Hardness	YS (MPa)	UTS (MPa)	Elog. (%)	CS (MPa)	FS (MPa)	IS (J or J mm^{-2})	Ref.
1	AA7075	Stir casting	67 HV	--	115	--	--	136	--	[59]
	AA7075/(5B_4C)		69 HV	--	133	--	--	143	--	
	AA7075/(10B_4C)		71 HV	--	149	--	--	153	1.5 J	
	AA7075/(15B_4C)		75 HV	--	172	--	--	161	--	
	AA7075/(0.1GNPs+10B_4C)		75 HV	--	159	--	--	195	2 J	
	AA7075/(0.2GNPs+10B_4C)		78 HV	--	167	--	--	260	3.5 J	
	AA7075/(0.3GNPs+10B_4C)		74 HV	--	165	--	--	243	2.8 J	
2	AA2024	Stir casting	117 HV	--	53.9	4.43	332.19	--	2.8 J	[65]
	AA2024/(0.15GNPs)		122.1 HV	--	47.2	3.03	383.40	--	3 J	
	AA2024/(0.3GNPs)		113.6 HV	--	96.4	3.80	389.98	--	2 J	
	AA2024/(0.15GNPs+1WC)		123.3 HV	--	156.7	3.13	381.57	--	4.5 J	
	AA2024/(0.3GNPs+1WC)		113.4 HV	--	229.9	3.58	384.67	--	8.5 J	
	AA2024/(0.15GNPs+2WC)		122.3 HV	--	242.8	3.77	398.05	--	1.5 J	
	AA2024/(0.3GNPs+2WC)		112 HV	--	184.2	4.61	362.06	--	4 J	
	AA2024/(0.15GNPs+3WC)		105.6 HV	--	101.6	4.33	375.29	--	2 J	
	AA2024/(0.3GNPs+3WC)		113 HV	--	89.1	4.47	359.14	--	1.8 J	
3	AA7010	Stir casting	106 HV	--	40	--	200	--	--	[67]
	AA7010/(1GNPs+2TiC)		135 HV	--	48	--	200	--	--	
	AA7010/(1.5GNPs+2.5TiC)		142 HV	--	52	--	360	--	--	
	AA7010/(2GNPs+3TiC)		170 HV	--	148	--	430	--	--	
	AA7010/(2.5GNPs+3.5TiC)		155 HV	--	136	--	370	--	--	
4	AA6061/(6GNPs+4SiC)	Semi solid stir casting or compocasting	102 HV	--	214	--	--	--	--	[17]
	AA6061/(4GNPs+6SiC)		116 HV	--	237	--	--	--	--	
	AA6061/(6GNPs+6SiC)		128 HV	--	253	--	--	--	--	
5	AA8011	Stir casting	47 HV	--	134.56	40.17	--	--	--	[128]
	AA8011/(1GNPs+3B_4C)		56 HV	--	154.46	26.7	--	--	--	
	AA8011/(1GNPs+6B_4C)		64 HV	--	161.32	22.7				
	AA8011/(1GNPs+9B_4C)		63 HV	--	159.11	24.03	--	--	--	
6	AA2024	Semi solid stir casting or compocasting	64.6 BHN	--	169.02	29.99	--	--	--	[18]
	AA2024/(10B_4C)		90.22 BHN	--	185.59	18.71	--	--	--	
	AA2024/(0.25GNPs+10B_4C)		91.03 BHN	--	186.28	17.03	--	--	--	
	AA2024/(0.5GNPs+10B_4C)		104.07 BHN	--	201.22	16.75	--	--	--	
	AA2024/(0.75GNPs+10B_4C)		109.86 BHN	--	214.95	16.12	--	--	--	
	AA2024/(1GNPs+10B_4C)		107.57 BHN	--	184.55	14.42	--	--	--	
7	AA1060	Powder metallurgy	30 HV	60.0	90.0	42.0	--	--	--	[28]
	AA1060/(0.5GNSs)		48.9 HV	71.1	121.0	48.8	--	--	--	
	AA1060/(1GNSs)		59.7 HV	71.2	121.1	55.6	--	--	--	
	AA1060/(2GNSs)		61.6 HV	67.4	117.3	41.1	--	--	--	
	AA1060/(1GNSs+20SiC)		67.8 HV	42.4	171.3	50.8	--	--	--	

Table 1. *Cont.*

Sl. No.	Composite System (wt.%)	Manufacturing Method	Hardness	YS (MPa)	UTS (MPa)	Elog. (%)	CS (MPa)	FS (MPa)	IS (J or J mm^{-2})	Ref.
8	AA5457	Stir casting	65 BHN	160	230	--	--	--	0.12 J mm^{-2}	[30]
	AA5457/(2GNPs+2SiC)		78 BHN	185	270	--	--	--	0.15 J mm^{-2}	
	AA5457/(4GNPs+4SiC)		89 BHN	200	290	--	--	--	0.18 J mm^{-2}	
	AA5457/(6GNPs+6SiC)		102 BHN	215	310	--	--	--	0.21 J mm^{-2}	
9	AA6061/(0.5GNPs+6B_4C)	Powder metallurgy (Fabricated)	78.3 HV	--	162.6	--	--	--	--	[60]
	AA6061/(0.5GNPs+6B_4C)	PM+T6	91.2 HV	--	195	--	--	--	--	
	AA6061/(0.5GNPs+6B_4C)	PM+T651	96.7 HV	--	205	--	--	--	--	
10	Al2024	Powder semi solid processing + Friction stir processing	129.5 HV		401					[26]
	Al2024/(0.25GNPs+0.25SiC)		151.1 HV		457					
	Al2024/(0.4GNPs+0.4SiC)		167.9 HV		510					
	Al2024/(0.5GNPs+0.5SiC)		192.6 HV		589					
	Al2024/(0.75GNPs+0.75SiC)		173.7 HV		529					
11	AA6063/(10SiC+2FA)	Stir casting	63.5 HV		82.3			168.4	3.7 J	[31]
	AA6063/(2GNPs+10SiC+2FA)		67.4 HV		126.7			224.2	5.4 J	
	AA6063/(4GNPs+10SiC+2FA)		81.1 HV		180.3			334.8	6.5 J	
	AA6063/(6GNPs+10SiC+2FA)		76.8 HV		142.6			261.6	5.9 J	
12	AA6061	Stir casting	51 BHN	83	117	11.2	--	--	--	[70]
	AA6061/(1GNPs+5Al_2O_3)		58 BHN	91	128	5.2	--	--	--	
	AA6061/(1GNPs+10Al_2O_3)		70 BHN	108	158	4.6	--	--	--	
	AA6061/(1GNPs+15Al_2O_3)		87 BHN	142	190	4.1	--	--	--	
13	AA6061	Ultrasonic assisted stir casting	68.6 HV	--	66.7	--	321.3	270.7	--	[82]
	AA6061/(2Al_2O_3)		76.7 HV	--	154.7	--	436	310.7	--	
	AA6061/(2GNPs)		85.7 HV		166.7		472	310.7		
	AA6061/(0.5GNPs+2Al_2O_3)		89.9 HV	--	173.3	--	594.7	336.0	--	
	AA6061/(1GNPs+2Al_2O_3)		92.7 HV	--	186.7	--	665.3	373.3	--	
	AA6061/(1.5GNPs+2Al_2O_3)		88.3 HV	--	144.0	--	585.3	320.0	--	
	AA6061/(2GNPs+2Al_2O_3)		82.2 HV	--	126.7	--	553.3	316.0	--	
	AA6061/(2.5GNPs+2Al_2O_3)		89.7 HV	--	150.7	--	597.3	336.0	--	
14	AA2024	Laser powder bed fusion		234.0	330	9.0	--	--	--	[72]
	AA2024/(1ZrO_2)			221.2	352	14.3	--	--	--	
	AA2024/(0.2GNPs+1ZrO_2)			247.1	382	16.0	--	--	--	
	AA2024/(0.4GNPs+1ZrO_2)			246.7	349	8.9	--	--	--	
15	AA1100	Accumulative roll bonding	51 HV	28	59	18	--	--	--	[89]
	AA1100/(0.1rGO)			41	69	9	--	--	--	
	AA1100/(1 ZrO_2)			45	77	11	--	--	--	
	AA1100/(0.05rGO+0.45ZrO_2)		66 HV	50	82	15	--	--	--	
	AA1100/(0.09rGO+0.91ZrO_2)		92 HV	76	103	14	--	--	--	
	AA1100/(0.14rGO+1.36ZrO_2)		113 HV	91	114	8	--	--	--	

Table 1. *Cont.*

Sl. No.	Composite System (wt.%)	Manufacturing Method	Hardness	YS (MPa)	UTS (MPa)	Elog. (%)	CS (MPa)	FS (MPa)	IS (J or J mm^{-2})	Ref.
16	AA7075	Stir casting	60 HV	--	146	8.5	--	--	8.5 J	[71]
	AA7075/(0.5GNPs+1TiO_2)		89 HV	--	219	7.3	--	--	13.5 J	
	AA7075/(0.5GNPs+3TiO_2)		91 HV	--	225	7.1	--	--	12.5 J	
	AA7075/(1GNPs+1TiO_2)		107 HV	--	240	6.4	--	--	10.5 J	
	AA7075/(1GNPs+3TiO_2)		112 HV	--	251	6.2	--	--	11.5 J	
	AA7075/(2GNPs+1TiO_2)		102 HV	--	242	6	--	--	10.5 J	
	AA7075/(2GNPs+3TiO_2)		84 HV	--	210	5.8	--	--	7 J	
17	AA6061	Stir casting	74 HV	52.62	63.48	1.2	--	178	8 J	[74]
	AA6061/(1GNPs+3CeO_2)		96 HV	56.96	72.14	2.16	--	222	10 J	
	AA6061/(3GNPs+3CeO_2)		112 HV	73.08	113.67	3.13	--	262	13 J	
	AA6061/(3GNPs+1CeO_2)		98 HV	60.75	88.82	2.79	--	238	10.5 J	
18	AA5056	Powder metallurgy	83 HV	105	116	6.4	--	--	--	[97]
	AA5056/(2GNPs+0.5CNTs)		88 HV	116	124	6	--	--	--	
	AA5056/(3GNPs+0.5CNTs)		98 HV	126	132	5.9	--	--	--	
	AA5056/(5GNPs+0.5CNTs)		96 HV	120	130	5.3	--	--	--	
19	Pure Al	Composite flake assembly process	--	205	250	17.3	--	--	--	[98]
	Pure Al/(0.335CNTs)		--	220	275	14.8	--	--	--	
	Pure Al/(0.408rGO)		--	244	300	12.1	--	--	--	
	Pure Al/(0.029rGO+0.143CNTs)		--	271	320	13	--	--	--	
	Pure Al/(1.005CNTs)		--	260	326	12.6	--	--	--	
	Pure Al/(1.226rGO)		--	270	331	5.9	--	--	--	
	Pure Al/(0.088rGO+0.431CNTs)		--	358	415	8.2	--	--	--	
	Pure Al/(2.025CNTs)		--	326	370	4.6	--	--	--	
	Pure Al/(2.47rGO)		--	290	310	2.1	--	--	--	
	Pure Al/(0.177rGO+0.869CNTs)		--	405	430	3.2	--	--	--	
20	AA5083	Rheo-squeeze casting	58 BHN	115	200	12.5	460	--	--	[93]
	AA5083/(0.25GNSs+0.25CNTs)		62 BHN	125	215	7.5	490	--	--	
	AA5083/(0.5GNSs+0.5CNTs)		68 BHN	128	225	7.4	540	--	--	
	AA5083/(0.75GNSs+0.75CNTs)		74 BHN	135	255	6.8	660	--	--	
	AA5083/(1GNSs+1CNTs)		86 BHN	170	300	8	590	--	--	
	AA5083/(1.5GNSs+1.5CNTs)		88 BHN	120	210	5.3	460	--	--	
21	AA7076	Stir Casting	83 BHN	124	106	13.8	--	--	--	[104]
	AA7076/(0.25GNPs+0.25CF)		75 BHN	130	162	11.4	--	--	--	
	AA7076/(0.375GNPs+0.375CF)		103 BHN	138	178	10.2	--	--	--	
	AA7076/(0.5GNPs+0.5CF)		122 BHN	142	188	9.6	--	--	--	
	AA7076/(0.75GNPs+0.75CF)		99 BHN	130	180	9.1	--	--	--	

Table 1. *Cont.*

Sl. No.	Composite System (wt.%)	Manufacturing Method	Hardness	YS (MPa)	UTS (MPa)	Elog. (%)	CS (MPa)	FS (MPa)	IS (J or J mm^{-2})	Ref.
22	AA6061	Ultrasonic assisted stir casting	42 HRB	87.25	120.19	15.24	--	--	6.72 J mm^{-2}	[95]
	AA6061/(0.5GO+2.5CNTs)		58 HRB	99.96	156.08	16.89	--	--	7.45 J mm^{-2}	
	AA6061/(1GO+2CNTs)		62 HRB	107.56	168.06	17.24	--	--	8.32 J mm^{-2}	
	AA6061/(1.5GO+1.5CNTs)		65 HRB	110.28	173.74	18.24	--	--	9.67 J mm^{-2}	
	AA6061/(2GO+1CNTs)		67 HRB	115.32	187.23	20.35	--	--	10.8 J mm^{-2}	
	AA6061/(2.5GO+0.5CNTs)		78 HRB	130.52	201.35	22.8	--	--	11.1 J mm^{-2}	
23	Pure Al	PM + Hot extrusion	--	99	159	25.5	--	--	--	[92]
	Pure Al/(0.25GNPs+0.25CNTs)		--	136	214	19.6	--	--	--	
	Pure Al/(0.5GNPs+0.5CNTs)		--	153	239	15.1	--	--	--	
	Pure Al/(0.75GNPs+0.75CNTs)		--	171	292	16.5	--	--	--	
	Pure Al/(1GNPs+1CNTs)		--	201	342	16.4	--	--	--	
24	Pure Al	BM + Hot extrusion	--	131	173	26.52	--	--	--	[103]
	Pure Al/(1.5rGO)		--	316	353	30.28	--	--	--	
	Pure Al/(1.5CNTs)		--	275	384	35.28	--	--	--	
	Pure Al/(0.375rGO+1.125CNTs)		--	318	448	27.2	--	--	--	
	Pure Al/(0.75rGO+0.75CNTs)		--	329	453	28.6	--	--	--	
	Pure Al/(1.125rGO+0.375CNTs)		--	348	460	31.63	--	--	--	
25	AA7075	Stir casting	84.8 BHN	113.773	139.187	12.2	--	--	--	[118]
	AA7075/(6Beryl)		105.8 BHN	165.705	188.433	9.4	--	--	--	
	AA7075/(2GNPs+6Beryl)		126.7 BHN	188.352	231.587	7.2	--	--	--	
26	Pure Al	Stir casting	58 HV	99	164.5	9.5	--	--	12 J	[124]
	Pure Al/(0.5GNPs+0.5MD)		67 HV	105	173.1	7.9	--	--	7.5 J	
	Pure Al/(1GNPs+0.5MD)		75 HV	107	179.1	7.7	--	--	8 J	
	Pure Al/(1.5GNPs+0.5MD)		83 HV	110	189.8	7.1	--	--	8.5 J	
	Pure Al/(2GNPs+0.5MD)		91 HV	131	217.9	6.9	--	--	9 J	
	Pure Al/(2.5GNPs+0.5MD)		84 HV	113	194	6.3	--	--	8 J	
27	AA6111	Semisolid stir casting or compocasting	--	232	319	20.4	--	--	--	[112]
	AA6111/(3ZrB_2)		--	270	372	26.1	--	--	--	
	AA6111/(0.1GNPs)		--	272	392	17.2	--	--	--	
	AA6111/(0.1GNPs+3ZrB_2)		--	339	426	15.4	--	--	--	
28	AA6111/(0.1GNPs+3ZrB_2)	Semisolid stir casting or compocasting	--	325	378	7.8	--	--	--	[19]
	75% reduction/(0.1GNPs+3ZrB_2)		--	345	398	10.8	--	--	--	
	83% reduction/(0.1GNPs+3ZrB_2)		--	342	426	15.4	--	--	--	
	92% reduction/(0.1GNPs+3ZrB_2)		--	360	442	11.7	--	--	--	

Table 1. *Cont.*

Sl. No.	Composite System (wt.%)	Manufacturing Method	Hardness	YS (MPa)	UTS (MPa)	Elog. (%)	CS (MPa)	FS (MPa)	IS (J or J mm^{-2})	Ref.
29	AA2024/(0.5GNPs+1Rgf)	Stir casting	--	--	248	--	346	--	--	[126]
	AA2024/(1GNPs+1Rgf)		--	--	308	--	433	--	--	
	AA2024/(1.5GNPs+1Rgf)		--	--	298	--	415	--	--	
	AA2024/(2GNPs+1Rgf)				305		377	--	--	
	AA2024/(0.5GNPs+3Rgf)		--	--	356		487	--	--	
	AA2024/(1GNPs+3Rgf)		--	--	343		546	--	--	
	AA2024/(1.5GNPs+3Rgf)		--	--	320		417	--	--	
	AA2024/(2GNPs+3Rgf)		--	--	298		415	--	--	
	AA2024/(0.5GNPs+5Rgf)		--	--	323		525	--	--	
	AA2024/(1GNPs+5Rgf)		--	--	303		582	--	--	
	AA2024/(1.5GNPs+5Rgf)		--	--	316		400	--	--	
	AA2024/(2GNPs+5Rgf)		--	--	341		405	--	--	
30	AA6111	Semisolid stir casting or compocasting	--	232	319	20.4	--	--	--	[113]
	AA6111/(3ZrB_2)		--	270	372	26.1	--	--	--	
	AA6111/(0.3GNPs)		--	303	412	15.7	--	--	--	
	AA6111/(0.3GNPs+3ZrB_2)		--	349	434	13.8	--	--	--	
31	AA7075	Stir casting	105 HV	--	144	--	--	--	--	[116]
	AA7075	Squeeze casting	109 HV	--	190	--	--	--	--	
	AA7075/(1GNPs+0.5hBN)	Squeeze casting	114 HV	--	201	--	--	--	--	

Severe Plastic Deformation (SPD) and secondary thermo-mechanical processes during secondary processing yielded superior refinement in the microstructure of the HAMCs. Notably, FSP and hot rolling were critical for eliminating voids and triggering dynamic recrystallization [19,26,28]. A composite of Al2024/(GNPs+SiC) reached a UTS of 589 MPa using PSSP combined with FSP, which broke reinforcement clusters better than liquid routes [26]. Hot rolling reduction up to 92% in AA6111 composites enhanced UTS to 442 MPa by transforming coarse grains into fine equiaxed structures (7.10 to 4.25 μm) [19].

Advanced architectural design strategies, such as the 3D interconnected network or flake assembly, have successfully broken the strength-ductility trade-off [98,103]. A flake design and extrusion strategy for Al/(rGO+CNTs) achieved a UTS of 460 MPa with a remarkable 31.6% elongation [103]. The justification provided was that CNTs acted as anchors while RGO sheets provided planar bridging, creating a robust structural skeleton that hindered crack propagation [98,103]. Further, additive manufacturing and squeeze casting offered high-precision fabrication of the HAMCs. L-PBF followed by T6 heat treatment in AA2024/(GNPs+ZrO_2) composites achieved the absolute highest UTS of 624 MPa [72]. Squeeze casting, solidifying under high pressure, significantly eliminates porosity compared to stir casting, improving the UTS of graphene reinforced Al7075 hybrids by 31.25% [116]. Across all routes, mechanical deterioration occurred beyond optimal reinforcement limits, i.e., typically 1–2 wt.% of graphene due to agglomeration [31,97].

In short, the AA2024/(GNPs+ZrO2) composite system processed through L-PBF and T6 treatment provided the greatest UTS of 624 MPa [72], followed by the 589 MPa UTS of the Al2024/(GNPs+SiC) composite system synthesized through PSSP+FSP [26]. In case of the best strength-ductility balance, the Al/(rGO+CNTs) HAMC imparted a UTS of 460 MPa and an elongation of 31.6% [103]. Further, the Al2024/(GNPs+SiC) composite processed via PSSP+FSP exhibited the highest hardness value of 192.6 HV [26], followed by 170 HV of the AA7010/(GNPs+TiC) composite fabricated via UASC [67]. The maximum grain refinement along with a UTS of 442 MPa was observed for the AA6111/(GNPs+ZrB_2) composite produced via semisolid stir casting and hot rolling [19].

Additionally, mechanical performances of graphene reinforced HAMCs across divergent processing regimes are compiled in Table 2. The comparative meta analyses reveal that advanced solid-state and additive configurations (such as L-PBF and PSSP+FSP) yielded the highest absolute UTS, while the HAMCs processed through liquid metallurgy routes together with assistance of high-energy cavitation or rheo-squeeze mechanism could achieve an enhancement in strength up to 350% by leveraging multi-scale reinforcement weight-percentage thresholds.

6.2. Assessment of the Tribological Properties of the HAMCs

The tribological performances of the HAMCs are subjected to the selection of the composite systems and their fabrication techniques as well. A comparison of the wear properties of the graphene reinforced HAMCs is drawn along with their synthesizing routes (see Table 3).

The addition of 2 wt.% GNPs and 0.5 wt.% marble dust (MD) to pure Al reduced the wear rate by 41% to 2.6×10^{-3} mm^3 m^{-1} (at 60 N, 0.63 m s^{-1}), attributed to the combined effect of carbonaceous and industrial waste [124]. Advanced variants like vacuum-assisted and ultrasonicated stir casting reported by Somayajula [95] further optimized tribological performances. Using vacuum eliminated oxidation while ultrasonication broke clusters, leading to a minimum COF of 0.295 with a wear value of 120 μm for systems with 2 wt.% GO and 1 wt.% CNTs in Al6061. Furthermore, Sandeep et al. [37] highlighted that electromagnetic stir casting ensured superior uniform dispersion, with 17 wt.% SiC and 3 wt.% GNPs in Al319 providing a wear rate of 0.0333 mm^3 m^{-1} (at 20 N) by preventing thermal softening of the matrix in reference to that of 0.0809 mm^3 m^{-1} of the base material, with a reduction in wear rate of 59%. Other stir-cast systems such as AA8011/(1GNPs+6B_4C) achieved a wear rate of 2.87×10^{-3} mm^3 m^{-1} and a COF of 0.346, a 50.9% improvement justified by grain refinement [128].

Powder metallurgy provides better control over nano-reinforcement distribution. Daha et al. [88] concluded that a hybrid containing 0.3 wt.% rGO and 5 wt.% Al_2O_3 in pure Al resulted in a remarkably low mass loss of only 0.038 g. The justification is graphene's superior lubricant characteristics, which created a smooth surface texture during sliding [88]. However, Kumar et al. [109] indicated a threshold value of reinforcement content; while 4 wt.% GNPs enhanced wear resistance by 71.3% (reducing wear loss to 0.2 g), the HAMCs beyond 4 wt.% GNPs quantity led to heterogeneous distribution and triggered porosity due to van der Waals forces [109].

Table 2. Cross category mechanical performance analysis of graphene reinforced HAMCS.

Reinforcement Category	Fabrication Technique	Best System Identified (wt.%)	Max UTS (MPa)	Maximum UTS Increase (%)	Best Reinforcement Threshold (wt.%)	Comments
Carbides Group	Powder semi solid Processing + Friction Stir Processing	Al2024/(0.5GNP+0.5SiC)	589	+47%	1.0 wt.% (0.5GNP+0.5SiC)	Secondary FSP operations induce severe plastic deformation, triggering dynamic recrystallization, extreme matrix refinement, and the mechanical breakdown of secondary phase clusters [26].
	Stir Casting	AA2024/(0.15GNPs+2WC)	243	+350%	2.15 wt.% (0.15GNP+2.0WC)	Establishment of a dense, multi-scale load-sharing synergy between the heavy, rigid WC particulates and the high-aspect-ratio planar GNPs [65].
Oxides Group	Laser Powder Bed Fusion + T6 Thermal Aging	AA2024/(0.2GNP+1ZrO_2)	624 (Post-T6)	+180%	1.2 wt.% (0.2GNP+1.0ZrO_2)	L-PBF engineers a highly controlled, ultra-fine bimodal microstructure, while post-processing T6 artificial aging adds a secondary layer of precipitate strengthening [72].
	Ultrasonic-Assisted Stir Casting	AA6061/(1GNPs+2Al_2O_3)	185	+172%	3.0 wt.% (1.0GNP+2.0Al_2O_3)	Intense transient acoustic cavitation forces generated by ultrasonic probes induce local de-agglomeration of carbon clusters and significant matrix grain refinement [82].
Carbonaceous Group	High-Energy Ball Milling + Hot Extrusion	Al/(1.125rGO+0.375CNT)	460	+161.8%	1.5 wt.% (3:1 rGO to CNT ratio)	Formation of a 3D interconnected nanostructural network where 1D CNTs act as spatial anchors and 2D rGO sheets bridge matrix grain boundaries to delay micro-cracking [103].
	Rheo Squeeze Stir Casting	AA5083/(1GNs+1CNTs)	300	+50.0%	2.0 wt.% (1.0GNS+1.0CNTs)	Seamless integration via nano-preform billet manufacturing, suppressing density-driven particle rejection at the solid-liquid boundaries [93].
Other/Fibers Group	Semi solid stir casting with ultrasonic assisted	AA6111/(0.1GNPs+3ZrB_2)	442	+17%	3.5 wt.% (0.1GNPs+3ZrB_2)	Severe hot rolling (92% deformation) shatters GNP and ZrB_2 clusters, refining grains to 4.25 μm. This maximizes dislocation density and strain hardening, yielding significant strengthening while preserving elongation above 10% [19].
	Stir Casting	AA2024/(0.5GNP+3Rgf)	356	+43.5% (w.r.t. 1Rgf+0.5GNPs)	3.5 wt.% (0.5GNP+3.0Rgf)	Homogeneous macroscopic blending reduces overall casting porosity and promotes an uniform load distribution across the fibrous waste phases [126].

Rgf: R-glass fiber.

Table 3. Comparison of tribological properties of graphene reinforced hybrid Al matrix composites.

Sl. No.	Composite System (wt.%)	Manufacturing Method	Wear Type	Test Condition	Wear Rate (× 10^{-3} mm^3 m^{-1}) [CoF] at Different Load					Reference
					20 N	40 N	60 N	80 N	100 N	
1	Pure Al	Stir casting	Pin on disc (Adhesive wear)	SV: 0.63 m s^{-1}	2.8 [0.660]	3.5 [0.630]	4.4 [0.600]	5.1 [0.570]	5.6 [0.540]	[124]
	Pure Al/(0.5GNPs+0.5MD)				2.6 [0.561]	3.1 [0.536]	3.8 [0.510]	4.6 [0.485]	5.2 [0.459]	
	Pure Al/(1GNPs+0.5MD)				2.3 [0.495]	2.7 [0.473]	3.5 [0.450]	4.2 [0.428]	4.7 [0.405]	
	Pure Al/(1.5GNPs+0.5MD)				2.2 [0.440]	2.6 [0.420]	3.0 [0.400]	3.6 [0.380]	4.3 [0.360]	
	Pure Al/(2GNPs+0.5MD)				1.9 [0.385]	2.3 [0.368]	2.6 [0.350]	3.1 [0.333]	3.7 [0.315]	
	Pure Al/(2.5GNPs+0.5MD)				2.0 [0.363]	2.5 [0.347]	2.8 [0.330]	3.2 [0.314]	3.9 [0.297]	
2	Pure Al	Stir casting	Pin on disc (Adhesive wear)	SV: 1.83 m s^{-1}	4.8 [0.561]	6.1 [0.536]	7.5 [0.510]	8.3 [0.485]	8.9 [0.459]	[124]
	Pure Al/(0.5GNPs+0.5MD)				4.5 [0.477]	5.2 [0.455]	6.4 [0.434]	7.8 [0.412]	8.4 [0.390]	
	Pure Al/(1GNPs+0.5MD)				3.9 [0.421]	4.5 [0.402]	5.8 [0.383]	6.9 [0.363]	7.9 [0.344]	
	Pure Al/(1.5GNPs+0.5MD)				3.7 [0.374]	4.3 [0.357]	5.1 [0.340]	5.9 [0.323]	7.1 [0.306]	
	Pure Al/(2GNPs+0.5MD)				3.2 [0.327]	3.9 [0.312]	4.5 [0.298]	5.3 [0.283]	6.2 [0.268]	
	Pure Al/(2.5GNPs+0.5MD)				3.5 [0.309]	4.2 [0.295]	4.9 [0.281]	5.5 [0.267]	6.7 [0.253]	
					Wear rate (×10^{-3} mm^3 m^{-1}) [CoF] at Different Load					
					10 N	20 N	30 N			
3	Al-Si Alloy	Pressure infiltration	Reciprocating ball on flat method (Adhesive wear)	SD: 500 m; SV: 0.08 m s^{-1}	16.96 [0.784]	27.68 [0.805]	33.90 [0.900]			[58]
	Al-Si Alloy/(48.46B_4C)				13.25 [0.607]	23.60 [0.658]	29.52 [0.702]			
	Al-Si Alloy/(0.21GNPs+47.38B_4C)				12.22 [0.587]	19.12 [0.619]	25.74 [0.658]			
	Al-Si Alloy/(0.42GNPs+47.29B_4C)				9.30 [0.521]	16.92 [0.572]	22.08 [0.611]			
	Al-Si Alloy/(0.84GNPs+47.1B_4C)				14.96 [0.562]	24.06 [0.654]	27.36 [0.701]			
					Wear rate (×10^{-3} mm^3 m^{-1}) [CoF] at Different Load					
					10 N	15 N	20 N			
4	Al319	Stir casting	Pin on disc (Adhesive wear)	SD: 600 m; SV: 2 m s^{-1},	13.4	39.3	80.9			[37]
	Al319/(20SiC)				27.4	33.8	39.9			
	Al319/(5GNPs)				23.6	28.6	48.1			
	Al319/(5GNPs+15SiC)				30.8	37.1	85.3			
	Al319/(3GNPs+17SiC)				11.2	14.5	33.3			
	Al319/(1GNPs+19SiC)				49.2	63.1	81.3			
5	Al319	Stir casting	Pin on disc (Adhesive wear)	SD: 2400 m; SV: 2 m s^{-1}	14.8	55.4	67.9			[37]
	Al319/(20SiC)				11.4	13.4	63.1			
	Al319/(5GNPs)				12.1	19.9	43.1			
	Al319/(5GNPs+15SiC)				17.6	69.1	53.9			
	Al319/(3GNPs+17SiC)				14.6	24.5	58.8			
	Al319/(1GNPs+19SiC)				28.5	46.8	65.6			
					Wear rate (×10^{-3} mm^3 m^{-1}) [CoF] at Different Load					
					10 N	20 N	30 N			
6	AA7076	Stir casting	Pin on disc (Adhesive wear)	SD: 750 m; SV: 1.51, 2.92, 4.34 m s^{-1}	2.91	3.82	3.82			[104]
	AA7076/(0.25GNPs+0.25CF)				2.76	3.34	4.19			
	AA7076/(0.375GNPs+0.375CF)				2.42	2.84	3.87			
	AA7076/(0.5GNPs+0.5CF)				2.04	2.79	3.47			
	AA7076/(0.75GNPs+0.75CF)				1.79	2.50	2.80			
7	AA8011	Stir casting	Pin on disc (Adhesive wear)	Load: 30 N; SD: 2148 m; SV: 2.387 m s^{-1}	5.87 [0.363]					[128]
	AA8011/(1GNPs+3B_4C)				3.96 [0.352]					
	AA8011/(1GNPs+6B_4C)				2.87 [0.346]					
	AA8011/(1GNPs+9B_4C)				3.16 [0.349]					

Table 3. *Cont.*

Sl. No.	Composite System (wt.%)	Manufacturing Method	Wear Type	Test Condition	Specific Wear Rate ($\times10^{-3}$ mm^3 N m^{-1})	Reference
					10 N	
8	AA1060 AA1060/(0.5GNS) AA1060/(1GNS) AA1060/(2GNS) AA1060/(1GNS+20SiC)	Powder metallurgy + Friction stir processing	Reciprocating ball on flat method (Adhesive wear)	Load: 10 N; SD: 15 m; SV: 500 mm min^{-1}	22 [0.52] 18 [0.48] 14 [0.45] 11 [0.43] 7 [0.41]	[28]
					Specific Wear Rate ($\times10^{-3}$ mm^3 N m^{-1}) [CoF]	
					10 N	
9	AA5457 AA5457/(2GNPs+2SiC) AA5457/(4GNPs+4SiC) AA5457/(6GNPs+6SiC)	Stir casting	Pin on disc (Adhesive wear)		23 [0.53] 18 [0.51] 16 [0.49] 14 [0.47]	[30]
					Depth of Wear (µm) [CoF]	
					10 N	
10	AA6061 AA6061/(0.5GO+2.5CNTs) AA6061/(1GO+2CNTs) AA6061/(1.5GO+1.5CNTs) AA6061/(2GO+1CNTs) AA6061/(2.5GO+0.5CNTs)	Ultrasonic assisted stir casting	Pin on disc (Adhesive wear)	Load: 10 N, Speed: 300 rpm	127 [0.365] 124 [0.340] 121 [0.315] 122 [0.320] 120 [0.295] 123 [0.335]	[95]
11	AA7075 AA7075/(10TiB_2) AA7075/(2GNPs+10TiB_2) AA7075/(4GNPs+10TiB_2) AA7075/(6GNPs+10TiB_2) AA7075/(8GNPs+10TiB_2)	Powder metallurgy	Pin on disc (Adhesive wear)	Load: 10, 20 and 30 N; SD: 400–800 m; SV: 1 m s^{-1}	0.67 0.58 0.48 0.2 0.33 0.56	[109]
					Wear Loss (g)	
					10 N	
12	Pure Al/(0.3rGO) Pure Al/(0.6rGO) Pure Al/(5Al_2O_3) Pure Al/(10Al_2O_3) Pure Al/(0.3rGO+5Al_2O_3) Pure Al/(0.3rGO+10Al_2O_3) Pure Al/(0.6rGO+5Al_2O_3) Pure Al/(0.6rGO+10Al_2O_3)	Powder metallurgy	Pin on disc (Adhesive wear)	Load: 11 N; Speed: 909 rpm	0.567 0.288 0.594 0.841 0.038 0.375 0.078 4.982	[88]

SV: Sliding velocity; SD: Sliding distance; MD: Marble dust.

The pressure infiltration method detailed by Polat et al. [58] was observed to be highly effective. Coating B_4C (47.2 wt.%) particles with 0.42 wt.% GNPs in Al-Si alloy reduced wear rates to 9.30×10^{-3} mm^3 m^{-1} (at 10 N) and a COF of 0.521 from 16.96×10^{-3} mm^3 m^{-1} and 0.784. The GNPs acted as solid lubricants, protecting the matrix and thus reducing the abrasive effect of hard B_4C on counter-faces. Finally, Wang et al. [28] demonstrated that two-pass FSP combined with ball milling led to extreme grain refinement of 4.9 μm along with the lowest COF of 0.41 and a specific wear rate of 0.007 mm^3 N^{-1} m^{-1} for Al1060/(1GNS+20SiC).

In brief, tribological performances of the HAMCs are highly dependent on the synergy between processing routes and reinforcement combinations. Among liquid metallurgy routes, electromagnetic stir casting provided the best overall wear rate for automotive applications, specifically the Al319/(3GNPs+17SiC) system with a low wear rate of 0.0333 mm^3 m^{-1} [37]. Vacuum-assisted ultrasonicated stir casting using Al6061/(2GO+1CNTs) provided the minimum reported COF of 0.295 and a reduced wear depth of 120 μm due to the formation of a stable lubricating tribo-layer [95]. In PM, the Al/(0.3rGO+5Al_2O_3) composite achieved the lowest mass loss (0.038 g), indicating excellent bulk wear resistance [88]. Finally, PM followed by FSP of Al1060/(1GNS+20SiC) was proved ideal for surface lubrication and grain refinement, yielding a COF of 0.41 and a specific wear rate of 0.007 mm^3 N^{-1} m^{-1}, significantly lower than the 0.52 COF of unreinforced powder matrix [28]. Those improvements across all routes are primarily justified by the crack bridging effect of graphene, refined grain boundaries, and the load-bearing capacity of hard ceramic particulates [28].

Further, an overview of the tribological performances of the HAMCs across various fabrication techniques is presented in Table 4. The comparative meta analyses outline about the extent of resistance to high-strain delamination provided by hard ceramic (carbides and oxides) reinforced HAMCs, whereas dual-carbonaceous setups and sustainable green-waste fillers in the Al matrix relied on shear-induced exfoliation to drastically lower COFs.

Table 4. Cross category tribological performance analysis of graphene reinforced HAMCs.

Category	Fabrication Technique	Best System Identified (wt.%)	Lowest Wear/ COF Values	Comments
Carbide	Semi-solid Stir Casting	GNPs+B_4C: (AA8011/(1GNPs+6B_4C))	Wear: 2.87×10^{-3} mm^3 m^{-1}; COF: 0.346	Optimal grain refinement and grain boundary pinning by hard B_4C; graphene acts as a solid lubricant [128].
	Electromagnetic Stir Casting	GNPs+SiC: (Al319/(3GNPs+17SiC))	Wear: 11.2×10^{-3} mm^3 m^{-1} (at 10 N);	Electromagnetic mixing ensures superior uniform dispersion, minimizing porosity to 4.28% [37].
Oxide	Powder Metallurgy	RGO+Al_2O_3: [Al/(0.3RGO+5Al_2O_3)]	Mass Loss: 0.038 g (94% reduction vs. GNP alone)	Synergistic effect of Al_2O_3 particles inducing Orowan barrier mechanism and RGO creating a smooth, self-lubricating surface [88].
	Stir Casting	GNPs+CeO_2: [Al6061/(3GNPs+3CeO_2)]	Specific Wear: 0.303 mm^3 N^{-1} m^{-1}; COF: 0.411	Fine grain size and strong interfacial bonding between nanoparticles and matrix [74].
Carbonaceous	Vacuum-assisted & Ultrasonicated Stir Casting	GO+CNTs: [Al6061/(2GO+1CNTs)]	COF: 0.295 (Overall Lowest); Wear depth: 120 μm	Vacuum eliminates oxidation; ultrasonication prevents particle clustering; GO forms a stable, protective lubricating tribo-film [95].
	Stir Casting	GNPs+CF: [AA7076/(0.75GNPs+0.75CF)]	Wear: 1.79×10^{-3} mm^3 m^{-1}	Hard ceramic particulates collected at grain boundaries allow the composite to withstand heavy strain [104].
Other (Waste/Green)	Stir Casting	GNPs+Marble Dust [Al/(2GNPs+0.5MD)]	Wear: 1.9×10^{-3} mm^3 m^{-1}; COF: 0.315	Synchronous between industrial waste (marble dust) filler and carbonaceous lubricant (GNPs) minimizes material removal and metal-to-metal contact [124].

CF: Carbon Fiber; COF: Coefficient of friction.

6.3. Methodological Completeness and Processing reliability Mapping

Critical analysis of the 115 compiled literature sources revealed a clear disparity between volume percents of reinforcements and manufacturing processes. Notably, an approximate of 30–40% of the reviewed studies represented highly optimized, high-impact standards with verified microstructural evolution, interfacial reactions, and mechanical/tribological properties. Conversely, a substantial portion of the remaining literature appearing in rapid-dissemination venues or conference proceedings presented a baseline implementation of conventional SC. While those in conference proceedings often claimed positive trends, they lacked rigorous microstructural evidences, such as high-resolution electron microscopy or phase quantification. The fabrication technique of SC has been dominant in terms of the volume of the literature reported on graphene reinforced HAMCs; nonetheless,

its success is highly conditional and often unverified unless paired with advanced, modified melt interventions, as summarized in Tables 3 and 4.

7. Applications of GNPs Reinforced HAMCs

The choice of Al alloys as a matrix is dictated by the compelling need to have vehicles with low fuel consumption and reduced emissions for a sustainable future. Because of their high strength-to-weight ratio, Al alloys are considered to be an alternative to conventional steels and to the more expensive superalloys. Al-based composites have contributed to such growth by improving the strength and hardness of the aluminum matrix, broadening the application field to more highly rated regimes [5,13]. AMCs, particularly HAMCs reinforced with GNPs and ceramic/metallic particles, have gained significant attention due to their unique combination of lightweight characteristics, high specific strength, improved wear resistance, and enhanced thermal and electrical properties. Notably, the incorporation of GNPs into hybrid reinforcement systems significantly improves load transfer capability, crack resistance, thermal stability, and conductivity, thereby enhancing the overall mechanical and multifunctional behaviour of the composites under severe mechanical and thermal operating conditions [129,130]. These attributes make those HAMCs greatly suitable for advanced structural and functional applications where conventional Al alloys may not provide sufficient performance. In the automobile industry, AMCs are increasingly employed in components such as piston, connecting rod, driveshaft, brake drum and rotor, engine block, cylinder heads and liners, gear components, suspension arms, and mechanical seals, etc., where improved wear resistance and reduced weight contribute to better fuel efficiency and lower emissions [5,8,20,131]. Similarly, in the aerospace sector, the AMCs are being explored for aircraft components (like stabilizers, fuselage, ventral fins, exit guide vanes of engine fan, covers of fuel access, etc.), turbine components, satellite parts and infrastructure components (like power transmission conductor cables, nuclear waste containment, etc.) due to their high strength-to-weight ratio and improved fatigue resistance [129]. In addition, HAMCs are being widely adopted in sports and recreational equipment such as bicycle frames, golf club shafts and heads, baseball bats, skating shoes, and rackets [131]. The broad industrial utilization of mono-reinforced AMCs together with the advanced HAMCs across sectors such as automobile, aerospace, electrical/electronics, marine, defence, and sports equipment is illustrated in Figure 19. Notably, Al-based MMCs and HAMCs have found increasing application in automotive, aerospace, and transportation industries owing to their high specific strength, enhanced wear resistance, and superior tribological performances [4,8]. Further, significant efforts have been made to replace conventional grey cast iron for brake components and pistons with Al-based MMCs possessing ceramic or hybrid reinforcements, resulting in substantial weight reduction and improved performance. More broadly, MMCs with graphene being one of the hybrid reinforcements have contributed to lightweight design strategies in automobiles, trains, bicycles, and aerospace structures, meeting energy efficiency and sustainability objectives [5].

In addition to structural and automotive needs, AMCs and HAMCs as well are gaining importance in electrical and electronic systems due to their improved thermal conductivity and heat dissipation capabilities, which are beneficial for heat sinks, electronic packaging, and power transmission components [25]. The marine industry benefits from these materials because of their corrosion resistance and lightweight properties, which improve durability and efficiency in shipbuilding and offshore structures. In the defence sector, HAMCs are used in lightweight armour systems and military vehicle components where high stiffness, impact resistance, and structural reliability are matters of concern [132]. As shown in Figure 19, the diverse application potential of AMCs and HAMCs across multiple industries drives a continuous research effort toward developing advanced hybrid reinforcement systems, particularly those incorporating graphene-based nanomaterials for next-generation lightweight engineering applications. In short, graphene-reinforced HAMCs have demonstrated significant improvements in strength, stiffness, and thermal and electrical conductivities, offering potential applications in electronics, energy storage, sensing, and advanced structural components.

From a techno-economic perspective, transitioning these HAMCs to wide-scale industrial manufacturing requires scalability, cost estimation, project viability, etc. Notably, the procurement cost of graphene is high; therefore, mass-produced variants or sustainable, waste-derived secondary reinforcements may offer an economically viable alternative [5,131]. Further, scaling up solid-state routes remains constrained by geometric die limits, whereas liquid-state routes face critical technological barriers such as poor wettability, cluster/agglomeration of reinforcements, and the localized formation of brittle Al_4C_3. While conventional mono-reinforced composites enjoy high commercial deployment, the graphene reinforced hybrid systems currently occupy an intermediate industrial readiness level (typically a technology readiness level of 4–5). Therefore, bridging this gap requires moving beyond a controlled laboratory standard to a scaled, robust real-life environment.

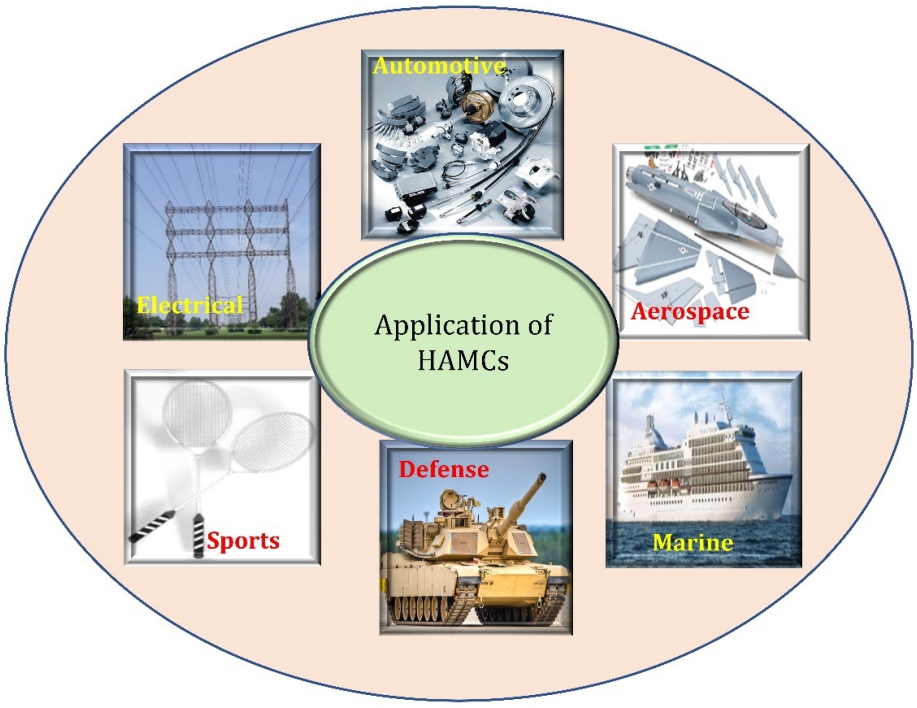

Figure 19. Major application areas of hybrid aluminum matrix composites.

8. Challenges, Research Gaps, and Future Perspectives

The integration of GNPs with secondary reinforcements in Al alloys has unlocked significant potential, yet critical processing and structural bottlenecks hindering the widespread industrial adoption of graphene reinforced HAMCs. A primary challenge, highlighted in the literature, is the severe trade-off between nano-dispersion homogeneity and nano-interfacial integrity [14]. While liquid metallurgy routes like stir casting offer scalability, they are severely limited by density-driven buoyancy and the local agglomeration of non-wetting carbon phases. Conversely, solid-state methods such as PM maintain better physical distribution but often suffer from incomplete matrix densification and uncontrolled formation of interfacial carbides, triggering severe structural embrittlement of the composites. The dual-reinforcement strategy in HAMCs may intensify these complexities by introducing multiple heterogeneous interfaces that require simultaneous optimization [131]. Since the interface between the Al matrix and the GNP reinforcement ultimately governs load transfer, thermal dissipation, and crack retardation [131,133] managing those overlapping boundaries represents the most critical barrier to maximizing the HAMCs performance.

8.1. Interfacial and Processing Challenges

To understand the core vulnerabilities of the HAMCs, the current review article addresses distinct chemical, thermodynamic, and wetting barriers occurred at the carbon-metal boundary during manufacturing:

(a) Thermochemical instability: When the melt temperature exceeds 650 °C in liquid casting routes, or during prolonged high-temperature solid-state sintering cycles, reactive Al atoms chemically attack the defective prism edges and basal planes of the graphene lattice [14,131]. This interfacial degradation follows the thermodynamic equation: $4Al + 3C \rightarrow Al_4C_3$ [15].

While a sub-nanometer, discontinuous carbide layer can occasionally act as a localized mechanical anchor to assist shear load transfer; however, excessive thermal exposure drives the growth of coarse, needle-like Al_4C_3 precipitates that act as severe stress concentrators. Furthermore, as Al_4C_3 is highly hygroscopic, it may react with atmospheric moisture to trigger rapid galvanic corrosion, accelerating the catastrophic embrittlement of the hybrid composite and destroying its structural durability [14,131].

(b) Wetting barriers and the metal-coated graphene countermeasure: To bypass the inherent wetting limitations of carbon and isolate the pristine graphene lattice from direct contact with molten Al, depositing continuous, nanometer-scale metallic layers onto the GNP surfaces has emerged as a premier boundary modification strategy [133]. As demonstrated by Liu et al. [133], surface metallization fundamentally transforms the non-wetting carbonaceous interface into a highly compatible, metallic outer shell. This modification drastically reduces contact wetting angle of the liquid Al during processing, thus ensuring clean, void-free matrix

infiltration and complete matrix encapsulation without requiring extreme, structurally damaging consolidation temperatures.

(c) Diffusion boundaries and Cu/Ni interlayer mitigation: Among the available surface modifications, the deposition of Cu or Ni interlayers provides a highly effective, dual-functioning protective shield to the HAMCs [133]. During thermal consolidation, Ni or Cu interlayer serves as a sacrificial diffusion barrier that physically blocks carbon migration into the surrounding liquid Al pool, effectively suppressing Al_4C_3 nucleation and crystallization. Simultaneously, the interlayer partially dissolves into the matrix to form stable intermetallic phases (such as Al_3Ni), thereby creating an atomistically coherent bond, ensuring seamless shear stress transfer while balancing the classic trade-off between dispersion homogeneity and local interfacial integrity [14].

(d) Phase agglomeration and solution via in-situ synthesis methods: Complementing external coatings, in-situ synthesis routes offer an alternative path to engineer pristine, contamination-free interfaces directly within the matrix. The work by Chen et al. [26] on the in-situ growth of SiC on GNPs highlighted the value of generating secondary ceramic phases directly on the graphene surface via controlled internal chemical reactions. By synthesizing these hybrid phases inside the melt, the resulting boundaries were completely free of organic residues, processing contaminants, and oxide scaling [26]. Notably, these in-situ grown ceramic nanoparticles mechanically pin the nano-sheets to prevent agglomeration or buoyancy-driven flotation, while simultaneously acting as geographical barriers that shield the core graphene sheets from direct chemical attack by the aggressive Al melt [26,131].

8.2. Key Research Gaps

A pronounced processing paradox exists within liquid metallurgy, where conventional stir casting dominates general literature due to its low cost and operational simplicity, yet high-impact publications utilizing ambient stir casting remain scarce. Standard casting alone cannot overcome the poor wettability and density-driven buoyancy of graphene, leading to severe reinforcement agglomeration and high residual porosity. Premium, high-performance studies achieve success almost exclusively by bypassing conventional methods in favor of advanced, high-energy liquid-state methodologies such as ultrasonic-assisted stir casting (which shatters GNP clusters via acoustic cavitation), semi-solid rheocasting (which mechanically traps phases within a high-viscosity liquid-solid zone), and squeeze casting (which applies high solidification pressure). A major research gap remains in standardizing these advanced hybrid liquid routes into continuous, cost-effective industrial workflows rather than keeping them restricted to small laboratory batches.

Beyond fabrication limitations, a critical testing gap exists regarding the long-term stability and dynamic performance of HAMCs under realistic operational conditions. Most current literature including prominent studies by Adediran et al. [33] and Kumar and Singh [17] focuses heavily on room-temperature, quasi-static tensile properties and short-term wear. There is a severe scarcity of data evaluating high-cycle fatigue, fracture toughness, and high-temperature creep resistance, all of which are non-negotiable performance thresholds for aerospace structures and automotive engine components [115,134]. Additionally, while dry sliding wear is extensively documented, HAMCs behavior under lubricated or corrosive environments remains severely under-explored, requiring deeper validation to move beyond lab-scale observations to real-world structural applications.

Finally, future research must pivot toward coupling advanced processing with secondary operations and predictive multi-scale modeling to bridge microstructural and scaling gaps. Synthesizing routes must systematically combine primary treatments, such as ultrasonic cavitation, with secondary thermo-mechanical processing like hot rolling or friction stir processing to achieve simultaneous macro-dispersion and localized microstructural toughening. This physical scaling should be supported by computational models capable of predicting complex, multi-phase reinforcement interactions and localized interfacial damage under stress. Ultimately, scaling these highly engineered laboratory architectures to match industrial-throughput and large-scale manufacturing demands remains the next vital milestone for mature HAMCs development [115,134].

8.3. Future Perspective and Commercialization

Transitioning GNP-reinforced HAMCs from academic novelties to mainstream structural standards requires a decisive shift toward manufacturing reliability and predictable performance capability of the HAMCs [3,11,135–137]. Rather than abandoning traditional foundry routes, research must focus on standardizing advanced liquid metallurgy techniques like ultrasonic-assisted stir casting, semi-solid rheocasting, and squeeze casting to provide low-cost, high-volume pathways for automotive and aerospace production of the HAMCs. This could be accompanied by pre-treatment interfacial engineering of the reinforcement. Pre-processing methods such as in-

situ growth of SiC on GNPs [26] or surface metallization [133] may successfully resolve critical foundry issues like particle buoyancy, poor matrix wetting, and carbide degradation by optimizing the interface prior to the incorporation into the matrix.

Conversely, several high-performance frontiers remain limited to laboratory scales due to low throughput, prohibitive processing costs, or fundamental knowledge gaps. For instance, additive manufacturing via laser powder bed fusion offers exceptional microstructural control, yet laser-induced thermal degradation of the graphene lattice, micro-cracking, and severe anisotropy keep it firmly at the lab scale. Similarly, computational modeling must transcend basic macro-scale formulas to develop multi-scale simulations capable of predicting localized failure at the complex graphene-metal interface, thus requiring extensive empirical validation before industrial tool deployment [33]. In short, the commercial realization of the HAMCs depends on balancing low-cost scalability with advanced microstructural control through robust processing, dynamic testing, and predictive modelling, which may dictate the future research trend of graphene reinforced HAMCs.

Author Contributions

S.D.: data curation, analysis, investigation, methodology, validation, writing (original draft). S.S.: data curation, investigation, methodology, supervision, validation, writing (original draft) and editing. D.D.: conceptualization, resources, supervision, validation, writing (review and editing). All authors have read and agreed to the published version of the manuscript.

Funding

This research received no external funding.

Institutional Review Board Statement

Not applicable.

Informed Consent Statement

Not applicable.

Data Availability Statement

Data will be made available on request.

Conflicts of Interest

The authors declare no conflict of interest.

Use of AI and AI-Assisted Technologies

No AI tools were utilized for this paper.

References

1. Zhou, M.Y.; Ren, L.B.; Fan, L.L.; et al. Progress in research on hybrid metal matrix composites. *J. Alloys Compd.* **2020**, *838*, 155274.
2. Sharma, M.; Dwivedi, V.K. A review on performance analysis of aluminum matrix composites with different reinforcement materials. *J. Eng. Appl. Sci.* **2026**, *73*, 91.
3. Liu, B.; Sun, J.; Zhao, J.; et al. Hybrid graphene and carbon nanotube-reinforced composites: Polymer, metal, and ceramic matrices. *Adv. Compos. Hybrid Mater.* **2025**, *8*, 1.
4. Kar, A.; Sharma, A.; Kumar, S. A critical review on recent advancements in aluminium-based metal matrix composites. *Crystals* **2024**, *14*, 412.
5. Rohatgi, P.; Weiss, D.; Srivatsan, T.S.; et al. Solidification processing of aluminum alloy metal matrix composites for use in transportation applications. *Metall. Mater. Trans. A* **2024**, *55*, 4867–4881.
6. Ceschini, L.; Dahle, A.; Gupta, M.; et al. *Aluminum and Magnesium Metal Matrix Nanocomposites*; Springer: Singapore, 2017; pp. 19–20.
7. Zhou, T.; Lei, M.; Xu, J. Recent progress in the development and properties of aluminum matrix composites reinforced with graphene: A review. *Mater. Today Sustain.* **2024**, *25*, 100674.

8. Krstić, J.; Jovanović, J.; Gajević, S.; et al. Application of metal matrix nanocomposites in engineering. *Adv. Eng. Lett.* **2024**, *3*, 180–190.
9. Gajević, S.; Miladinović, S.; Ivanović, L.; et al. A review on mechanical properties of aluminium-based metal matrix nanocomposites. *Tribol. Mater.* **2023**, *2*, 114–127.
10. Wakhi Anuar, N.F.B.; Salleh, M.S.; Omar, M.Z.; et al. Wear properties of graphene-reinforced aluminium metal matrix composite: A review. *Rev. Adv. Mater. Sci.* **2023**, *62*, 20220326.
11. Lava Kumar, P.; Lombardi, A.; Byczynski, G.; et al. Recent advances in aluminium matrix composites reinforced with graphene-based nanomaterial: A critical review. *Prog. Mater. Sci.* **2022**, *128*, 100948.
12. Chen, W.; Yang, T.; Dong, L.; et al. Advances in graphene reinforced metal matrix nanocomposites: Mechanisms, processing, modelling, properties and applications. *Nanotechnol. Precis. Eng.* **2020**, *3*, 189–210.
13. Borgonovo, C.; Apelian, D. Manufacture of aluminum nanocomposites: A critical review. *Mater. Sci. Forum* **2011**, *678*, 1–22.
14. Li, Z.; Fan, G.; Tan, Z.; et al. A versatile method for uniform dispersion of nanocarbons in metal matrix based on electrostatic interactions. *Nano-Micro Lett.* **2016**, *8*, 54–60.
15. Divakar, S.; Sardar, S.; Sah, S.; et al. A state-of-the-art review on SiC and MWCNTs reinforced hybrid metal matrix composites: Processing, properties, and applications. *Hybrid Adv.* **2025**, *10*, 100454.
16. Sehgal, A.; Sharma, V.K.; Gautam, P.S.; et al. Forging the future: Exploring aluminium AA-6061 composites through stir casting for advanced applications and future innovations. *Evergreen* **2025**, *12*, 806–826.
17. Kumar, D.; Singh, S. Enhancing friction and wear performance in hybrid aluminum composites through grey relational analysis. *Res. Eng. Struct. Mater.* **2024**, *10*, 943–956.
18. Vinod Kumar, R.; Reddappa, H.N.; Chandrashekar, A.; et al. Stir-cast Al2024-based composite reinforced with boron carbide and graphene particles: Mechanical and dry sliding wear characteristics. *Eng. Rep.* **2024**, *6*, e12850.
19. Guan, C.; Chen, G.; Kai, X.; et al. Evolution of microstructure and mechanical properties of graphene nanoplates and ZrB2 nanoparticles reinforced AA6111 composites during hot rolling deformation. *J. Alloys Compd.* **2022**, *920*, 165910.
20. Sharma, S.K.; Gajević, S.; Sharma, L.K.; et al. Progress in aluminum-based composites prepared by stir casting: Mechanical and tribological properties for automotive, aerospace, and military applications. *Lubricants* **2024**, *12*, 421.
21. Yang, L.; Zhou, B.; Ma, L.; et al. Architectured interfacial interlocking structure for enhancing mechanical properties of Al matrix composites reinforced with graphene nanosheets. *Carbon* **2021**, *183*, 685–701.
22. Ikumapayi, O.M.; Akinlabi, E.T.; Pal, S.K.; et al. A survey on reinforcements used in friction stir processing of aluminium metal matrix and hybrid composites. *Procedia Manuf.* **2019**, *35*, 935–940.
23. Ghalehbandi, S.M.; Malaki, M.; Gupta, M. Accumulative roll bonding—A review. *Appl. Sci.* **2019**, *9*, 3627.
24. Alam, M.A.; Ya, H.B.; Azeem, M.; et al. Advancements in aluminum matrix composites reinforced with carbides and graphene: A comprehensive review. *Nanotechnol. Rev.* **2023**, *12*, 20230111.
25. Lin, F.; Ren, M.; Zhu, L.; et al. Graphene-reinforced aluminium matrix nanocomposites: Fabrication, properties and applications. *Adv. Nanocompos.* **2025**, *2*, 59–85.
26. Chen, L.; Qi, Y.; Fei, Y.; et al. Enhanced mechanical properties and thermal conductivity for GNPs/Al2024 composites with in situ SiC nanorods. *Met. Mater. Int.* **2021**, *27*, 4263–4270.
27. Moustafa, E.B.; Abushanab, W.S.; Melaibari, A.; et al. The effectiveness of incorporating hybrid reinforcement nanoparticles in the enhancement of the tribological behavior of aluminum metal matrix composites. *JOM* **2021**, *73*, 4338–4348.
28. Wang, C.; Zhu, X.; Fan, Y.; et al. Microstructure and properties of aluminum–graphene–SiC matrix composites after friction stir processing. *Materials* **2024**, *17*, 979.
29. Hemalatha, K.; Ashwin, R.; Santhanam, M.; et al. Experimental study on behaviour of SiC and graphene on AL7075 hybrid metal matrix composite. *Mater. Today Proc.* **2020**, *39*, 26–30.
30. Lakshmaiya, N.; Vijetha, K.; Doss, A.S.A.; et al. Dual-scale evaluation of hybrid Al-SiC/graphene composites: Mechanical properties and deep learning-driven machinability insights. *Results Eng.* **2025**, *27*, 105742.
31. Vishnoi, M.; Kumar, N.; Maurya, M.; et al. Stir cast AA 6063/graphene/SiC/fly ash composite: Assessment of microstructural and mechanical properties. *Russ. J. Non-Ferr. Met.* **2025**, *66*, 259–272.
32. Patil, S.; Chinchanikar, S. Investigation on the mechanical properties of stir-cast Al7075-T6-based nanocomposites with microstructural and fractographic surface analysis. *Obrab. Met.* **2025**, *27*, 236–251.
33. Adediran, A.A.; Edoziuno, F.O.; Adesina, O.S.; et al. Mechanical characterization and numerical optimization of aluminum matrix hybrid composite. *Mater. Sci. Forum* **2022**, *1065*, 47–57.
34. Singh, S.; Angra, S.; Kumar, D. Optimization of hardness and tensile strength of stir cast hybrid aluminum metal matrix composite using grey relational analysis. In Proceedings of the 2022 International Conference on Computational Modelling, Simulation and Optimization (ICCMSO), Pathum Thani, Thailand, 23–25 December 2022.
35. Reddy, M. R.; Gugulothu, S. K.; Krishnaiah, T.; et al. Enhanced mechanical properties and machinability of Al-Cu-SiC-GNP smart hybrid composite using machine learning optimization. *Arab. J. Sci. Eng.* **2026**, *51*, 2433–2454.

36. Radha, A.; Vijayakumar, K.R. An investigation of mechanical properties on aluminum 6063 reinforced with silicon carbide and graphene nano particle by stir casting technique-metal matrix hybrid composites. *Int. J. Appl. Eng. Res.* **2015**, *10*, 228–231.
37. Sandeep, B.; Laxminarayana, P.; Kishore, K. Microstructure & tribological behavior of hybrid Al 319 metal matrix composite reinforced with SiC & graphe nano powder. *J. Bio-Tribo-Corros.* **2025**, *11*, 14.
38. Sandeep, B.; Kishore, K.; Laxminarayana, P. Wear, corrosion and microstructural analysis on SiC–GNP-reinforced Al319 composite fabricated through electromagnetic stir casting. *Surf. Rev. Lett.* **2025**, 2550156. https://doi.org/10.1142/S0218625X25501562.
39. Praveen Kumar, A.; Aadithya, S.; Dhilepan, K.; et al. Influence of nano reinforced particles on the mechanical properties of aluminium hybrid metal matrix composite fabricated by ultrasonic assisted stir casting. In Proceedings of the International Conference on Modelling, Simulation and Control (ICMSC-2015), San Francisco, USA, CA, 21–23 October 2015.
40. Tile, P.S.; Thomas, B. Influence of graphene/h-BN and SiC/h-BN reinforcing particles on microstructural, mechanical and tribological characteristics of Al7075-based hybrid nanocomposites. *Eng. Res. Express* **2024**, *6*, 025577.
41. Reddy, M.R.; Gugulothu, S.K.; Krishnaiah, T.; et al. Machinability evaluation and multi-objective optimization of Al-Cu-SiC-graphene nano-platelets hybrid composite using water jet machining and machine learning approaches. *Materwiss. Werksttech.* **2025**, *56*, 1367–1383.
42. Jauhari, S.; Prashantha Kumar, H.G.; Anthony Xavior, M. Synthesis and characterization of AA 6061-graphene-SiC hybrid nanocomposites processed through microwave sintering. *IOP Conf. Ser. Mater. Sci. Eng.* **2016**, *149*, 012086.
43. Prashantha Kumar, H.G.; Anthony Xavior, M. Encapsulation and microwave hybrid processing of Al 6061-graphene-SiC composites. *Mater. Manuf. Process.* **2018**, *33*, 19–25.
44. Zhang, J.; Liu, Q.; Yang, S.; et al. Microstructural evolution of hybrid aluminum matrix composites reinforced with SiC nanoparticles and graphene/graphite prepared by powder metallurgy. *Prog. Nat. Sci. Mater. Int.* **2020**, *30*, 192–199.
45. Zhang, J.; Qian, M.; Jia, Z.; et al. Strength-plasticity relationship and intragranular nanophase distribution of hybrid (GNS + SiCnp)/Al composites based on heat treatment. *Materials* **2024**, *17*, 2460.
46. Puchý, V.; Andrejovská, J.; Sedlák, R.; et al. Friction properties of alumina–silicon carbide–silver–graphene nanoplatelet self-lubricating composite prepared by SPS technique. *Lubricants* **2025**, *13*, 3.
47. Raheja, G.S.; Singh, S.; Prakash, C. Development of hybrid Gr/SiC reinforced AMCs through friction stir processing. *Mater. Today Proc.* **2021**, *50*, 539–545.
48. Zhao, D.; Yu, X.; Suo, Z.; et al. Synergistic effect of nano-SiC and in-situ exfoliated graphene on enhancing mechanical and tribological properties of Al5052 composites via friction stir processing. *J. Alloys Compd.* **2026**, *1050*, 185836.
49. Huang, C.W.; Huang, Y.F.; Aoh, J.N. Strengthening mechanisms of aluminum matrix composite containing Cu-coated SiC particles produced by friction stir processing. *J. Chin. Inst. Eng.* **2019**, *42*, 653–663.
50. Maddaiah, K.C.; Kumar, G.V.; Pramod, R. Studies on the mechanical, strengthening mechanisms and tribological characteristics of AA7150-Al_2O_3 nano-metal matrix composites. *J. Compos. Sci.* **2024**, *8*, 97.
51. Ghazanlou, S.I.; Eghbali, B. Fabrication and characterization of GNPs and CNTs reinforced Al7075 matrix composites through the stir casting process. *Int. J. Miner. Metall. Mater.* **2021**, *28*, 1204–1214.
52. Sah, S.; Sardar, S.; Guha, A.; et al. Electrical Discharge Machining of Hybrid Metal Matrix Composites: A Comprehensive Review. *Int. J. Adv. Manuf. Technol.* **2025**, *136*, 447–526.
53. Anand, G.; Sardar, S.; Sah, S.; et al. Multi-objective optimization to enhance surface integrity in WEDM for Al-matrix composite: A comparative assessment of self-weight adjusting MCDMs and objective weight integrated hybrid TOPSIS methods. *Results Surf. Interfaces* **2025**, *18*, 100467.
54. Anand, G.; Sardar, S.; Guha, A.; et al. Surface integrity characteristics and multi-response optimization in wire-EDM of Al–Al3Fe composites. *Arab. J. Sci. Eng.* **2024**, *49*, 15289–15324.
55. Ajithkumar, J.P.; Anthony Xavior, M. Mechanical, microstructural and electrical properties of Al7075/SiC based hybrid composites with nano B^4C, graphene and CNT reinforcements. *J. Phys. Conf. Ser.* **2022**, *2198*, 012049.
56. Abbas Shafqat, Q.; Rafi-Ud-Din; Shahzad, M.; et al. Mechanical, tribological, and electrochemical behavior of hybrid aluminum matrix composite containing boron carbide (B_4C) and graphene nanoplatelets. *J. Mater. Res.* **2019**, *34*, 3116–3129.
57. Tripathy, S.K.; Senapati, A.K. An extensive analysis of mechanical and tribological studies of Al6061 alloy based hybrid composite reinforced with B4C and graphene. *Mater. Today Proc.* **2021**, *44*, 2808–2812.
58. Polat, S.; Sun, Y.; Çevik, E.; et al. Investigation of wear and corrosion behavior of graphene nanoplatelet-coated B4C reinforced Al-Si matrix semi-ceramic hybrid composites. *J. Compos. Mater.* **2019**, *53*, 3549–3565.
59. Radha, A.; Suresh, S.; Ramanan, G.; et al. Processing and characterization of mechanical and wear behavior of Al7075 reinforced with B4C and nano graphene hybrid composite. *Mater. Res. Express* **2019**, *6*, 1265c5.
60. Xavior, M. Assessing the effect of heat treatment and tempering conditions on the properties of graphene/B4C reinforced Al6061 composites. *Adv. Mater. Process. Technol.* **2025**, *11*, 3879–3890.

61. Parasuraman, B.; Michael, A.X. Effect of T6 tempering on the wear and corrosive properties of graphene and B4C reinforced Al6061 matrix composites. *J. Manuf. Mater. Process.* **2025**, *9*, 82.
62. Wang, X.; Jiang, X.; Sun, H.; et al. Microstructures and mechanical properties of Al nanocomposites hybrid-reinforced with B4C, carbon nanotubes and graphene nanoplatelets. *Mater. Sci. Eng. B* **2023**, *293*, 116457.
63. Kala, K.L.; Krupakaran, R.L.; Gangula, V.R.; et al. Application of grey Taguchi method for optimization of EDM process parameters on stir casted aluminium hybrid metal matrix composites. In Proceedings of the International Conference on Advances in Design, Materials, Manufacturing and Surface Engineering for Mobility, Chennai, India, 27 October 2023.
64. Kala, L.K.; Madhuri, K.; Reddy, D.; et al. Optimization of machining parameters based on desirability function analysis for stir casted aluminium hybrid metal matrix composites. In Proceedings of the International Conference on Advances in Design, Materials, Manufacturing and Surface Engineering for Mobility (ADMMS'25), Chennai, India, 7 February 2025.
65. Subburaj, A.; Antony Joseph Decruz, A.M.M.; Chandra Moorthy, V.A.; et al. Mechanical characterization and micro-structural analysis on AA2024 hybrid composites reinforced with WC and graphene nanoparticles. *Trans. Indian Inst. Met.* **2022**, *75*, 1721–1730.
66. Khoshaim, A.B.; Moustafa, E.B.; Alazwari, M.A.; et al. An investigation of the mechanical, thermal and electrical properties of an AA7075 alloy reinforced with hybrid ceramic nanoparticles using friction stir processing. *Metals* **2023**, *13*, 124.
67. Duvvarapu, A.; Katrenipadu, S.P.; Gurugubelli, S.N. Microstructural behavior and mechanical properties of AA7010/TiC/graphene hybrid nanocomposite synthesized by stir casting. *Trans. Indian Inst. Met.* **2024**, *77*, 1835–1845.
68. Lingaraju, S.V.; Hatti, G.; Jadhav, M.R.; et al. Investigation on tribological behavior of Al7075-TiC/graphene nano-composite using Taguchi method. *J. Bio-Tribo-Corros.* **2024**, *10*, 110.
69. Gatamorta, F.; Enginsoy, H.M.; Bayraktar, E.; et al. Recycled "A1431 + A1050" based composites reinforced with "TiC" ceramic powders for aeronautical applications. In *Mechanics of Composite, Hybrid and Multifunctional Materials, Fracture, Fatigue, Failure and Damage Evolution*; River Publishers: New York, NY, USA, 2025; Volume 3, pp. 35–40.
70. Boppana, S.B.; Dayanand, S.; Murthy, B.V.; et al. Development and mechanical characterisation of Al6061-Al_2O_3-graphene hybrid metal matrix composites. *J. Compos. Sci.* **2021**, *5*, 155.
71. Chaurasia, R.; Sarangi, S.K. Synergistic effect of graphene nanoplatelets and titanium dioxide nanopowder-reinforced aluminium nanohybrid composites on mechanical properties. *Funct. Compos. Struct.* **2024**, *6*, 025012.
72. Wei, P.; Chen, Z.; Yao, S.; et al. Enhancing strength and ductility of graphene and ZrO_2 nanoparticles hybrid reinforced AA2024 composite fabricate by laser powder bed fusion. *Compos. Part A: Appl. Sci. Manuf.* **2024**, *185*, 108378.
73. Yaqoob, B.; Pasha, R.A.; Awang, M.; et al. Comparison of mixing strategies and hybrid ratio optimization for mechanical properties enhancement of Al-CeO_2-GNP's metal matrix composite fabricated by friction stir processing. *Metallogr. Microstruct. Anal.* **2019**, *8*, 534–544.
74. Kumar, D.; Singh, S.; Angra, S. Synergistic effects of graphene and ceria nanoparticulates on microstructure and mechanical behavior of stir-cast hybrid aluminum composite. *Trans. Indian Inst. Met.* **2024**, *77*, 2699–2709.
75. Kumar, D.; Singh, S.; Angra, S. Dry sliding wear and microstructural behavior of stir-cast Al6061-based composite reinforced with cerium oxide and graphene nanoplatelets. *Wear* **2023**, *516–517*, 204615.
76. Abeens, M.; Brucely, Y.; Paulraj, G.; et al. Preparation and characterization of Al8011 TiO_2 and nano graphene hybrid composite mechanical and wear behavior. *Mater. Today Proc.* **2023**, *in press*. https://doi.org/10.1016/j.matpr.2023.04.192.
77. Kishore, K.L.; Padal, K.T.B. Effect of graphene nano platelets on microstructural and wear behavior of AA7075/Al2O3 nano composites. *Mater. Today Proc.* **2022**, *62*, 4424–4431.
78. Al Oraimi, S.; Al Abri, A.; Krishnan, P.K. Development and microstructural characterization of recycled waste reinforced aluminum hybrid composites for mechanical applications. In Proceedings of the 11th World Congress on Mechanical, Chemical, and Material Engineering (MCM'25), Paris, France, 19–21August 2025.
79. Mahenran, T.; Nadar Rajammal, V.K.K. Mechanical and morphological investigation of aluminium 7075 reinforced with nano graphene/aluminium oxide/Inconel alloy 625 using ultrasonic stir casting method. *Rev. Compos. Mater. Av.* **2022**, *32*, 181–189.
80. Harish, P.; Siddiq, S.; Srikanth, V.M.; et al. Effect of alumina and graphene on mechanical and tribological behaviour of Al-7075 hybrid composite. *Appl. Eng. Lett.* **2019**, *4*, 79–87.
81. Ganesh, M.; Atgur, V. Fabrication and mechanical characterization of stir cast AA7075 (graphene alumina) nano hybrid composite. *Int. J. Veh. Struct. Syst.* **2025**, *17*, 671. https://doi.org/10.4273/ijvss.17.4.20.
82. Soni, S.K.; Ganatra, D.; Mendiratta, P.; et al. Microstructure and mechanical characterization of Al2O3/graphene reinforced Al6061 based hybrid nanocomposites. *Met. Mater. Int.* **2022**, *28*, 545–555.
83. Mohammed, A.S.; Alahmari, T.S.; Laoui, T.; et al. Mechanical and thermal evaluation of aluminum hybrid nanocomposite reinforced with alumina and graphene oxide. *Nanomaterials* **2021**, *11*, 1225.
84. Khan, M.F.; Mohammed, A.S.; Toor, I.U.H. A comprehensive evaluation of electrochemical performance of aluminum hybrid nanocomposites reinforced with alumina (Al_2O_3) and graphene oxide (GO). *Metals* **2024**, *14*, 1057.

85. Elshina, L.A.; Muradymov, R.V.; Kvashnichev, A.G.; et al. Synthesis of new metal-matrix Al–Al_2O_3–graphene composite materials. *Russ. Metall.* **2017**, *2017*, 631–641.
86. Sadoun, A.M.; Najjar, I.M.R.; Wagih, A. Electroless-plating of Ag nanoparticles on Al_2O_3 and graphene nano sheets (GNs) for improved wettability and properties of Al-Al_2O_3/GNs nanocomposites. *Ceram. Int.* **2021**, *47*, 10855–10865.
87. Jafarzadeh, E.; Ghalandari, L. Evaluation of mechanical properties, corrosion resistance, and microstructure of an Al 1wt% graphene-Al_2O_3 hybrid composite sheet produced by accumulative roll bonding. *J. Ultrafine Grained Nanostruct. Mater.* **2024**, *57*, 222–235.
88. Daha, M.A.; Nassef, B.G.; Nassef, M.G.A. Mechanical and tribological characterization of a novel hybrid aluminum/ Al_2O_3/RGO composite synthesized using powder metallurgy. *J. Mater. Eng. Perform.* **2021**, *30*, 2473–2481.
89. Fattahi, M.; Rostami, M.; Amirkhanlu, F.; et al. Fabrication of aluminum TIG welding filler rods reinforced by ZrO2/reduced graphene oxide hybrid nanoparticles via accumulative roll bonding. *Diam. Relat. Mater.* **2019**, *99*, 107528.
90. Haja Syeddu Masooth, P.; Jayakumar, V.; Bharathiraja, G.; et al. Analysis of wire-cut electric discharge machining behaviour of AA6061/C/ZrO2 hybrid nano composites using Taguchi's method. *Mater. Res. Express* **2024**, *11*, 045006.
91. Naik, H.R.M.; L., H.M.; Malik, V.; et al. Effect of microstructure, mechanical and wear on Al-CNTs/graphene hybrid MMC's. *Adv. Mater. Process. Technol.* **2022**, *8*, 366–379.
92. Yang, L.; Pu, B.; Zhang, X.; et al. Manipulating mechanical properties of graphene/Al composites by an in-situ synthesized hybrid reinforcement strategy. *J. Mater. Sci. Technol.* **2022**, *123*, 13–25.
93. Elshalakany, A.B.; Tirth, V.; El-Kashif, E.; et al. Characterization and mechanical properties of stir-rheo-squeeze cast AA5083/MWCNTs/GNs hybrid nanocomposites developed using a novel preform-billet method. *J. Mater. Res. Technol.* **2021**, *10*, 1195–1209.
94. Perla, V.R.; Suraparaju, S.K.; Thimmarayappa, M.; et al. Effect of wire electrical discharge machining process parameters of Al-6082 hybrid nano metal matrix composites. *Mater. Today Proc.* **2020**, *43*, 551–556.
95. Prasad Somayajula, V.S.; Krishna Kumar, T.S.; Morampudi, P.; et al. Mechanical and tribological analyses of Al6061-GO/CNT hybrid nanocomposites by combined vacuum-assisted and ultrasonicated stir casting method. *J. Mech. Behav. Mater.* **2025**, *34*, 20250049.
96. Kumar, V.; Nagegowda, K.U.; Boppana, S.B.; et al. Wear behavior of aluminium 6061 alloy reinforced with coated/uncoated multiwalled carbon nanotube and graphene. *J. Met. Mater. Miner.* **2021**, *31*, 17–24.
97. Reddy, N.C.; Girish, B.M.; Satish, B.M.; et al. Investigation of mechanical and wear behaviour of Al5056-carbon nanotube-graphene hybrid MMCs using powder metallurgy route. *J. Mines Met. Fuels* **2023**, *71*, 1906–1918.
98. Li, Z.; Fan, G.; Guo, Q.; et al. Synergistic strengthening effect of graphene-carbon nanotube hybrid structure in aluminum matrix composites. *Carbon* **2015**, *95*, 419–427.
99. Heydari, A.; Khoramishad, H.; Alikhani, H.; et al. The effect of graphene-oxide nanoplatelets on the high-velocity impact response of glass laminate aluminum reinforced epoxy. *Phys. Mesomech.* **2021**, *24*, 65–76.
100. Chen, X.; Qian, F.; Bai, X.; et al. Formation of the orientation relationship-dependent interfacial carbide in Al matrix composite affected by architectured carbon nanotube. *Acta Mater.* **2022**, *228*, 117758.
101. Xu, Z.Y.; Li, C.J.; Wang, Z.; et al. Balancing the strength and ductility of graphene oxide-carbon nanotube hybrid reinforced aluminum matrix composites with bimodal grain distribution. *Mater. Sci. Eng. A* **2020**, *796*, 140067.
102. Sadeghi, B.; Cavaliere, P.; Velashjerdi, M.; et al. High strength and conductivity: Functional gradient design in reduced graphene oxide+ carbon nanotube hybrid Al nanolaminated composites. *Mater. Sci. Eng. A* **2026**, *951*, 149628.
103. Sadeghi, B.; Cavaliere, P.; Velashjerdi, M.; et al. A 3D interconnected CNT-RGO hybrid networks for Al matrix composites: Unveiling a new pathway to superior strength-ductility balance. *Compos. Part. B Eng.* **2025**, *305*, 112746.
104. Patil, A.; Banapurmath, N.R.; Hunashyal, A.M.; et al. Development and performance analysis of novel cast AA7076-graphene amine-carbon fiber hybrid nanocomposites for structural applications. *Biointerface Res. Appl. Chem.* **2022**, *12*, 1480–1489.
105. Kumar, R.; Shringi, D.; Bairwa, K.N. Numerical validation of thermal conductivity of Al6061 based hybrid nano metal matrix composite filled with nanoparticles of Ni and Cr. *Mater. Res. Express* **2021**, *8*, 115011.
106. Pu, B.; Mesguich, D.; Estournès, C.; et al. Al matrix composites reinforced by *in situ* synthesized graphene–Cu hybrid layers: Interface control by spark plasma sintering conditions. *J. Mater. Sci.* **2022**, *57*, 6266–6281.
107. Pu, B.; Zhang, X.; Chen, X.; et al. Exceptional mechanical properties of aluminum matrix composites with heterogeneous structure induced by *in-situ* graphene nanosheet-Cu hybrids. *Compos. Part. B Eng.* **2022**, *234*, 109731.
108. Saxena, P.; Bongale, A. Classification of faults in friction stir processed composites using a machine learning and ensemble learning approach. *Mater. Res. Express* **2024**, *11*, 116507.
109. Lokesh Kumar, J.; Gurusamy, P.; Gayathri, N.; et al. Influence of graphene nanoplates and titanium diboride particulate on wear and interfacial bonding properties of sintered aluminium alloy composites. *Diam. Relat. Mater.* **2024**, *144*, 111035.
110. Maheswara Rao, C.; Durga Prasad, K.G.; Venkata Subbaiah, K.; et al. Analysis of corrosion polarization behaviour in GNP/TiB_2 reinforced hybrid Al–Mg-Si-MMNCs for marine environments. *J. Inst. Eng. Ser. D* **2025**, *106*, 1557–1566.

111. Vishnoi, M.; Rai, S.; Verma, N.; et al. Stir cast AA 6351/graphene/TiB_2/rice husk ash composite: Fabrication and assessment of mechanical properties. *Proc. Inst. Mech. Eng. Part C J. Mech. Eng. Sci.* **2024**, *238*, 4575–4586.
112. Guan, C.; Zhao, Y.; Chen, G.; et al. Synergistic strengthening and toughening of copper coated graphene nanoplates and in situ nanoparticles reinforced AA6111 composites. *Mater. Sci. Eng. A* **2021**, *822*, 141661.
113. Guan, C.; Chen, G.; Kai, X.; et al. Strengthening-toughening of graphene nanoplates and *in situ* ZrB_2 nanoparticles reinforced AA6111 matrix composites with discontinuous layered structures. *Mater. Sci. Eng. A* **2022**, *853*, 143750.
114. Qian, W.; Kai, X.; Tao, R.; et al. Investigation on high-temperature creep property and mechanism of AA6111 matrix composites reinforced by *in-situ* ZrB_2 nanoparticles. *Mater. Charact.* **2023**, *196*, 112620.
115. Guan, C.; Chen, G.; Kai, X.; et al. Transformation of dislocation strengthening mechanisms induced by graphene nanoplates and ZrB_2 nanoparticle in nanolaminated Al matrix composites. *Mater. Charact.* **2023**, *199*, 112773.
116. Agarwal, P.; Kishore, A.; Kumar, V.; et al. Fabrication and machinability analysis of squeeze cast Al 7075/h-BN/graphene hybrid nanocomposite. *Eng. Res. Express* **2019**, *1*, 015004.
117. Reddy, K.S.T.; Manohar, H.S.; Manjunath, G.; et al. Synthesis and characterization of silicon nitride and graphite reinforced aluminium hybrid metal matrix composites. *Mater. Today Proc.* **2020**, *45*, 304–306.
118. Patil, S.; Raju, B.S.; Haneef, M.; et al. Reinforcement with graphene nano platelets and beryl in Al7075 matrix composites. *Mater. Today Proc.* **2020**, *45*, 27–33.
119. Patil, S.; Ahmed, S.A.; Gunaki, P.; et al. Investigations on machinability behavior in turning of Al7075/beryl/graphene nano platelets hybrid composites with multilayer coated carbide insert using Taguchi and statistical techniques. *Key Eng. Mater.* **2022**, *937*, 55–66.
120. Patil, S. Influence of multi directional forging on hardness and wear behaviour of Al7075-beryl-graphene hybrid MMCs. *J. Metall. Mater. Eng.* **2022**, *12*, 116–123.
121. Patil, S.; Haneef, M.; Seenappa, S. A statistical analysis of optimization of wear behavior of Al7075-beryl-graphene hybrid composites using Taguchi technique. *Mater. Today Proc.* **2020**, *20*, 195–201.
122. Patil, S.; Haneef, M. Tribological behavior and hardness properties of heat treated Al 7075-beryl-graphene hybrid metal matrix composites. *Int. J. Recent Technol. Eng.* **2019**, *8*, 4808–4815.
123. Wadi, V.T.; Göçer, A.; Karamiş, M.B. Tribological characteristics of GNPs and HNTs as lubricant additives in an aluminum-based hybrid composite-steel contact. *Arab. J. Sci. Eng.* **2022**, *47*, 9099–9118.
124. Chaurasia, R.; Kumari, N.; Cep, R.; et al. Development and performance evaluation of green aluminium metal matrix composites reinforced with graphene nanopowder and marble dust. *Nanotechnol. Rev.* **2025**, *14*, 20250233.
125. Bawa'neh, H.; Lababneh, B.; Malkawi, A.M.; et al. Investigation of the mechanical properties of an aluminum (Al 6061-T6)/graphene/bentonite hybrid nanocomposite experimentally and through finite element analysis study. *Mater. Adv.* **2024**, *6*, 1031–1041.
126. Dhananjaya Kumar, L.K.; Sripad Kulkarni, S.; Deepu, J.N.; et al. Investigation of mechanical & corrosion properties of graphene, R-glass fiber reinforced aluminium 2024 hybrid composites. *Mater. Today Proc.* **2020**, *43*, 1684–1693.
127. Ahmed, N.A.; Choudhury, A.B.S.; Kumar, S.; et al. Tribological study of AA7075-graphene-kaolin hybrid composite fabricated through powder metallurgy route. In *Recent Trends in Mechanical Engineering*; Lecture Notes in Mechanical Engineering series; Springer, Singapore, 2024.
128. Michael, A.; John, E.R. Thermo-mechanical, tribological and microstructural properties of aluminium AA8011/B4C/graphene based hybrid composites. *Trans. Indian Inst. Met.* **2024**, *77*, 1217–1228.
129. Rawal, S.P. Metal-matrix composites for space applications. *JOM* **2001**, *53*, 14–17.
130. Saleh, B.; Jiang, J.; Fathi, R.; et al. 30 years of functionally graded materials: An overview of manufacturing methods, applications and future challenges. *Compos. Part. B Eng.* **2020**, *201*, 108376.
131. Surappa, M.K. Aluminium matrix composites: Challenges and opportunities. *Sadhana* **2003**, *28*, 319–334.
132. Siengchin, S. A review on lightweight materials for defence applications: Present and future developments. *Def. Technol.* **2023**, *24*, 1–17.
133. Liu, G.; Zhao, N.; Shi, C.; et al. In-situ synthesis of graphene decorated with nickel nanoparticles for fabricating reinforced 6061Al matrix composites. *Mater. Sci. Eng. A* **2017**, *699*, 185–193.
134. Andilab, B.; Emadi, P.; Sydorenko, M.; et al. Influence of GNP additions on the microstructure, mechanical properties, and electrical conductivity of cast A319 aluminum alloy. *Int. J. Met.* **2024**, *18*, 3047–3061.
135. Elizalde-Herrera, F.J.; Flores-Soto, P.A.; Mora-Cortes, L.F.; et al. Recent development of graphene-based composites for electronics, energy storage, and biomedical applications: A review. *J. Compos. Sci.* **2024**, *8*, 481.
136. Md Ali, A.; Omar, M.Z.; Hashim, H.; et al. Recent development in graphene-reinforced aluminium matrix composite: A review. *Rev. Adv. Mater. Sci.* **2021**, *60*, 801–817.
137. Matli, P.R.; Guttikonda, M.; Gopal, K.R.; et al. Processing, microstructure and performance of aluminium metal matrix composites for engineering applications—A review. *Prog. Compos. Mater.* **2025**, *1*, 6.